ACOUSTIC CHARACTERIZATION OF A MULTI-ROTOR SUAS AS A FIRST STEP TOWARDS DETECTION AND IDENTIFICATION VIA ACOUSTIC SIGNATURE

By

JORDAN AMBROSE FEIGHT

Bachelor of Science in Mechanical Engineering
West Virginia University
Morgantown, West Virginia
2014

Bachelor of Science in Aerospace Engineering
West Virginia University
Morgantown, West Virginia
2014

Submitted to the Faculty of the
Graduate College of the
Oklahoma State University
in partial fulfillment of
the requirements for
the Degree of
MASTER OF SCIENCE
July, 2017

ACOUSTIC CHARACTERIZATION OF A MULTI-ROTOR SUAS AS A FIRST STEP TOWARDS DETECTION AND IDENTIFICATION VIA ACOUSTIC SIGNATURE

Thesis Approved:

DR. JAMEY JACOB

Thesis adviser

DR. BRIAN ELBING

DR. RICHARD GAETA

Name: Jordan Ambrose Feight

Date of Degree: JULY 2017

Title of Study: ACOUSTIC CHARACTERIZATION OF A MULTI-ROTOR SUAS AS A FIRST STEP TOWARDS DETECTION AND IDENTIFICATION VIA ACOUSTIC SIGNATURE

Major Field: MECHANICAL AND AEROSPACE ENGINEERING

ABSTRACT:

In this study, the noise produced by a multi-rotor aircraft is recorded and characterized with the main goal to understand the signature for the use of detection and identification. The need for this technology spawns from multiple situations where sUAS are being used with malicious intent to perform illegal acts, such as delivering contraband to prisoners. The aircraft of choice is a small unmanned aerial system, the 3DR Iris+. The aircraft is tested in multiple different testing environments as well as different setups to investigate specific parameters and how they affect the acoustic signature of the system. The parameters under inspection are the following: rotor RPM, the number of rotors, distance and angle of microphone array from the noise source, and the environment. The aircraft is shown to be detectable in all the testing environments, while there are promising results for the identification. The results indicate that there are potential effects on the signature due to the aircraft structure, however, this requires further investigation. Also, there is no apparent effect on fundamental acoustic signature due to the environment. The significant factors that arise from this study are the operational state of the aircraft and the microphone location (or the directivity of the noise source). The results show that as the angle between the rotor plane and the microphone increases so does the overall sound pressure level of the system.

ACKNOWLEDGEMENTS

The author would like to thank his advisor, Dr. Jamey Jacob, who gave him the idea for this project and provided much needed direction in his research. His committee member, Dr. Richard Gaeta, who pushed him to try harder and was his main source of information and knowledge on acoustics.

The author would also like to thank his colleagues Madison Ellis, Andrew Cole, and Aavron Estep for assisting with taking measurements and developing/testing equipment. Geoffrey Donnell, who was the designated pilot. Kristen McKinney, who provided assistance in taking measurements and designing components. Alvin Ngo, who provided intellectual support and reviewing of this work. Dr. Kedar Pai, who provided general guidance and support.

Finally, the author would like to acknowledge his mentors for their great example. Dr. Andrew Nix, who provided guidance and support and encouraged him to chase his dreams. From their similar professional interests to their dorky interests, he has always been a great friend the author. Dr. Jay Wilhelm, his previous employer and good friend. He provided great advice and support, and encouraged the author to never give up. Dr. Wade Heubsch, who encouraged the author to pursue his interest in graduate studies and sUAS.

Acknowledgements reflect the views of the author and are not endorsed by committee members or Oklahoma State University

TABLE OF CONTENTS

LIST OF TABLES

LIST OF FIGURES

NOMENCLATURE

3DR	3D Robotics
BARC	Broadband acoustic rotor codes
BPF	Blade passing frequency
BVI	Blade vortex interaction
CAD	Computer aided design
CCP	Constant current power
CFD	Computational fluid dynamics
D	Diameter
ESC	Electronic speed controller
f	Frequency, Hz
GIA	Gallagher-Iba Arena
GPS	Global Positioning System
Kv	Motor velocity constant
LCD	Liquid-crystal display
LIDAR	Light detection and ranging
LiPo	Lithium polymer
NCAA	National Collegiate Athletic Association
OASPL	Overall sound pressure level

OSU	Oklahoma State University
PVC	Polyvinyl chloride
R	Radius
RADAR	Radio detection and ranging
Re	Reynolds number
RPM	Revolutions per minute
sUAS	Small unmanned aerial system
T	Thrust
u	Uncertainty
UAFS	Unmanned Aircraft Flight Station
UAS	Unmanned aerial system
USB	Universal Serial Bus
VTOL	Vertical take-off and landing
θ	Angle from the Rotor plane to microphone location, within Roll plane, degrees
μ	Mean of a specified data set

CHAPTER I

1. INTRODUCTION

1.1. Motivation

There is a growing demand for Unmanned Aerial Systems (UAS) in a multitude of industries from agriculture to defense to even retail. A UAS is an aircraft without the possibility of direct human intervention from within or on the aircraft [1]. The UAS originated in the military domain and can be traced back to as early as 1916 [2]. The early versions of the UAS were used for multiple purposes from flying targets to attack missions [3]. The modern version of the battlefield UAS saw its introduction in the early 1970s [4]. While UAS may have begun with military use, it has branched out into the civilian sector and has become a major source for research, entertainment, and industry. These aircraft are being considered to preform everyday tasks from delivering packages to monitoring traffic on roads. The use for UAS is becoming broader as the industry begins to experiment with applications such as remote sensing and even crime scene investigation. With the increase of small Unmanned Aerial Systems (sUAS) in the airspace comes the inevitable increase of regulations for aspects such as who can operate the aircraft and noise pollution. What defines the UAS as small is the weight where the range is 0.55 – 55 pounds [1]. There are already government agencies, such as the Air Force, beginning to consider developing a national standard for the noise of sUAS [5].

This study will focus on the multirotor type of rotorcraft due to the increase in popularity and the effectiveness of this type of aircraft for everyday applications. Also, the noise produced by rotorcraft is generally considered to be a major annoyance. Of course, with consideration of the military uses, there will always be an interest with the noise reduction of aircraft. However, this research also seeks to utilize the noise produced by the aircraft for the benefit of detecting and potentially identifying the aircraft. The need for such systems arise from multiple situations where sUAS have been abused to perform illegal acts, such as delivering drugs and other contraband to prisoners [6].

Previous research has been published with similar goals [7], however the means of accomplishing the identification of the aircraft was through comparing the recording of the unknown target to a database of known acoustic signatures. While this method is feasible and currently being implemented [8], it requires previous knowledge of the aircraft. With the large influx of different sUAS in development and on the market, and considering the growth of the industry as well as the customizability of this technology, this may not be as viable. New systems are being created and implemented frequently and will require a large upkeep to keep this method viable. Therefore, it would be ideal to have a method to identify the aircraft without the database.

1.2. Details of Rotorcraft and sUAS

The sUAS used for this study is a rotorcraft, specifically a quadcopter known as 3DR Iris+ (shown in Figure 1-1) designed and developed by 3D Robotics (3DR). The distinction between a fixed-wing aircraft and a rotorcraft is that the rotorcraft is required to provide lift throughout the entire flight by rotating the rotors. A common type of rotorcraft is the helicopter. Helicopters are unique due to generally having only one main rotor and a tail rotor for yaw control, although there are configurations with more than one main rotor. However, quadcopters have four main rotors that are used to produce lift and to maneuver the aircraft through differential thrust and torque.

Although quadcopters are not a new technology, they have become far more popular in recent years, especially for sUASs. This can be attributed to the ever-tiny size of microprocessors that has allowed this technology to become much smaller and more easily acquired. This accomplishment has caused a revived interest in multi-rotors for the military, public, and commercial use. The design and flight regime of multi-rotors allow for a wide range of uses. This is partially due to the simple controls required to command this particular aircraft but mainly due to the vertical take-off and landing (VTOL) ability.

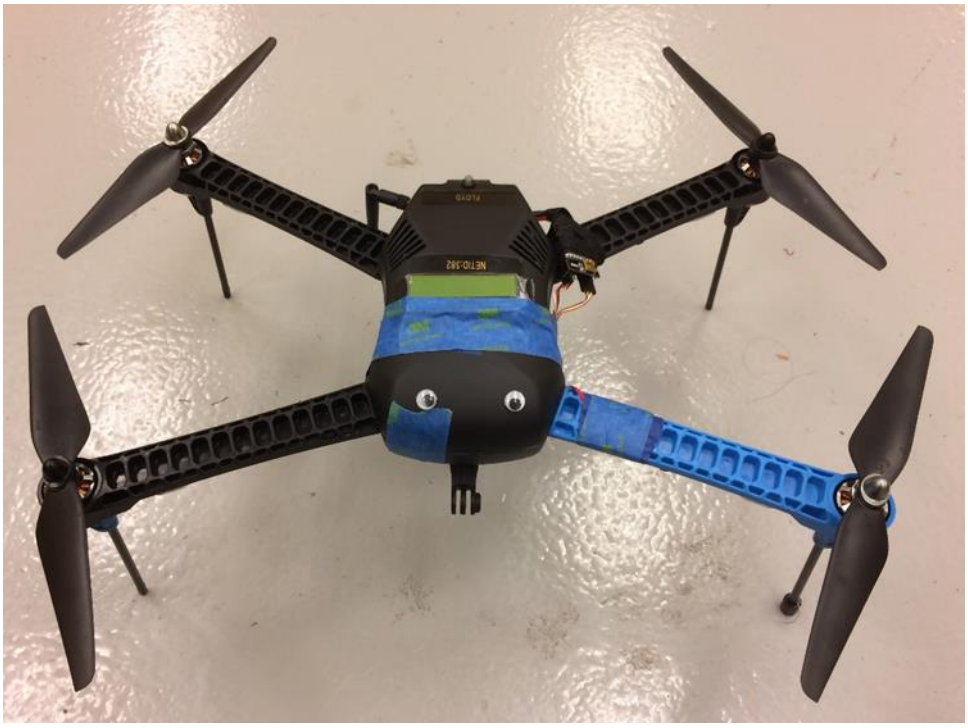

Figure 1-1: Selected aircraft, 3DR Iris+ with RPM datalogger and display attached

The rotorcraft functions under three forms of flight: axial flight, non-axial flight, and hover (as shown in Figure 1-2). Axial flight occurs when the axis of rotation of the rotor is in the direction of the airflow and can be seen during pure vertical climb, and pure vertical descent. Non-axial flight occurs everywhere axial flight does not, essentially when the flow over the rotor is not in line with the axis of rotation. Hover occurs when the vehicle maintains altitude and position. In general, rotorcraft spend most time in non-axial flight while transitioning from between locations. This

study however will not directly focus on either of these operations but instead will focus on simulating the hover operating state.

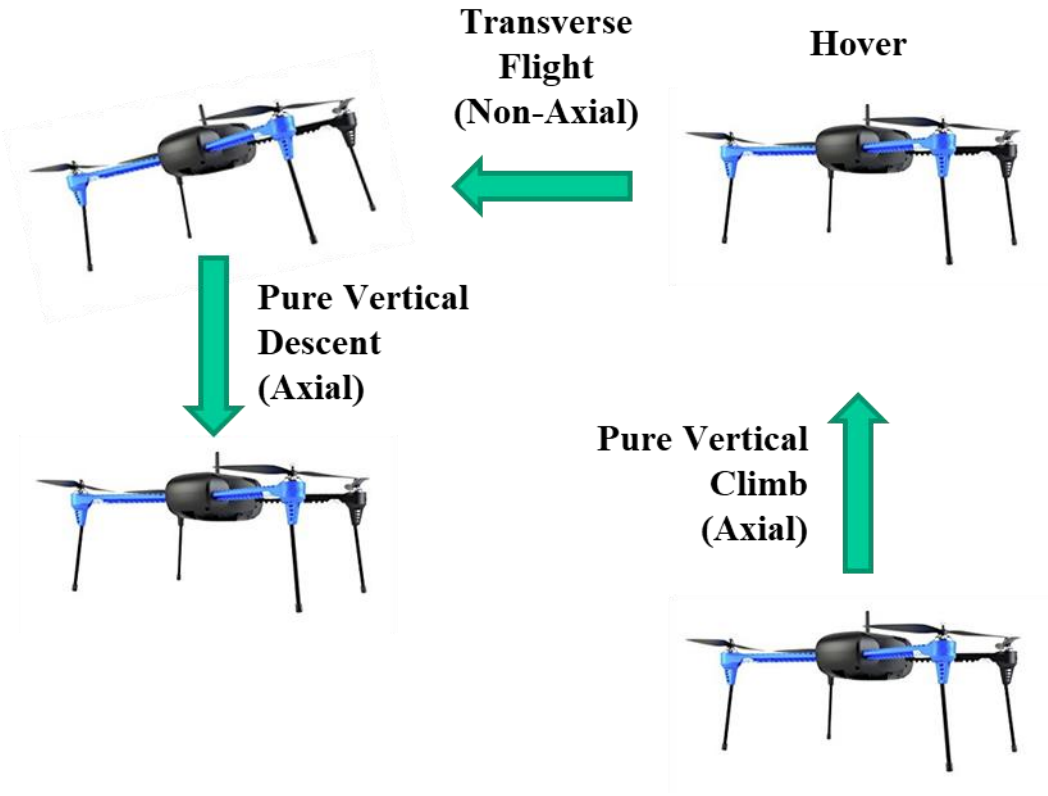

Figure 1-2: Forms of flight for rotorcraft

1.3. Levels of Awareness

When considering detection of the acoustic signature as a level of awareness, it is important to understand the differences between various levels. The determination of detection can be considered the same across multiple areas of focuses such as optics, infrared systems, and acoustics. The Army Night Vision Laboratory performed experiments on the ability to identify targets using analog sensors [9] and defined the levels of awareness as, "Detection", "Recognition" and "Identification." The terms were defined as followed:

- Detection: the ability to distinguish an object from the background
- Recognition: the ability to classify the object class (animal, human, vehicle)

- Identification: the ability to describe the object in details (a deer, a man with a hat, a Jeep)

While Johnson's experiments were specific to image processing, the terms and their definitions can be easily applied to another sensor technology. This study will consider Johnson's Criteria while investigating the acoustic signature of an aircraft. Detection, being the simplest level of awareness, has been researched and implemented through the means of RADAR, LIDAR, and acoustic sensing technologies since the early 1900s. When considering the detection of a noise source, the major variable is the level of background noise. For the use in a battlefield, noise rejection and cancelation are two signal processing techniques for reducing or removing the effects of background noise. This current work does not implement any noise rejection or cancelation, but does record and analyze the background noise to better understand the noise source.

The recognition and identification of a noise source involves two different techniques that utilize a database of known signals [8]. This is the current method used by the military for a multitude of different types of sensor technologies. Since the majority of the weapons or vehicles are known, it is easier and potentially faster to compare the measurements rather than analyze them. However, when considering sUAS and their ease of construction and customization as well as availability, acquiring a reliable database may be difficult. With this in consideration, the question of whether it is possible to recognize and/or identify the aircraft without the use of a database. The difficulty with this method comes into understanding the physical contributions to the noise source.

1.4. Rotor Noise

To characterize the noise generated by the aircraft, and to develop a detection method, it is important to understand the typical noise source mechanisms of rotary-wing vehicles, shown in Figure 1-3. These sources can be divided into deterministic components (thickness and loading noise) and non-deterministic components (broadband noise). Thickness noise is caused by the blade of the rotor displacing fluid as the rotor rotates and is highly dependent on the geometry of the

rotor. It is modeled as a monopole radiating from the tip of the blade and is discernable in the rotor plane [10]. Loading noise is caused by the sum of the forces exerted on the fluid by the airfoil, such as lift and drag. It is modeled as a dipole radiating from the surface of the blade and dominates above and below the rotor plane [11]. Loading noise is also typically separated into two sub-categories, steady and unsteady. There are many factors which can cause unsteady loading noise, for example fuselage interference, non-uniform upwash and downwash, and most notably blade vortex interaction (BVI). BVI is caused by the blade of the rotor passing within close proximity of the shed tip vortex of the previous blade. This causes impulsive changes in the aerodynamic loading resulting in highly directional impulsive loading noise [12]. The main take-away for unsteady loading noise is that the cause is rooted in impulsive changes in the aerodynamic loading. Broadband noise is typically described as fluctuation turbulence noise and has many factors which contribute to the its formation. Some examples of these factors are turbulence ingestion noise, blade wake interaction noise, and blade self-noise. High-speed impulsive noise is a high-intensity, in-plane noise associated with high advancing tip speeds [13]. For a further in-depth description of the noise sources of rotary-wing vehicles, refer to references listed in this section.

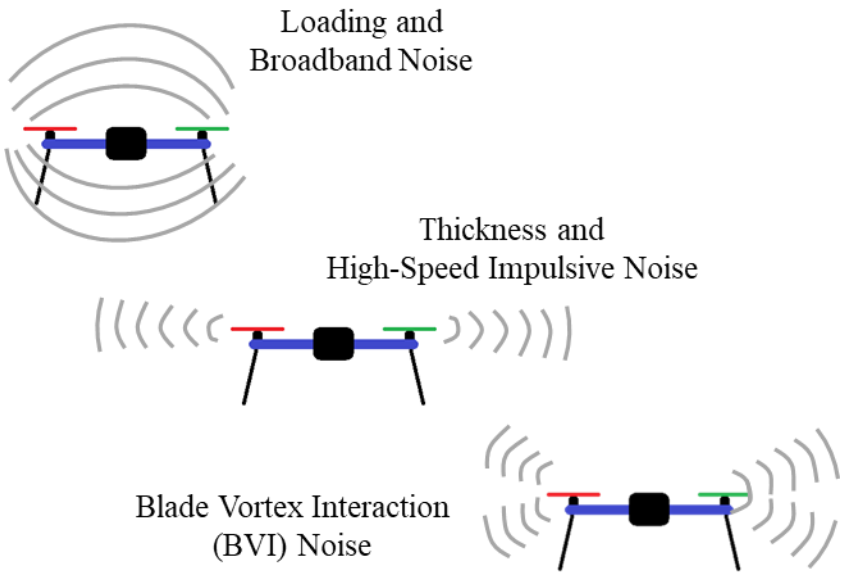

Figure 1-3: Rotor aerodynamic noise sources with associated directionalities, adapted from [13]

1.5. Goals and Objectives

The primary research question for the current study is as follows: Is it feasible to detect and/or identify an sUAS via the acoustic signature produced during flight operations? In order to investigate this question a baseline understanding of the noise source is required, both in how the aircraft operates and how it generates noise. The operation of sUAS is well established, however the emission of the noise is still uncertain and under investigation. The operation falls under the three forms of flight discussed previously: axial flight, non-axial flight, and hover. The major contributor to the noise emitted by sUAS is the rotor, which has multiple noise sources, and was also discussed previously. However, the majority of research in the past on this topic has been for larger rotors and flow regimes.

Another consideration for the noise source is the propagation pattern of the noise, also known as the directivity. This feature is of interest due to the aircraft having multiple rotors, which could have constructive and/or destructive effects on the propagation, considering each rotor has its own noise sources with their own directivity. Also, the directivity could play a large part in terms of the detectability of the aircraft, as well as gaining knowledge of how the aircraft is operating. As

for the identification of the aircraft, this will rely heavily on the characteristic features of the acoustic signature. Specifically, the features that are dependent on the type of aircraft, method of flight, or other properties of an aircraft that makes it definable or different. These features have yet to be fully defined and therein lies the main goal of the current study. To determine these features a set of objectives were designed for the current study focusing on the characterization of the acoustic signature of the sUAS. The objectives are as follows:

- To identify the characteristic features of the acoustic signature of sUAS rotorcraft.
- To determine the directivity of the noise produced by the aircraft
- To explore the changes in the features of the acoustic signature caused by:
    - Increasing throttle (RPM) of the motors
    - Having multiple rotor-motor subsystems
    - Recirculation and vibration
    - Flight environment
    - Aircraft operation

In terms of the features of acoustic signature, it is expected to be similar to that of typical rotorcraft and to contain large amounts of tonal noise due to the aircraft having multiple rotors. Lastly, it is expected that the loading noise and broadband noise will be dominate above and below the rotor plane, in comparison to the thickness noise, as shown in Figure 1-4.

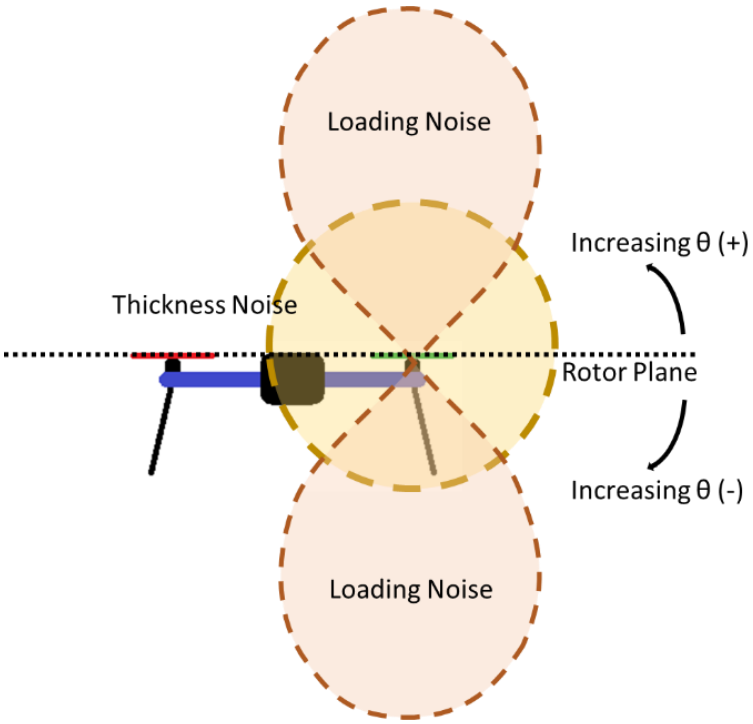

Figure 1-4: Expected directivity of rotor noise sources

CHAPTER II

2. PREVIOUS WORK

This chapter briefly reviews previous work regarding relevant research on rotor and propeller acoustics, specifically for sUAS. Many of the results presented in this chapter were also used for comparison of the results found through this study.

2.1. Quadcopter Acoustics and Aerodynamics

Intaratep [14] performed a study focusing on the aerodynamic and acoustic performance of the DJI Phantom II multi-rotor aircraft. A main goal of the study was to explore and determine of the effect of multiple rotor interaction, both in terms of aerodynamic and acoustic performance. The aircraft was selected due to popularity and accessibility and was modified with an alternate radio controller, which was used to control all 4 motors independently. This allowed for precise control inputs for each motor. The study also tested 4 different rotors sets (outlined in Table 2-1), to determine any effect on the thrust and noise produced due to blade geometry.

Table 2-1: Parameters of rotors under investigation [14]

Name	Model	Diameter (in)
Original DJI prop	9450	9.4
Aftermarket DJI prop	9443	9.4
Black carbon fiber prop	Replica of model 9443	9.4
White carbon fiber prop	T-Motor	9.0

The procedures used for this study focused on the acoustic performance of the rotors. However, thrust and acoustic measurements for the aircraft were performed simultaneously in the

Virginia Tech. anechoic chamber. The aircraft was mounted to a test stand and held level, in the upright position. All tests had the aircraft oriented to simulate the hover flight condition. The motor speeds were varied from approximately 1700 to 7900 RPM, at undefined intervals. The aircraft was tested with different rotor-motor configurations, related to the desired test. The procedures are shown in Table 2-2.

Table 2-2: Rotor configuration and procedure [14]

Number of activated rotors	Rotors tested
1	Original DJI rotor
2	Original DJI rotor, Aftermarket DJI rotor
4	Original DJI rotor, Aftermarket DJI rotor, Black carbon fiber, White carbon fiber

To determine the aerodynamic performance, a single load cell was used to measure static thrust produced by the aircraft. The load cell was integrated in the test stand. The aircraft was also attached to a suspension system consisting of steel cables to eliminate vibrations. To determine the acoustic performance, a single half-inch, pressure microphone (Bruel & Kjaer 4190) was used to measure noise produced by the aircraft. The distance from microphone to the center of aircraft is approximately 6 times the blade diameter.

In terms of the characterization of the acoustic signature, Intaratep observed that the motor noise contributes to the overall noise of the aircraft in the mid frequency range (600-6000 Hz). Also, the acoustic spectrum for the aircraft and each propeller is dominated by high and sustained tonal noise at the shaft rate, blade passing frequency (BPF), and their harmonics up to the mid frequencies (6k Hz). Intaratep also observed that at higher frequencies, the broadband noise dominates. These characteristics are shown in Figure 2-1. This led Intaratep to conclude that the domination of the BPF and the smaller shaft rate noise is similar to the typical acoustic spectrum of axial flow machines, in this specific flight condition.

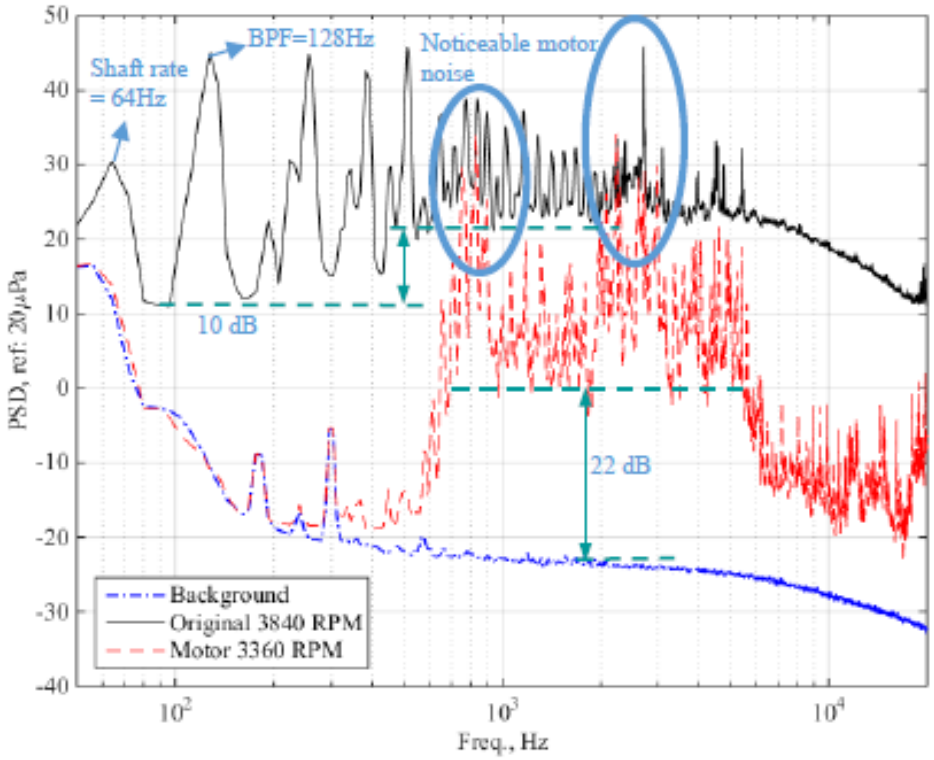

Figure 2-1: Power spectral density of the Original 9450 propeller compares to that of the unloaded motor running at nominal motor rotational speed of 4000 rpm and background noise in the anechoic chamber [14]

When considering the acoustic comparison between multiple rotor geometries, all four propellers are almost identical at low frequency, however, at high frequencies there are deviations in the broadband noise. It was speculated that this could be caused by potential laminar boundary layer vortex shedding noise. Also, the results showed a disconnect between the aerodynamic performance and the acoustic performance for some of the rotors under inspection. The black and white carbon rotors were shown to produced nearly identical thrust, however their noise spectra diverge at frequencies above 6000Hz. Also, the original and aftermarket rotors were shown to produce 40 to 50% less thrust than the black carbon rotor, however their noise spectrum displays similar broadband levels at high frequencies.

Lastly, it was determined that the noise increases when increasing the number of rotors as well as a decrease in aerodynamic performance due to the interaction between multiple rotors. The results showed, on average, the thrust was reduced by 5.8% when going from 1 to 2 rotors and then

7.3% when going from 1 to 4 rotors. The Thrust-RPM curve for the selected aircraft and the various rotor-motor configurations is shown in Figure 2-2.

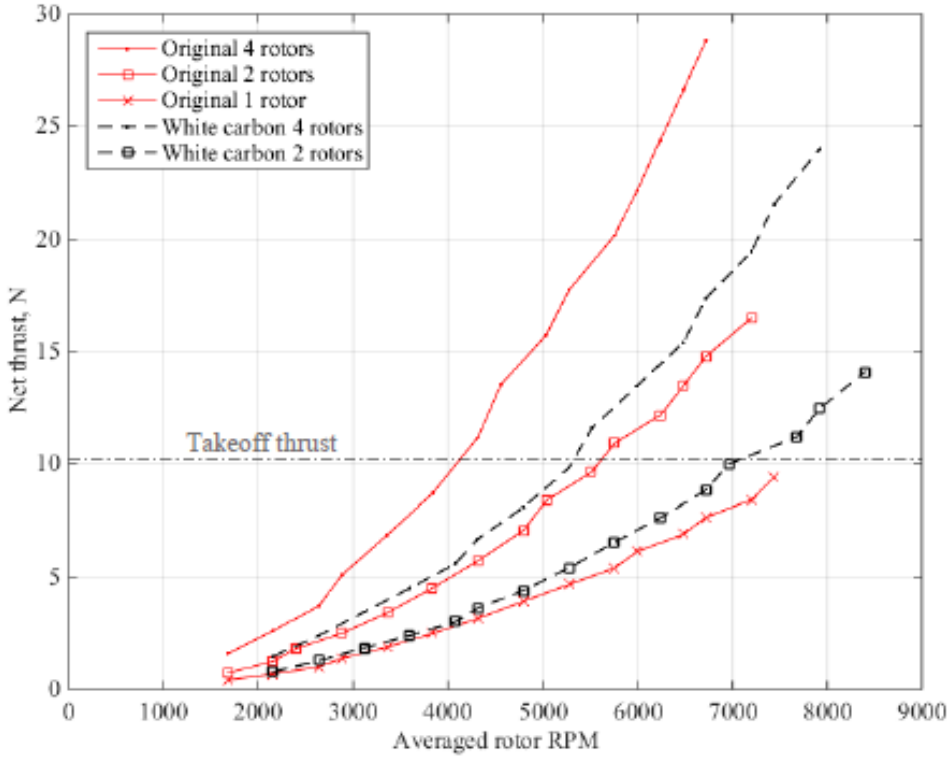

Figure 2-2: Static thrust of single and 2 rotor operation compares to 4 rotor operation for the DJI Phantom II, with Original 9450 and White Carbon propeller set [14]

The results for this study are particularly relevant for the current research due to the aircraft and propellers being comparable to the 3DR Iris+, which is the aircraft selected for the current research. This similarity will allow for a more direct comparison between the results of the studies, especially in terms of the characterization of the acoustic signature. This study was unique due to the focus being on the interaction between the multiple rotors and how it effects the aerodynamics and aeroacoustics. The findings for this effect directly aided the procedures used in the current study by providing a method for determining takeoff RPM. However, this study only considered a single microphone at static hover condition.

2.2. Rotor Noise Characterization

The purpose of the study, performed by Sinibaldi [15], was to investigate the effectiveness of a propeller design aimed at a low acoustic signature, specifically for the use on a small unmanned aerial system (sUAS). Typical propellers used on sUAS are designed with the purpose of good aerodynamic and structural properties and are considered to be noisy. This study aims to validate the design of the low noise propeller and provide a comparison between the aeroacoustic features of the low noise propeller and a conventional propeller. Two methods were employed, a numerical analysis and an experiment to replicate the numerical study. For both methods, the aerodynamic and aeroacoustic features were examined for both propeller types. The characteristics used to classify the propellers are the chord, pitch, and thickness distributions of the propeller. Both propellers were 2 bladed with a diameter of 0.6 meters.

For the analysis, two methods were employed to better understand the physics and to validate the data through means of comparison. The two methods were to develop mathematical models and perform a numerical analysis and to develop an experiment to replicate the numerical study. For numerical analysis, the model utilized the blade-elemental theory combined with the momentum theory to determine the aerodynamic loading on the propeller. For the aeroacoustic model, the harmonic noise is classically based on the analysis of the Ffowcs-Williams/Hawkings equation, however the broadband noise is based on the approach of Amiet [16], [17].

The experimental analysis concentrated on the three variables: RPM of the motor, thrust produced by the propeller, and the acoustic signature of the system. To measure the RPM, two independent external systems were used, a light emitting diode with corresponding receiver across the propeller plane and an Eagle Tree telemetry system. To measure the thrust, a three-component balance was used and evaluated the propellers in a wind tunnel of the Department of Mechanical and Aerospace Engineering of the University ‘‘La Sapienza.’’

For the acoustic measurements, 8 free field, 1/4 inch microphones were used and arranged within the chamber in varying locations with differing angular positions with respect to the

propeller plane (2D from center of propeller), and differing radius (2D and 10D). The propellers were driven by an electric brushless motor, which was mounted to a test stand. The propeller was operating in a static, simulated hover condition. All the acoustic measurements were performed within the square anechoic chamber located at the Research Centre of INAIL of Monteporzio Catone. The anechoic chamber was reported to have a low frequency cut off of 45 Hz.

It was observed that there was a satisfactory agreement for the aerodynamic thrust and the acoustic noise between the experimental and the analytical results, for both propellers. As for the directivity of the noise, it was observed that as the microphone moves toward the axial location the harmonic contribution becomes less evident, while the broadband term increases and overcomes the discrete tones, shown in Figure 2-3. This in turn causes the overall noise level to also increase. However, the conventional propeller had a different directivity pattern than the optimized propeller, which can be seen in Table 2-3. Table 2-3 shows the overall sound pressure levels (OASPL) measured for each configuration, summation of the acoustic energy from 0 Hz to 25 kHz. Lastly, the optimized propeller was verified to have a lower contribution on the overall noise of the system.

Table 2-3: Selected RPM values with corresponding parameters: OASPL (dB, unknown range) of the two systems propeller/motor at different angular positions [15]

	Thrust = 0.8 N		Thrust = 1.9 N	
Angle (degrees)	**Conventional (dB)**	**Optimized (dB)**	**Conventional (dB)**	**Optimized (dB)**
0	93.6	96.9	108	108.7
30	67.6	60	84.1	85.5
60	54.5	46.2	71.7	82.6
90	57.2	42.6	74.1	72.44

The results from this study provides a baseline in terms of the directivity of the noise but only in the roll plane of the aircraft. These results will allow for comparisons to be made with the findings of the current study, however this study only considered a single rotor-motor system rather than an entire aircraft.

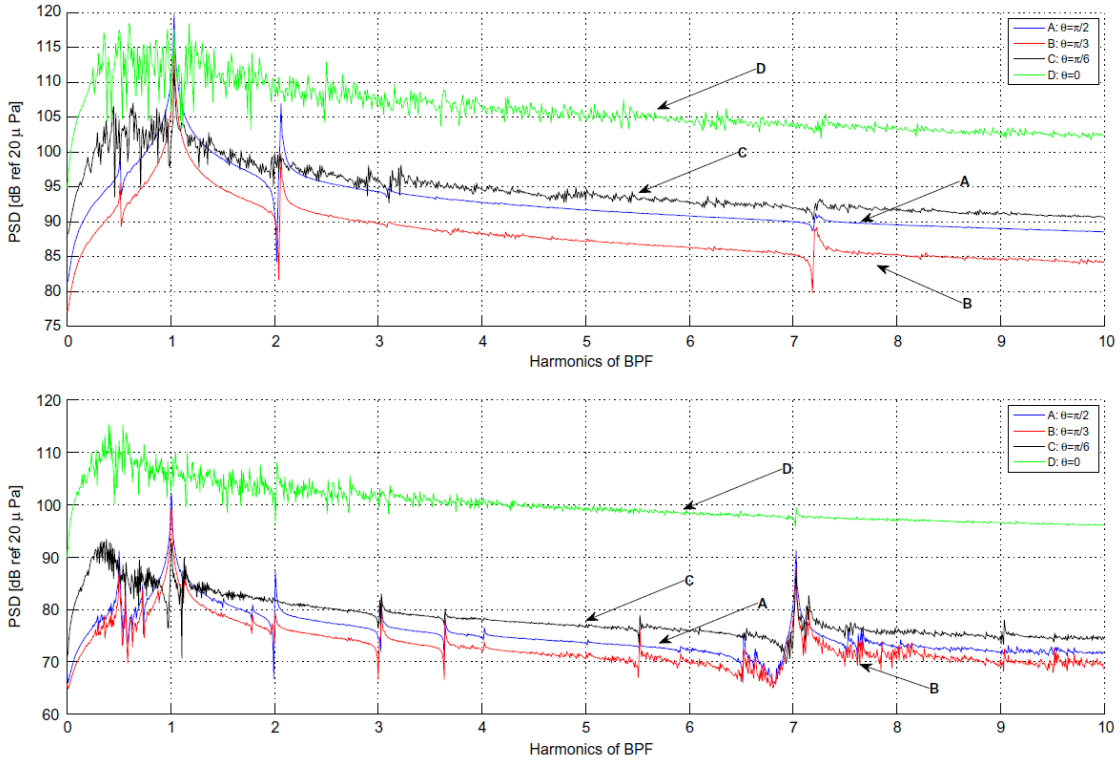

Figure 2-3: Directivity effect on the power spectral density distributions (PSD) of the propeller/motor noise produced by the conventional (top) and optimized (bottom) propellers at r = 2. T = 0.8 N, rotational frequency f = 16 Hz (top), f = 33 Hz (bottom) [15]

2.3. Further Rotor Noise Characterization & Rotor-Airframe Interaction Investigation

A study performed by Zawodny [13] focused on the acoustic and aerodynamic performance of a single rotor-motor system rather than a full sUAS system. Zawodny's study also compared the acoustic and aerodynamic performance of multiple different rotor geometries as well as a comparison to prediction software.

For this study, two different rotors were evaluated and compared, both in terms of aerodynamic and acoustic performance. These were selected based on research of common sUAS platform. The specifics for the rotor are shown in Table 2-4.

Table 2-4: Rotor parameters for Zawodny study

Rotor	Material	Diameter (in)	Weight (g)	Motor (Model)
DJI-CF rotor	Carbon Fiber	9.4	12.1	DJI (2212)
APC-SF rotor	Injection-Molded	11	15.0	3DR (2830-358)

To measure the noise of the system, five free-field microphones were arranged in an arc configuration at a radial distance of 75 inches from the motor hub. The microphones had a separation angle of 22.5 degrees, from 45 degrees below the rotor plane to 45 degrees above the rotor plane. The rotor-motor system was held by a test stand which oriented the rotor plane at 7.5 feet above the floor wedge tips of the anechoic chamber. All experiments were performed in the structural acoustic loads and transmission anechoic chamber facility at the NASA Langley Research Center. The interior dimensions for the chamber are approximately 31.6 x 25 x 15 feet, and is acoustically treated down to a cut-off frequency of 100 Hz. Only hover conditions were investigated in this study.

For the numerical prediction, either computational fluid dynamics (CFD) or blade element analysis were used for determining the aerodynamic loading. These results were used to compute the deterministic components of noise utilizing a Ffowcs Williams and Hawkings solver. The broadband noise is computed semi-analytically using the broadband acoustic rotor codes (BARC) software suite.

Zawodny observed that the spectrum for both rotors contained typical features such as a high-amplitude BPF tone, but also additional tonal content at the BPF harmonics and broadband noise, shown in Figure 2-4. Additionally, the results showed that the motor noise was a considerable contribution to the total noise and the broadband noise of the system in specific frequency bands. Zawodny also showed that as the RPM increases, so does the BPF amplitude and frequency. These results are similar to what has been presented in previous literature and will provide a strong baseline for comparison.

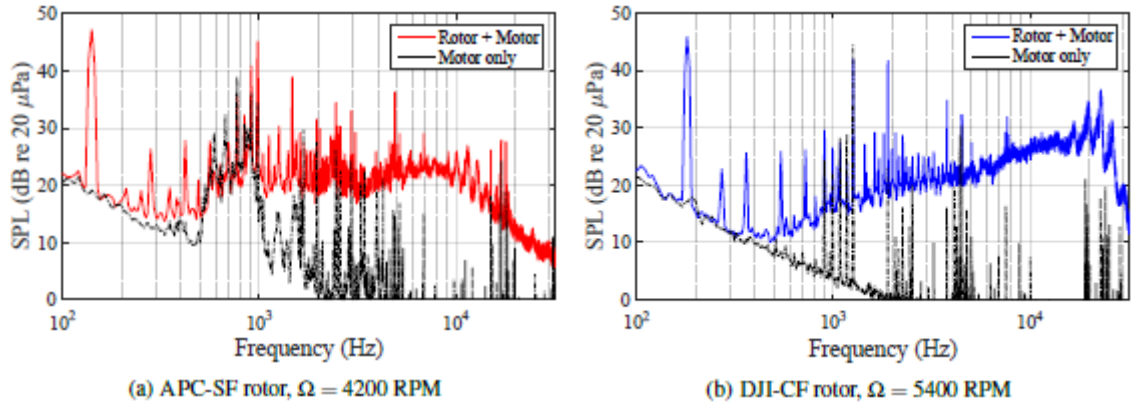

Figure 2-4: Acoustic narrowband spectral comparison of APC-SF and DJI-CF rotor-motor and motor-only configurations, at 45 degrees below the rotor plane [13]

Finally, Zawodny showed that the OASPL (100 – 20,000 Hz) increases as the angle from the rotor plane (θ) increases. These results are shown in Figure 2-5. The APC-SF rotor does not have the same pattern as the DJI-CF rotor, however at the higher RPM values the trend is present. The DJI-CF rotor most resembles the rotor that will be used in the current research, and therefore those results will be used for comparison. However, the results shown here are for a single rotor-motor system, without airframe structure. Therefore, these results may not be the most representative of the system noise.

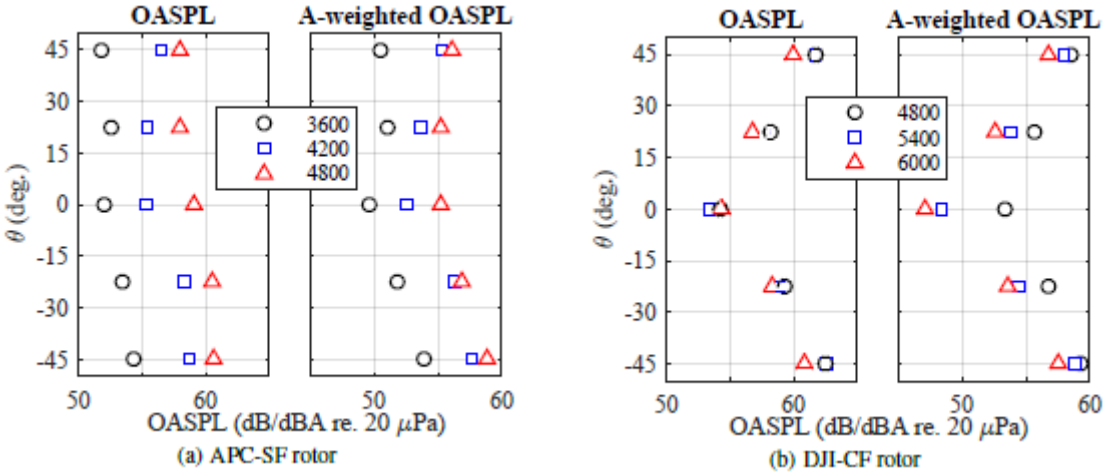

Figure 2-5: Un-weighted and A-weighted OASPL (100-20k Hz) partial directivity patterns for APC-SF and DJI-CF rotor-motor configurations [13]

Another study performed by Zawodny [18] , published at NASA workshop, focused on the acoustic performance of a single rotor-motor system but specifically on the rotor-airframe

interaction. The study considered two simple vehicle airframe configurations, such as a cone shape and a rod shape for the arm, and considered the separation distance between the rotor tip and the arm. Zawodny observed that there is a significant effect on the spectral content when the separation distance between the rotor tip and the arm is small, less than half the length of the rotor radius. For the rod shape and a separation distance less than half the length of the rotor radius, it was observed that the spectrum is harmonically rich (Figure 2-6a). For the cone shape and a separation distance less than half the length of the rotor radius, it was observed that there are variations in the BPF amplitude as the separation distance decreases, there is a faster harmonic roll-off than what was present for the rod shape, and there is more harmonic content at smaller separation distanced than what was present in the rod shape (Figure 2-6b). Finally, Zawodny also concluded that the broadband content does not change with the airframe configuration.

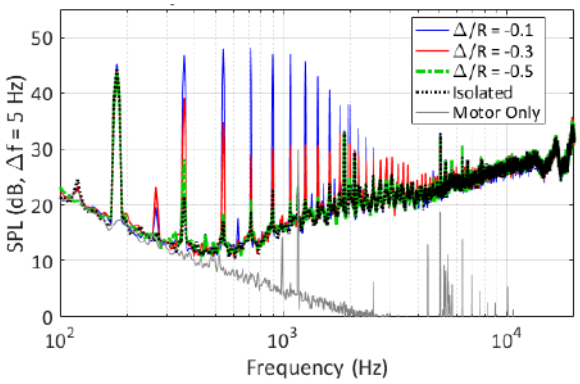

Figure 2-6a: Rotor-airframe results for rod shape airframe from Zawodny [18]

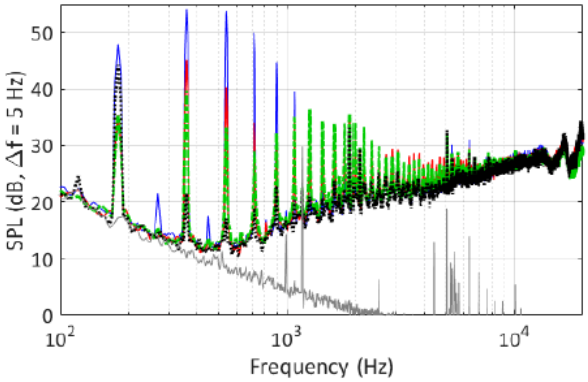

Figure 2-6b: Rotor-airframe results for cone shape airframe from Zawodny [18]

2.4. Summary of Previous Work

Going forward, the relevant results from the literature presented above when regarding the acoustic characterization of an aircraft are summarized in this section. It was shown that the signature contained typical features of rotor noise [13] [14], such as the shaft rate, BPF and harmonics, and broadband noise. The tonal noise dominated the low-mid frequencies while the broadband noise dominated the higher frequencies [14]. It was also shown that motor noise contributes to the overall noise of the aircraft [13] [14]. As for the directivity of the noise, it was

shown that as the microphone moves toward the axial location the harmonic contribution becomes less evident, while the broadband term increases [14]. Therefore, the OASPL increases as the angle from the rotor plane (θ) increases [13]. Additional tonal content, dubbed as rotor-airframe interaction noise, was present in the spectrum and considered a significant effect on the spectral content when the separation distance between the rotor tip and the arm is small [18]. The frequency location of such noise was shown to coincide with what would be harmonics of the shaft rate. Lastly, it was determined that noise increases when increasing the number of rotors as well as a decrease in aerodynamic performance due to the interaction between multiple rotors [15].

CHAPTER III

3. TECHNICAL APPROACH

Since there are many different testing setups for this study, this chapter has been structured in a way that will present the common elements found in each setup first and then further to explain the details in each respective subsection. To prevent confusion, the setups and their respective subsections have placed in an order based on the common elements.

3.1. Equipment

The aircraft used for this study was the Iris+, a quadcopter airframe developed by 3DRobotics (3DR) [19]. The Iris+ is an electric powered aircraft with an approximate weight of 3.21 lbf and length of 19.8 inches from motor-to-motor, diagonally. The aircraft is powered by an onboard 3cell, 11.1 V, LiPo battery and controlled by a 2.4 GHz radio transmitter. The aircraft was modified with the EagleTree Brushless Motor RPM Sensor V2, along with the EagleTree eLogger V4, and the EagleTree PowerPanel LCD Display. This allowed for the on-board logging and display of the motor RPM, which was used to set the RPM of all motors during tests. The aircraft also was equipped with the Pixhawk high-performance autopilot. This autopilot comes stock with two gyroscopes and accelerometers, magnetometer and a barometer. The autopilot is capable of multiple different flight modes but for this study only two are utilized: manual and loiter. A simple schematic of the 3DR Iris+ with necessary peripherals is shown in Figure 3-1.

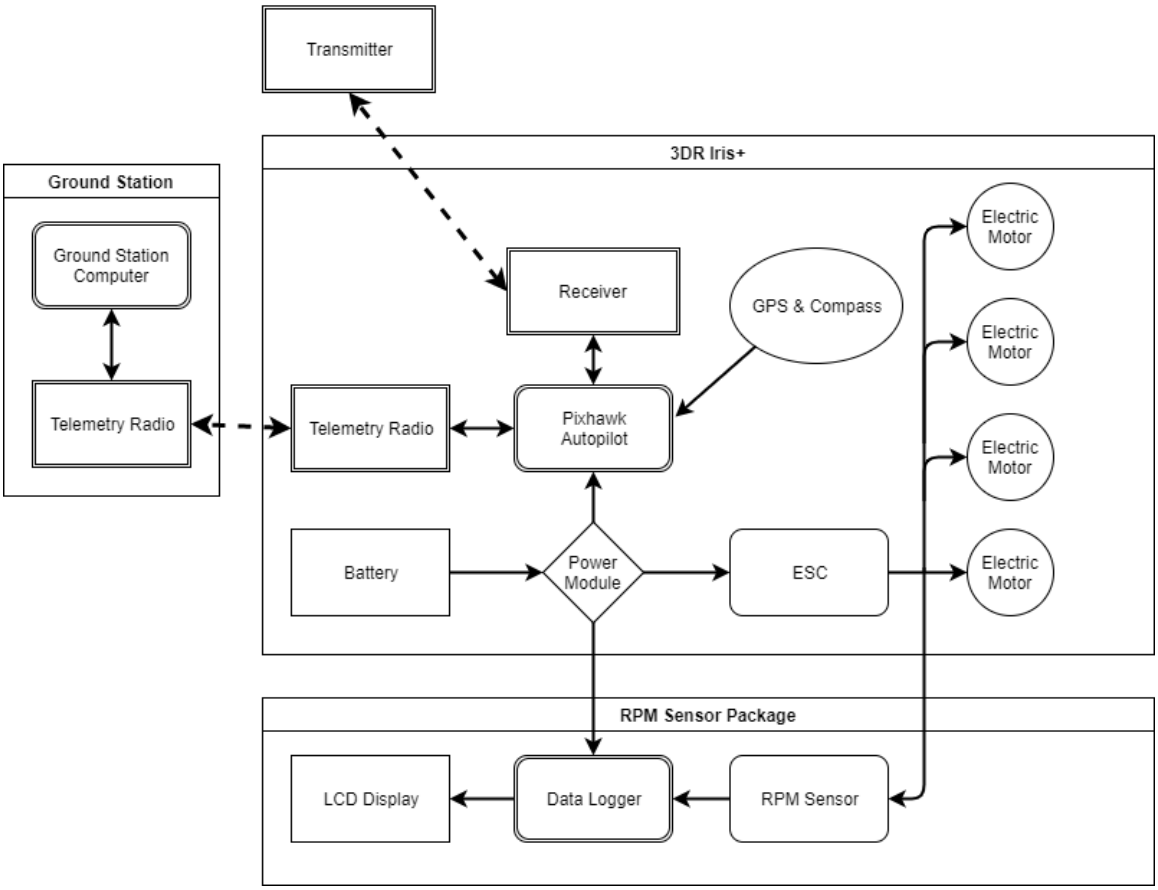

Figure 3-1: 3DR Iris+ schematic including ground station and RPM sensor modification

For all the following tests, the stock propellers were used (shown in Figure 3-2), which has a 9.5-inch diameter, 4.5-inch pitch, and is defined as a self-tightening rotor manufactured by Tiger Motor (model number: T9545-A) [20]. The airfoil for this rotor was determined empirically to be the Clark Y 11.7% smoothed [21]. The electric motors on the Iris+ have a Kv rating of 950 and was also manufactured by Tiger Motor. The stock electric motors on the Iris+ were also tested on a thrust stand to develop a baseline for the aerodynamic performance of the aircraft and to provide a validation method for future numerical analysis.

Figure 3-2: 3DR Iris+, self-tightening rotor manufactured by Tiger Motor (model number: T9545-A)

This aircraft was chosen for its availability, simple design, and open source capabilities. The aircraft was modified to allow for the control of each motor individually by terminating the signal to selected motors. The aircraft was also modified to allow for the bypass of the flight controller so that all electric motors could be controlled directly from the radio transmitter and spinning at approximately the same RPM. Figure 3-3 and Figure 3-4 show images of the modified aircraft.

Figure 3-3: 3DR Iris+ with motor selection modification

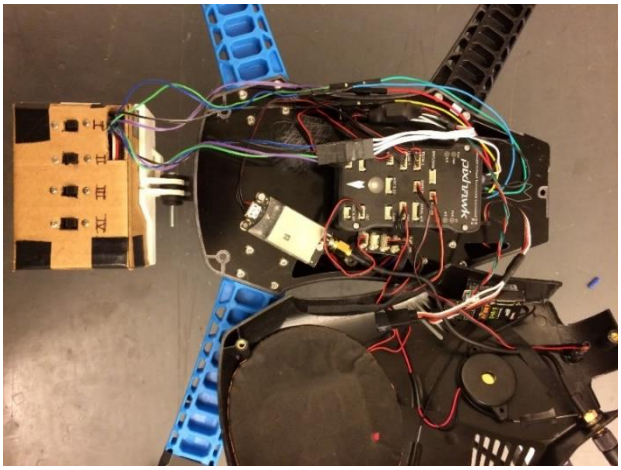

Figure 3-4: 3DR Iris+ with motor selection modification – outer case removed

The microphones used for the noise measurements were G.R.A.S. 1/2-inch prepolarized pressure microphones (Type 40AD) with an electronic noise floor of 16 dBA (OASPL) and flat response from 20 Hz to 10 kHz. Each microphone was accompanied with a G.R.A.S. 1/2-inch CCP preamplifier (Type 26CA) which has an operating frequency range from 2.5 Hz to 100 kHz. The microphones were calibrated with a G.R.A.S. Sound Calibrator type 42AB. Each microphone was

attached to a 50-foot coaxial cable (RG-6) which connected to an 8-channel National Instruments data acquisition system (PXIe-1082) that was used to convert the analog microphone signal into digital form and for Fast Fourier transform (FFT) analysis. The data was then recorded with the National Instruments SignalExpress and processed with Microsoft Excel and MATLAB.

3.2. Thrust Characterization for System

The measurement of thrust from a single rotor-motor system was used to acquire a Thrust-RPM curve which allowed for the takeoff thrust and RPM to be determined. Determining these values allowed for the creation of the testing matrix used for the static tests, described in later sections. With the baseline single rotor-motor values and the relationship discussed in Intaratep's study [14], the resultant values for the 4 rotor-motor case were determined.

The thrust stand used for these measurements was a RCbenchmark series 1520, complete with a load cell and a brushless electric motor RPM sensor, shown in Figure 3-5. The setup also included the E-flight 40-amp Lite Pro, SB Brushless electronic speed controller (ESC). The test stand was a small, desktop setup with a USB interface that allowed for the data to be logged on a PC. The thrust stand was securely mounted to reduce any vibrations when in operation. Before collecting the data, RPM measurements were conducted on the aircraft in actual flight conditions in order to gather a known limit for the system. The maximum RPM measured for this preliminary collection was 8640, while the minimum operating RPM was 1736. These were the 'soft' bounds used for the main data collection.

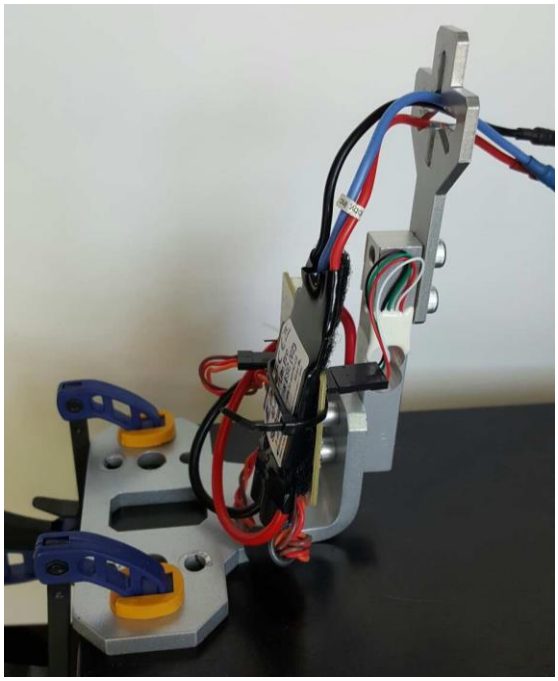

Figure 3-5: RCbenchmark series 1520 thrust stand with E-flight 40-amp Lite Pro ESC

For the main data collection, one of the stock motors from the aircraft was removed and attached to the thrust stand along with a rotor. The motor was controlled by a companion computer program for the thrust stand, which also recorded the voltage, amperage and RPM of the motor as well as the thrust of the system. For the test procedure, the motor was selected to operate at specified RPM values for approximately 30 seconds while the program collected the measured thrust values. The RPM range tested was from 1500 to 7500 with a step size of 250. To produce the Thrust-RPM curve, the RPM and corresponding thrust values were then averaged for each data set. The resulting values of this test (represented by the green line) are presented in Figure 3-6 along with the calculated multi-rotor values.

Using the single rotor dataset, the scaled multi-rotor dataset was calculated by simply multiplying the thrust values by the number of rotors (which was 4 for this aircraft). This was considered the ideal case, without losses, and is represented by the blue line in Figure 3-6. From the scaled multi-rotor dataset, the actual multi-rotor dataset, with losses, was calculated by using the relationship discussed in Intaratep's study [14], represented by the orange line in Figure 3-6.

The precision and bias uncertainties for the RPM and thrust measurements were found to be negligible, where both values were below 1%.

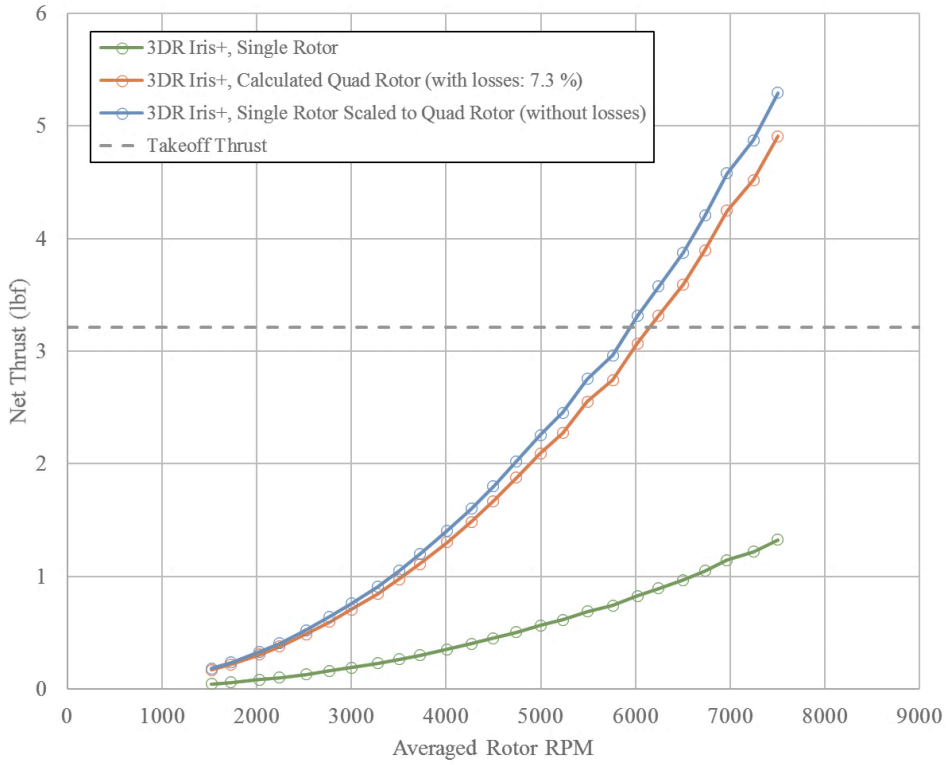

Figure 3-6: Static thrust of single rotor, scaled quad rotor, and actual quad rotor for the 3DR Iris+

3.3. Testing Environment

Three different environments were considered for all measurements discussed in the following sections, the OSU anechoic chamber, OSU Gallagher-Iba Arena (GIA) and the OSU Unmanned Aircraft Flight Station (UAFS). The OSU anechoic chamber dimensions are approximately 276 x 204 x 108 inches, from tip to tip of the foam wedges. The width of the foam wedges is 7.5 inches with a height of 12 inches. The chamber was previously tested to be anechoic at a frequency range of 250 Hz and higher. The purpose for this testing environment is to simulate “free field" conditions, where free field is referring to there being no reflected acoustic waves. This environment will also allow for the microphones to be isolated from external noises at frequencies above the low-frequency cut-off value as well as typical weather effects such as wind and

temperature changes. Figure 3-7 shown an image of the 3DR Iris+ within the anechoic chamber with a microphone array.

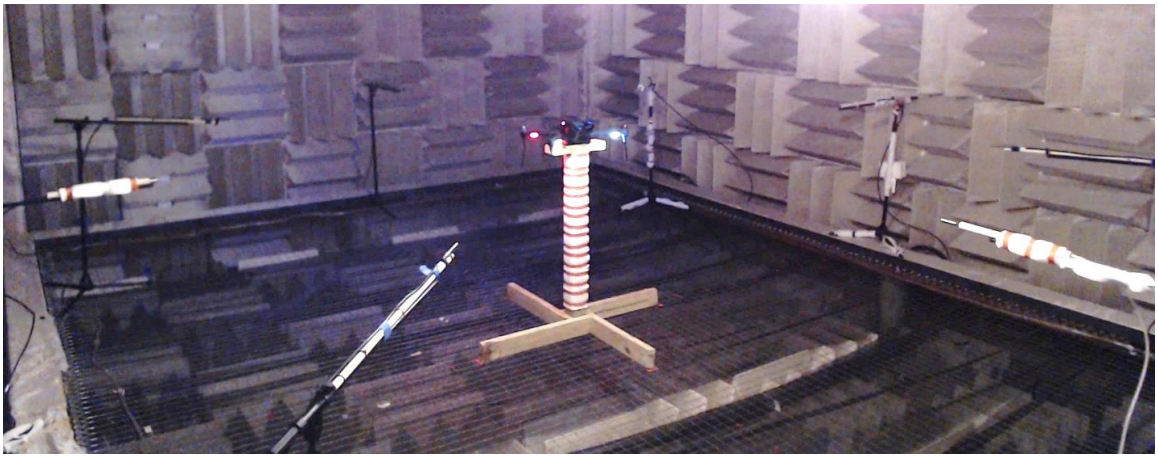

Figure 3-7: Anechoic chamber environment with Static, Rotor Plane Microphone Array, Hard Mount test setup at 7.6D and 3DR Iris+

The OSU GIA is the basketball arena on the OSU campus. The measurements were taken inside the arena, on the basketball court, and outside of operational hours. The exact dimensions of the arena are unclear but it can seat a total of 13,611 attendees with a ceiling approximately 120 feet high and has the standard NCAA men's college court size of 50 x 94 feet. The aircraft was located in the center of the court, with the microphone array positioned around it, as seen in Figure 3-8. The distance from the closest microphone to the seating area was approximately 18 feet. This environment was selected due to large amount of space, which was required for the hover measurements. However, the aircraft was unable to receive a GPS signal so it warranted the tether system. Also, there was a high amount of background noise due to the lighting, which was unable to be powered off.

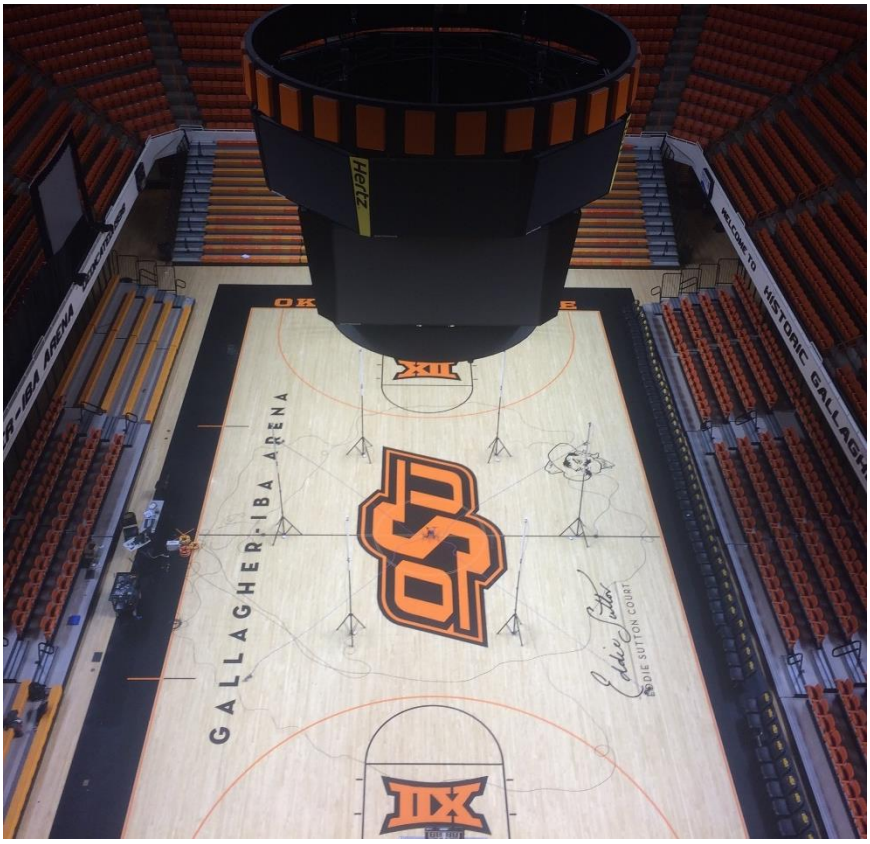

Figure 3-8: OSU Gallagher-Iba Arena with Hover, Rotor Plane Microphone Array test setup

The other environment utilized for the static measurements is the OSU UAFS, which is a test facility located 12 miles East of Stillwater, Oklahoma. The facility consists of two runways, an aircraft hangar, a control room, and a long pavilion, as shown in Figure 3-9. The surrounding area is mainly farm and pasture land with a low trafficked dirt road west of the main runway and buildings. The specific area used at the facility during the tests was between the southmost building and the main runway, approximately 50 feet from the building. In order to reduce unwanted external noise, all tests were performed at night between the times of 11 PM and 5 AM. During this time frame the weather is also typically calm with reduced wind speeds. The specific wind speeds for each test will be included along with the corresponding results and can be seen in

Table 6-1 in the Chapter 7, The Appendices. Figure 3-10 shows an image of the 3DR Iris+ being tested in hover flight at the OSU UAFS with a microphone array.

Figure 3-9: Oklahoma State University Unmanned Aircraft Flight Station [22]

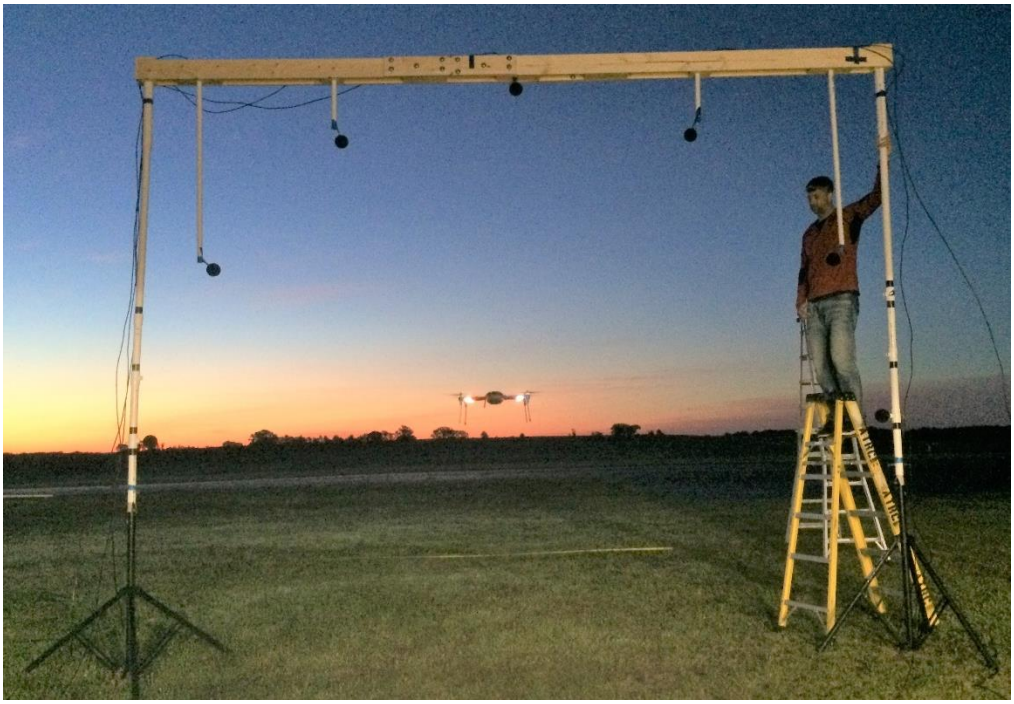

Figure 3-10: UAFS environment with microphone array test setup at 10D and 3DR Iris+

3.4. Static Acoustic Tests

To characterize the acoustic signature of the selected aircraft, the current study considered both static and hover measurements. The static measurements were performed with the aircraft

mounted to a test stand while the hover measurements were performed with the aircraft hovering under its own weight or with a tether system attached. The static measurements best represent the hover condition and will serve as the ideal case for the identification of the features within the acoustic signature. All measurements for the static tests were conducted on a stationary aircraft, fully fixed to a test stand. The aircraft was leveled with all rotors supplying directly vertical lift, relative to the aircraft. This section will focus on the static measurements and their setup, therefore the hover measurements are covered in more detail in later sections.

For the static measurements, multiple control parameters were considered and varied, such as the rotor RPM, the motor configurations, the microphone array, the test stand mount techniques, and the testing environment. As outlined earlier, these parameters were selected in order to characterize the effects on the acoustic signature due to the change in rotor RPM, the interaction between multiple rotors, recirculation and/or vibrations, and environment as well as to explore the directivity of the noise. When varying the RPM of the motor, the standard RPM values selected for this study are as follows: 5000 RPM ±120, 6900 RPM ±120, 7900 RPM ±120. These values were determined from the Thrust-RPM curve (Figure 3-6) and the takeoff weight of the aircraft. The RPM values were selected to represent the different phases of flight: descend, hover, climb/accelerate. Table 3-1 shows the selected operating conditions and the corresponding parameters.

Table 3-1: Selected RPM values with corresponding parameters

Throttle	BPF (Hz)	RPM	Tip Speed (ft/sec)	Mach # (Tip)	Re # (0.75R)	Thrust (lbf)
50%	168	5040	209	0.19	52000	2.2
75%	226	6780	282	0.25	70000	4.0
100%	262	7860	324	0.29	81000	5.5

When operating the aircraft for the static tests, the flight controller was bypassed so that all electric motors could be controlled directly, allowing for the motors to be spinning at approximately the same RPM. The main configurations of the motors for all static tests were loaded (with rotor)

and unloaded (motor only). The purpose of this was to be able to determine the effect the electric motor has on the overall system noise.

Two microphone arrays were considered for the static measurements: an array in the rotor plane and an array in the roll plane of the aircraft. The rotor plane is the specific plane in which the rotors are rotating (which is parallel to the yaw plane of the aircraft, but not coincident) and the roll plane is the plane in which the aircraft would perform the roll maneuver. For reference, Figure 3-11 shows an image displaying the planes of interest and their respective terminology, with respect to the aircraft. The descriptions of each setup will be further explained in their respective sections. The purpose of this was to characterize the directivity of the noise in both planes, with the hopes to develop a three-dimensional representation of the directivity.

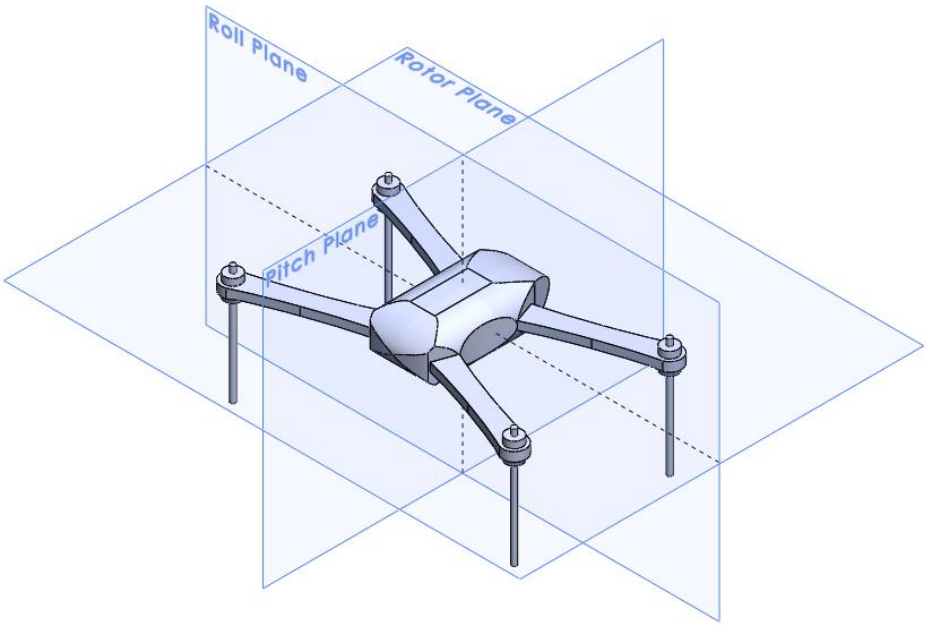

Figure 3-11: Geometric planes of interest

6.4.1. Static, Rotor Plane Microphone Array

For the following test setups, multiple microphones are located either directly within the rotor plane or slightly below the rotor plane (approximately 8 degrees). The purpose of this setup was to be able to examine the directivity of the noise in the rotor plane.

Two different aircraft mounting techniques were considered for the static measurements conducted in the rotor plane, a ‘soft mount’ and a ‘hard mount.’ The purpose for this was to explore the effect of vibrations on the acoustic signature when mounting the aircraft. The results of this specific test will hopefully shed light on the best method to mount the aircraft for static measurements.

Each mounting technique shared a common goal but also had individual goals. Both setups explored the effects due to the rotor RPM and motor noise. However, the ‘soft mount’ also explored the effects due to the interaction of multiple rotors, and tested the assumption of the Inverse-Square Law within the anechoic chamber at Oklahoma State University (OSU). Similarly, the ‘hard mount’ explored the effects due to recirculation and testing environment. This division was created due to the findings with the mounting technique. All tests performed with this microphone array setup was within the anechoic chamber and at the UAFS.

3.4.1.1. *Soft Mount Testing*

The mounting technique was designed to be a quick and simple mount that would allow for the aircraft to be mounted level without any potential obstructions. The aircraft sits in a small indention on a flat piece of wood covered with foam. The foam provides a small amount dampening for the aircraft and slightly helps prevent reflections of the acoustic waves. The aircraft is held in place with strong plastic zip-ties that weave though the arms and into the wood plate. The excess plastic on the end of the zip-ties were removed. The mount can be seen with the aircraft attached in Figure 3-12.

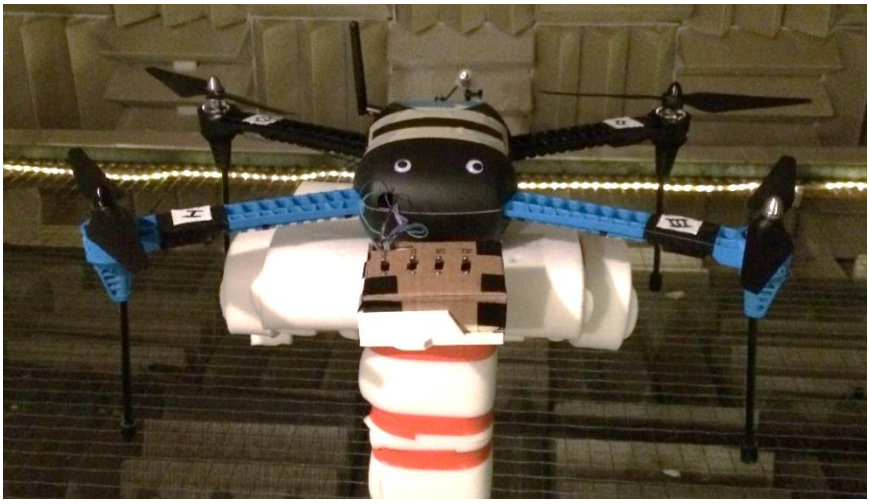

Figure 3-12: Soft Mount with attached 3DR Iris+ within Anechoic Chamber

For the testing setup, eight microphones were arranged in a circular array with the quadrotor located directly in the middle. Microphones were positioned at a radius of approximately 7.6D (72 inches) and 8.9D (84 inches) from the center of the quadrotor, where D is the diameter of each rotor. These radius values were selected due to the limitation of space within the anechoic chamber at OSU. A radius of 10D would have been preferred based on the conclusion presented by Ahuja [23]. The results from Ahuja showed that distances of 10D or greater are required to assure measurements are in the geometric far field. The microphone arrangement is presented in Figure 3-13 and Figure 3-14, where the distance value noted in Figure 3-14 is relative to the simulated floor of the testing environment.

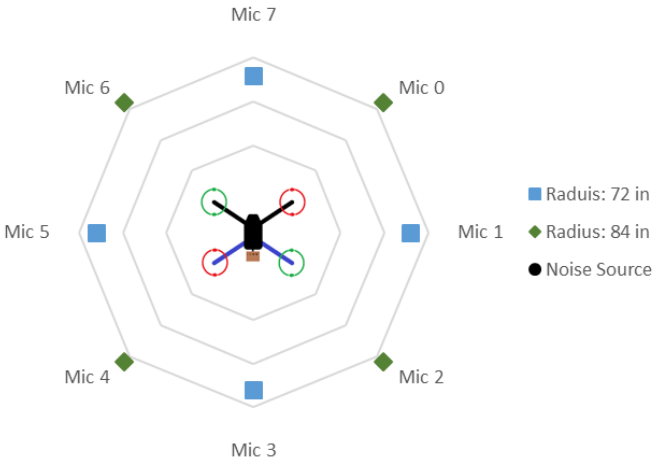

Figure 3-13: Microphone location for Static, Rotor Plane MicrophoneArray, Soft Mount test - Top view

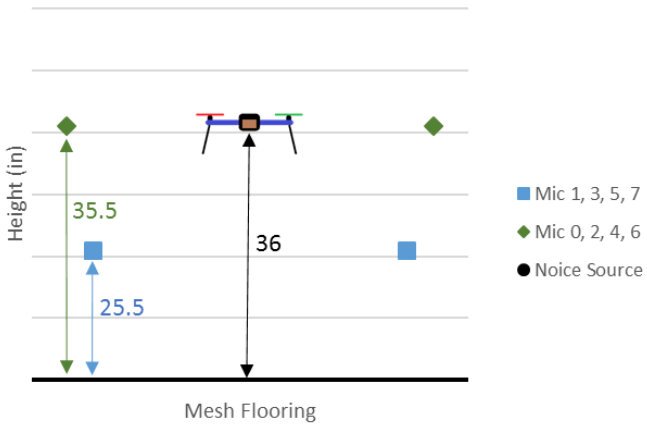

Figure 3-14: Microphone location for Static, Rotor Plane Microphone Array, Soft Mount test - Side view

The procedure focused on the investigation of the effects due to the interaction of multiple rotors. This was selected due to the requirement of the motors to be toggled between active and inactive. The measurements for this setup can be broken down into six groups with each group representing a different combination of active rotors. Paired with each these is a companion measurement that had just the motors operating without any rotors attached. The purpose of this was to see an effect of the motor noise on the overall noise of the system, if present. Table 3-2 and Figure 3-15 show the various configurations tested along with a schematic of which rotor combinations were used. Note that configurations 3 and 4 were tested to see if the rotation direction had any effect on the acoustic signature. Each configuration was tested at the three different throttle settings: 50% (5000 RPM ±120), 75% (6900 RPM ±120), and 100% (7900 RPM ±120).

Table 3-2: Varying Rotor-Motor Configurations

Configuration	Active Rotor
1a	I, II, III, IV
1b	I, II, III, IV (Motor Only)
2a	I, II, III
2b	I, II, III (Motor Only)
3a	I, II
3b	I, II (Motor Only)
4a	I, III
4b	I, III (Motor Only)
5a	I
5b	I (Motor Only)
6a	IV
6b	IV (Motor Only)

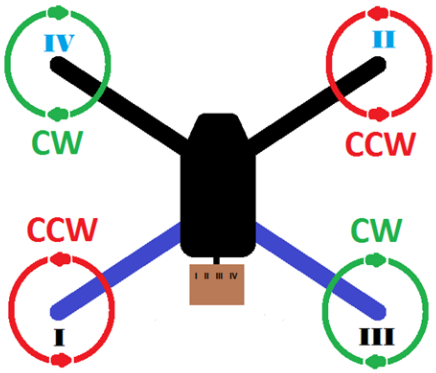

Figure 3-15: Electric Motor Location Convention

For selected measurements, microphones 1 and 5 were moved at different radii from the quadcopter center (see Figure 3-16). This was done to test the assumption of the Inverse-Square Law. The microphones were placed at a distance of 24, 40, 56 and 72 inches from the noise source. Each measurement was with a throttle setting of 100% (7900 RPM ±120) and had a foam windscreen attached to the microphone. G.R.A.S AM0069 foam windscreens were used to reduce the effect of possible recirculation of the propeller wash in the chamber.

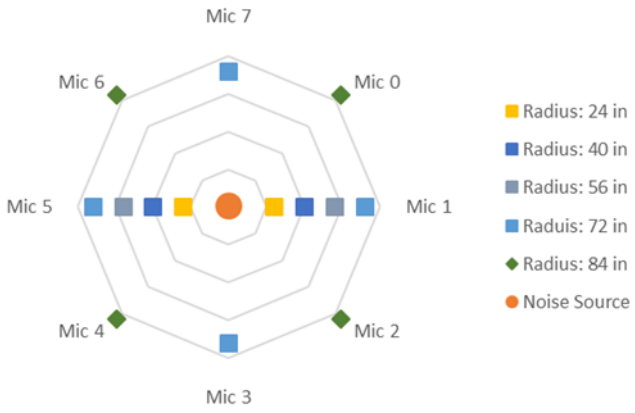

Figure 3-16: Microphone location Static, Rotor Plane Microphone Array, Soft Mount test - Top view

3.4.1.2. *Hard Mount Testing*

The mounting technique for this testing setup used the same test stand as the 'soft mount', however, the focus was to firmly secure the aircraft fuselage to the stand. This design traded the quick and easy, attach and remove feature of the 'soft mount' for a rigid clamp design, as shown in Figure 3-17 and Figure 3-18. The clamp design was created in the 2016 SOLIDWORKS 3D computer aided design (CAD) software package. The dimensions for the internal section of clamp are taken directly from the aircraft fuselage dimensions and are modeled for an exact fit. The mount was 3D printed with a Formlabs, Form 2 3D printer using the Formlabs Tough, Photopolymer Resin. The mount was attached directly to the test stand, via wood screws, in place of the wood plate used in the 'soft mount'.

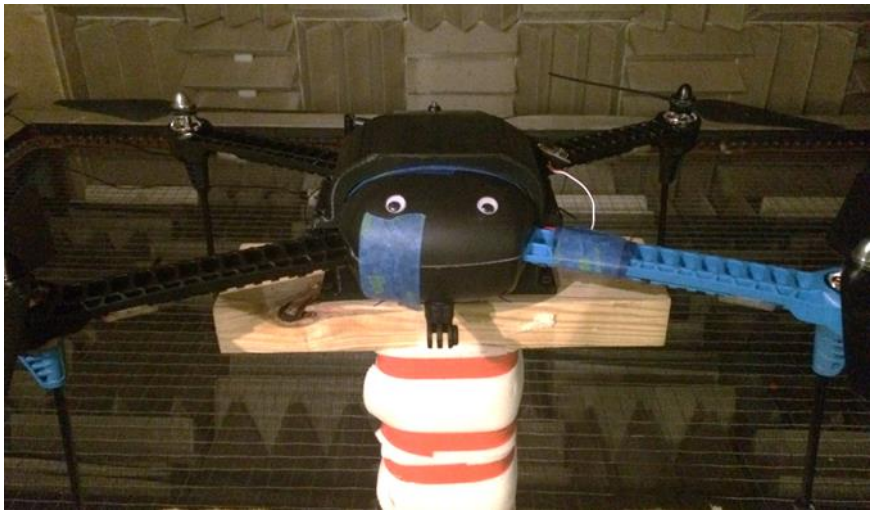

Figure 3-17: Hard Mount with attached 3DR Iris+ within Anechoic Chamber

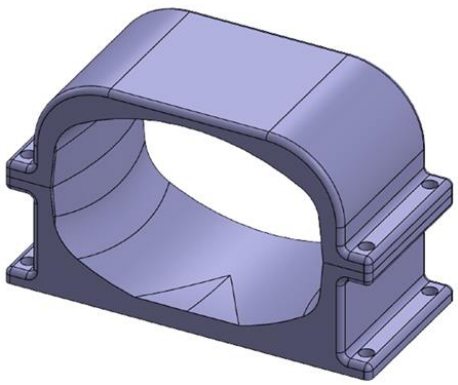

Figure 3-18: Hard Mount 3D CAD image from 2016 SOLIDWORKS

For this test setup, eight microphones were used and arranged in a circular array, with a radius of approximately 7.6D (72 inches) and again at 10D (95 inches) from the center of the quadrotor. The 7.6D radius was selected due to the limitation of space in the anechoic chamber used. The 10D radius was selected to assure measurements are in the geometric far field. Each microphone was held by a stand at 40 inches above the floor. The test stand was located in the center of the array, which oriented the aircraft to have the rotor plane also 40 inches above the floor. The microphone arrangement is presented in Figure 3-19 and Figure 3-20, where the distance value noted in Figure 3-20 is relative to the simulated floor of the testing environment.

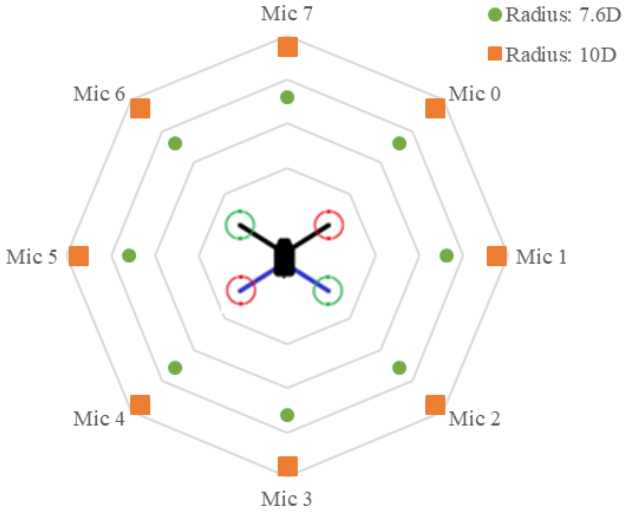

Figure 3-19: Microphone location for Static, Rotor Plane Microphone Array, Hard Mount test - top view

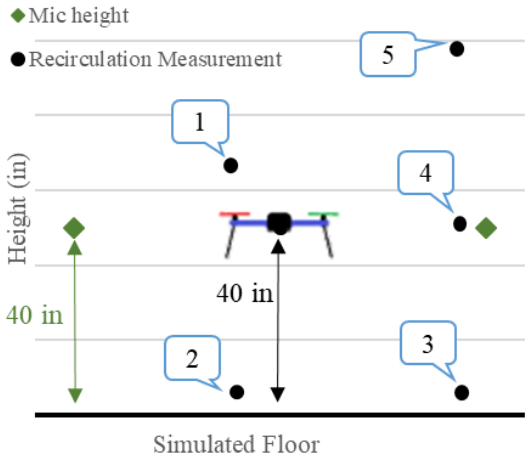

Figure 3-20: Microphone location for Static, Rotor Plane Microphone Array, Hard Mount - side view, with recirculation measurement locations

The measurements for this setup considered all four rotors active with a companion measurement that had just the motors operating without any rotors attached. Each configuration was tested at the three different throttle settings: 50% (5000 RPM ±120), 75% (6900 RPM ±120), and 100% (7900 RPM ±120).

Recirculation measurements were also performed with an Omega HHF5000 Digital anemometer, to detect the level of recirculation as this might affect the noise produced by the rotor. The measurements were taken with an Omega HHF500 digital anemometer. Figure 5, shows the

locations where each measurement was taken. For the locations 1 & 2, the measurements were taken radially, above and below each rotor. For the locations 3 – 5, the measurements were taken radially, at every microphone placement. This recirculation measurement procedure was used with the setup previously described and a modified version with large foam sheets placed under the test stand, shown in Figure 3-21. This was done in order to promote the occurrence of recirculation without introducing any unwanted reflections. All recirculation tests were performed only at 100% Throttle (7900 RPM ±120).

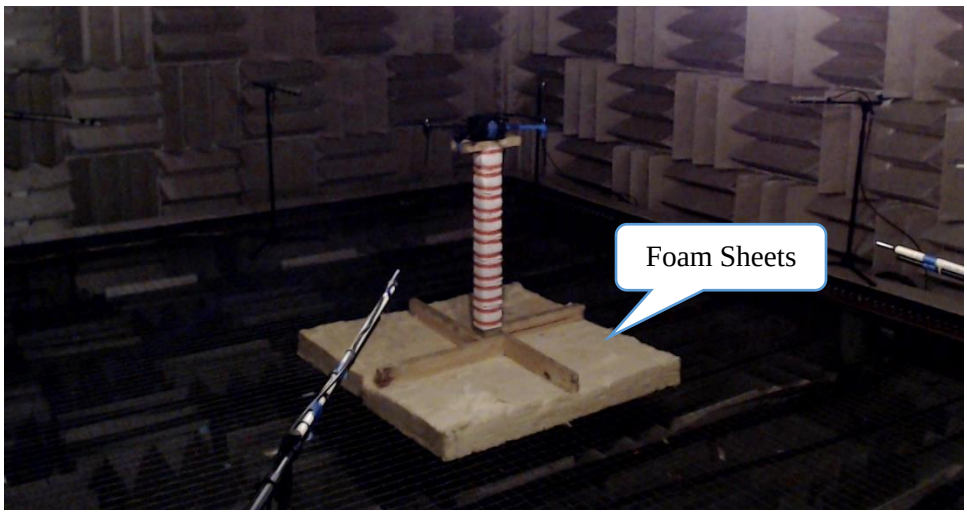

Figure 3-21: Recirculation measurements test with foam sheets

6.4.2. Static, Roll Plane Microphone Array

For the following test setup, multiple microphones are located directly within the roll plane of the aircraft. The purpose of this setup was to be able to examine the directivity of the system noise in the roll plane. Seven microphones were arranged in a semicircular array with a radius of approximately 10D (95 inches) and a radial separation of approximately 30 degrees, as shown in Figure 3-22. The aircraft was mounted to a test stand, using the custom 3D printed mounting technique discussed above. The rotor plane of the aircraft was approximately 40 inches above the ground, while the microphone plane was approximately 60 inches above the ground. This resulted in larger angle between the microphone locations and the rotor plane, as shown in Figure 3-23.

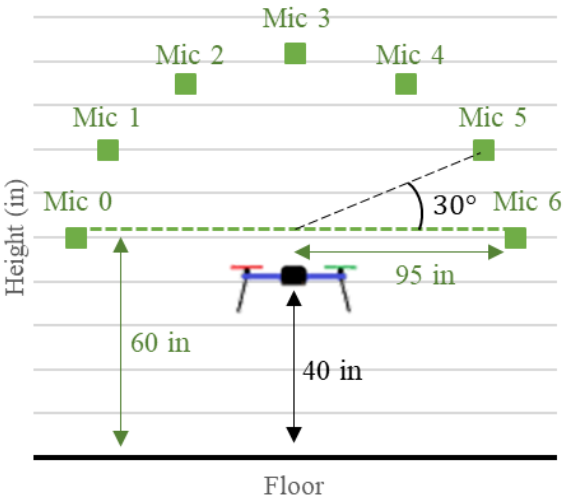

Figure 3-22: Microphone location for Static, Roll Plane Microphone Array test

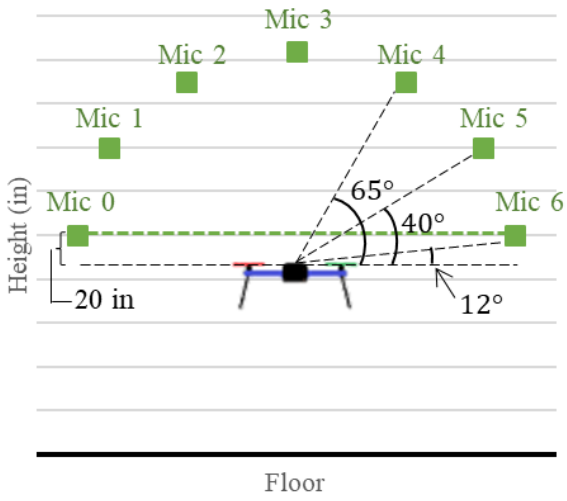

Figure 3-23: Equivalent angle between microphone and rotor plane due to aircraft height offset for Static, Roll Plane Microphone Array test

The microphone array was held in place by a large arc structure specifically designed for this setup, shown in Figure 3-24. The arc structure had seven ports for the microphones to be mounted, five of which were hanging and two were integrated into the supporting legs of the arc. The hanging microphones were rigidly attached to the arc structure through PVC piping and therefore were not left free floating. Each microphone was also equipped with a G.R.A.S AM0069 foam windscreen to assist in preventing unwanted pressure variations due to the wind, near the diaphragm. The measurements for this setup considered all four rotors active, but only tested at 100% Throttle (7900 RPM ±120). All tests performed with this microphone array setup was at the UAFS.

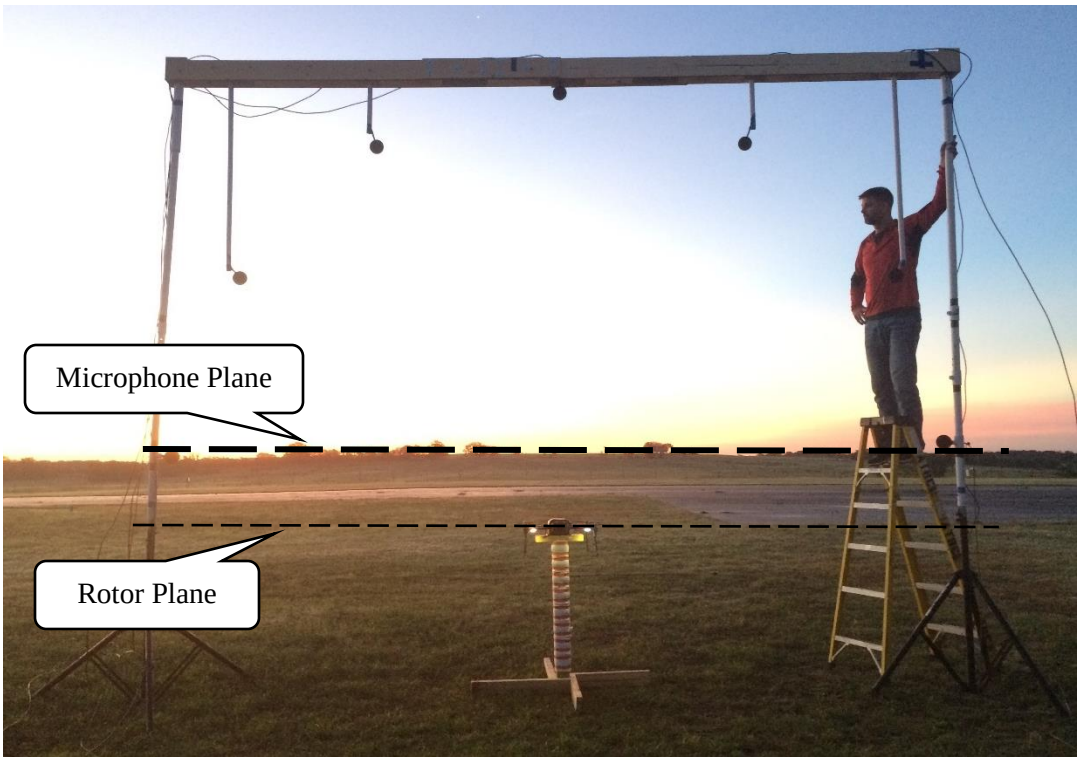

Figure 3-24: UAFS environment with Static, Roll Plane Microphone Array test setup at 10D and 3DR Iris+

3.5. Hover Acoustic Tests

To reiterate, the static measurements were performed with the aircraft mounted to a test stand while the hover measurements were performed with the aircraft hovering under its own weight or with a tether system attached. Another important difference between the static and hover tests is the onboard autopilot is now in control of the aircraft. This means the autopilot controls the motor RPM, which it varies in order to keep the aircraft level and stable, therefore the spectra will most likely have more tonal content due to the motors operating at different RPMs. There were no flyover measurements, rather only stationary measurements where the aircraft would hover at a specified location. The purpose for this was to allow for comparison between the static measurements and the hover measurements without having to consider more complexities like Doppler effect. The static measurements were designed to be a representation of what would be measured in an actual hover condition and therefore these hover measurements will allow for an assessment of this assumption.

For the hover measurements, there were less control parameters than what were discussed for the static measurements. The control parameters were the microphone array and the testing environment. The main goal of the hover measurements was to further explore the directivity of the noise above and below the rotor plane, while also collecting data of real world operations of the aircraft. To explore the directivity two microphone arrays were considered, an array in the rotor plane and an array in the roll plane of the aircraft. These arrays were set up similar to the static measurements with adjustments made to allow for the flight of the aircraft.

6.5.1. Hover, Rotor Plane Microphone Array

For this test, six microphones were used and arranged in a circular array with the aircraft operating in the middle. The microphones were positioned on large microphone stands at a radius of 20D (190 inches) from the center of the aircraft with approximately 60 degrees separating each microphone radially. The large microphone stands were used to allow the height of the microphone to be changed. The large radius was selected to assure that the measurements were in the geometric far field but also to allow for some distance between the aircraft and the microphones to reduce any potential risk of collision. The microphone arrangement is presented in Figure 3-25 and Figure 3-26, where the distance value noted in Figure 3-26 is relative to the simulated floor of the testing environment.

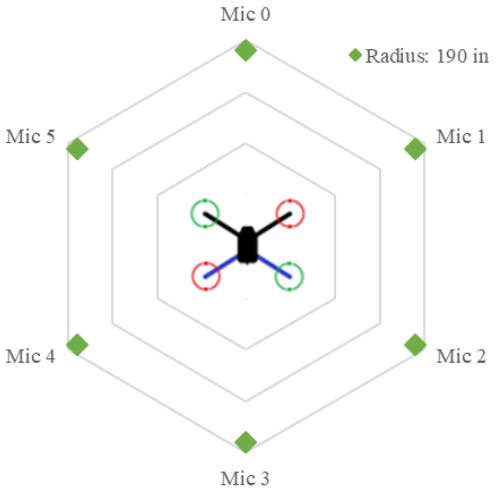

Figure 3-25: Microphone location for Hover, Rotor Plane Microphone Array test - top view

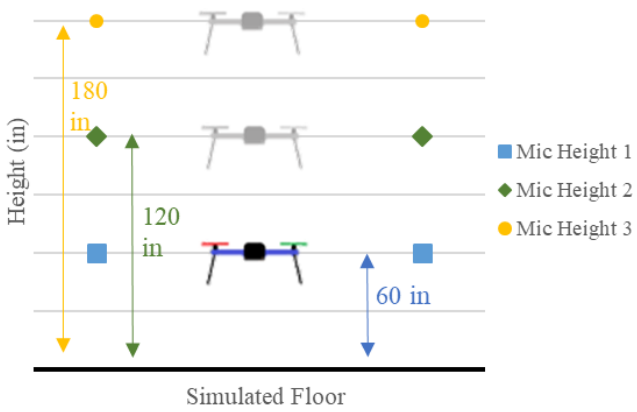

Figure 3-26: Microphone location for Hover, Rotor Plane Microphone Array - side view

The main purpose of this test setup is to further investigate the directivity of the noise generated by the aircraft. The parameters being varied are the microphone height (60, 120, 180 inches), aircraft altitude (60, 120, 180 inches), and the method of control (tethered or GPS hold). The procedure for the testing was as follows: the microphone height would be set and held constant while the aircraft would hover at a specified altitude and location for the duration of the measurement (30 seconds), then the aircraft would change its altitude where a new measurement would be taken, then finally the aircraft would change its altitude again for the last measurement. Once that set of measurements was completed the microphone height would be changed and the measurements would be repeated. In total, there will be nine measurements per control method, one for each height variation. The combination of each height measurement creates an effective microphone placement of in rotor-plane and approximately $\theta = 17.5^{\circ}$ and $\theta = 32.3^{\circ}$ above and below the rotor plane. The effective microphone locations, with respect to the aircraft, are presented in Figure 3-27.

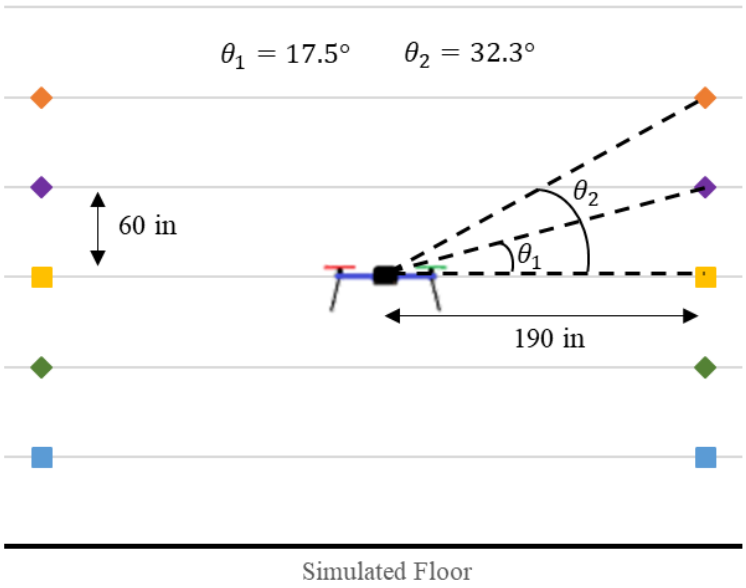

Figure 3-27: Effective microphone location Microphone location for Hover, Rotor Plane Microphone Array test - side view

The two control methods used for this test were, tethered and GPS hold. For the tethered condition, the aircraft was attached to a tether system that consisted of four separate weights (10 pound dumbbells) on the ground connected to the aircraft via 1/3-inch nylon rope. The rope was then attached to a custom mount on each arm of the aircraft, furthest inboard next to the fuselage. The purpose of the tether control method was to hold the aircraft position in a GPS denied environment. A photo of the tether system and the rope mounts are presented in Figure 3-28 and Figure 3-29.

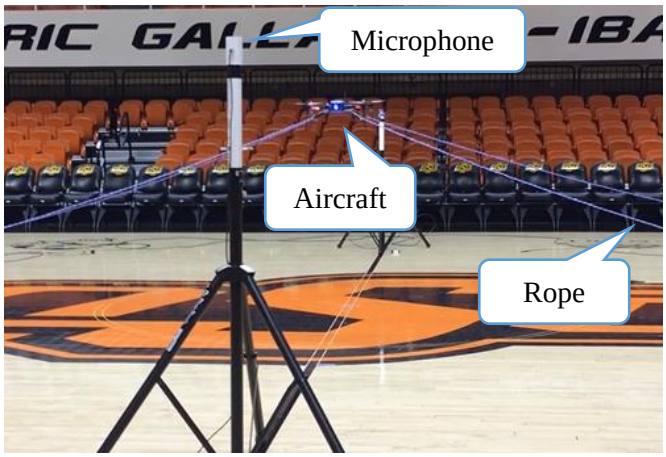

Figure 3-28: Tether system setup at OSU GIA with 3DR Iris+ in flight

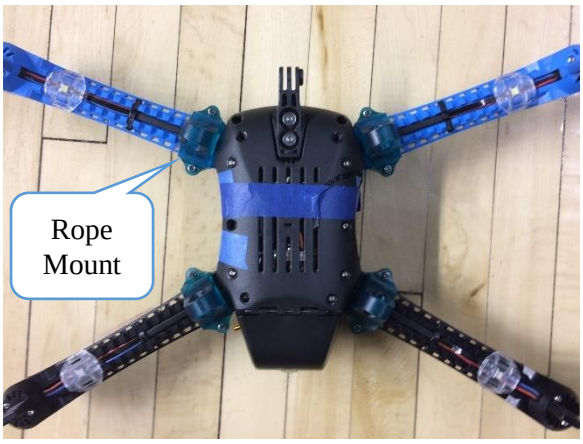

Figure 3-29: Location of rope mounts attached to 3DR Iris+ for tether system setup

The GPS hold condition was flown without the tether and relied solely on the on-board flight controller. For this control method, the aircraft operated in an environment with access to a GPS signal in which it would normally use to assist in holding its position. The test setup with the tether system attached and microphones at the maximum height of 180 inches, inside the OSU Gallagher-Iba Arena (GIA), is shown in Figure 3-30. All tests performed with this microphone array setup was within the GIA and at the UAFS.

Figure 3-30: OSU Gallagher-Iba Arena environment with Hover, Rotor Plane Microphone Array test setup, including tether, at 20D and 3DR Iris+

6.5.2. Hover, Roll Plane, Microphone Array

This setup utilizes the same equipment as the setup described in Section 3.6.4.2 with some differences. The purpose is also the same, to explore the directivity, but now adapted for hover measurements. The microphone placement and the structure holding them are identical between the two setups. The differences are in the operation of the aircraft and the testing procedure. For this test, the aircraft was flown rather than mounted to a test stand. The aircraft would hover at an altitude of 60 inches, which would orientate the rotor plane coincident with the microphone plane. Similar to the *Hover, Rotor Plane, Microphone Array* test procedure, the aircraft would hover at a specified altitude and location for the duration of the measurement (30 seconds). However, this procedure did not consider different altitudes for the aircraft or different heights for the microphones. Also, this setup did not consider multiple control methods and only focused on the GPS hold method. The microphone locations, with respect to the aircraft, are presented in Figure 3-31. All tests performed with this microphone array setup was at the UAFS.

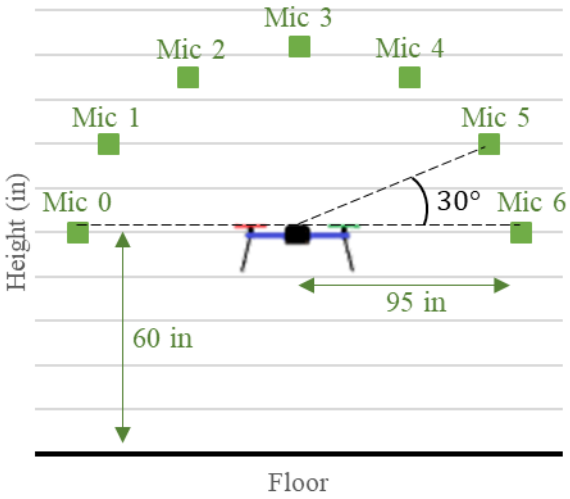

Figure 3-31: Microphone location for Hover, Roll Plane Microphone Array test

Reference Table 3-3 for a summary of all the different testing setups and configurations covered in this chapter.

Table 3-3: Testing setups and configurations considered

Setup	Control Type	Microphone Array	Environment
Static	Soft Mount	Rotor	Anechoic Chamber
Static	Hard Mount	Rotor	Anechoic Chamber
Static	Hard Mount	Rotor	UAFS
Static	Hard Mount	Roll	UAFS
Hover	Tether	Rotor	GIA
Hover	Tether	Rotor	UAFS
Hover	GPS hold	Rotor	UAFS
Hover	GPS hold	Roll	UAFS

3.6. Uncertainty Analysis

To analyze the uncertainty of the measurements for the narrowband data two methods were employed: precision uncertainty analysis and bias uncertainty analysis. Precision uncertainty is the random components typically involved with the repeatability of the measurement and parameters outside of control such as atmospheric conditions. Bias uncertainty is the systematic component involved with the resolution of the equipment used for the measurement. The precision uncertainty was determined by calculating the standard deviation (σ) of three different measurements, taken at three different times under the same conditions. The equation for the standard deviation is provided in Equation 1.

$$\sigma = \sqrt{\frac{1}{N}\sum_{i=1}^{N}(x_i - \mu)^2} \qquad (1)$$

Where σ is the standard deviation, N is the number of samples, x_i is the specific value in data set, and μ is the mean of the data set. The calculation for standard deviation was performed on each set of SPL values over the entire frequency spectrum. The step by step breakdown of this process is as follows:

- μ: the mean of the SPLs at each frequency value across the different measurements
- $(x_i - \mu)^2$: for each SPL value, subtract the mean and square the result

- $\frac{1}{N}\sum_{i=1}^{N}(x_i - \mu)^2$: determine the mean of the squared differences, also known as the variance
- $\sqrt{\frac{1}{N}\sum_{i=1}^{N}(x_i - \mu)^2}$: square root of the variance, which is the standard deviation

This resulted in a standard deviation spectrum that was then added to the narrowband data to obtain maximum and minimum uncertainty bounds. The bias uncertainty was determined by calculating the total bias value based off the uncertainty values of each instrument used in the sound pressure measurement. The equation for the total bias is presented in Equation 2 [24].

$$Total\ Bias = \sqrt{\sum (u)^2} \qquad (2)$$

The step by step breakdown of this process is as follows:

- $(u)^2$: square each uncertainty value
- $\sum(u)^2$: sum all squared uncertainty value
- $\sqrt{\sum(u)^2}$: take square root of sum

These induvial uncertainty values of the equipment were provided by the manufacture of the respective equipment and is presented in Table 3-4 as well as the total bias.

Table 3-4: Bias Uncertainty for Sound Pressure Measurement

Equipment	Uncertainty (u)
Microphone	±2 dB
Preamplifier	± 0.2 dB
Wire Connectors	± 0.05 dB/unit
Coaxial Cable	± 0.03 dB/100 feet
Total Bias	± 2.01 dB

When narrowband results are shown in this paper, the uncertainty is separated between the precision and bias results. Due to the complexity of frequency domain data, the uncertainty is shown with min and max bounds rather than error bars.

CHAPTER IV

4. FINDINGS

The results presented throughout this chapter are derived from the experimental setups discussed in Chapter III Technical Approach and presented regarding their relevance to the objectives and goals outlined in Chapter I.

4.1. Ambient Background Noise Characterization

Multiple measurements of ambient background noise were made during each test. The purpose of this was to determine the level of background noise in the testing environment which in turn will allow for the determination of which tones and other features are present in the background and not caused by the noise source under study. Understanding the ambient background noise also plays a key role when considering the detection of a noise source. If the background noise is too high, this will mask the target noise source and provide difficulties in detection. However, if there is a strong understanding of the background noise, then there is potential to filter out this noise in order to assist in the detection. When ambient spectra are shown, for the balance of this paper, it will be an average of all microphone ambient data for that measurement.

There are several things to note from this data before considering the noise source. For the anechoic chamber spectrum (shown in Figure 4-1), the electronic noise floor is observed approximately at 400 Hz and above. This is an important feature to consider since the presence of this shows that the acoustic pressure cannot be measured below this value. Also, what is believed

to be an electric noise tone is present at 120 Hz and another tone at 146 Hz. The cause of these are undetermined but the 120 Hz tone is believed to be due to a ground loop in the power line.

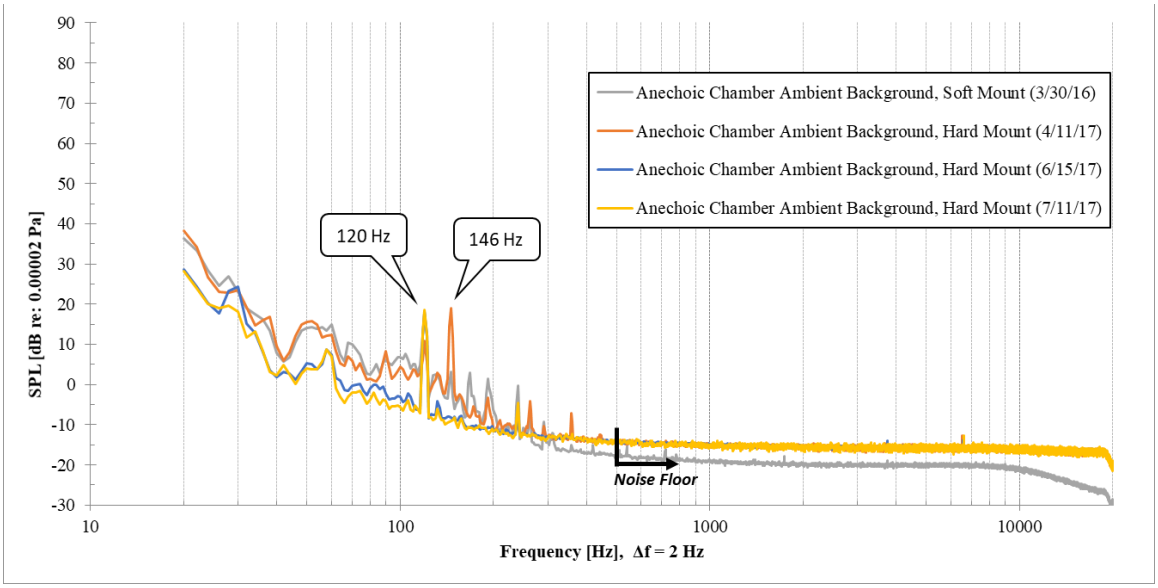

Figure 4-1: Comparison of narrowband acoustic spectra of OSU Anechoic Chamber ambient background noise

For the GIA ambient background spectrum (shown in Figure 4-2), a tone is present at 120 Hz along with harmonics. The cause of this is tone undetermined but is believed to be electric noise caused by lighting in the facility. There appears to be a tone present at 60 Hz which is the know frequency for utility line and therefore the tone at 120 Hz could be a harmonic. The lights used in the facility were powered on throughout all tests and were unable to be powered off due to limitations placed on the procedure by the facility manager. Also, the lights created a notable hum noise noticeable by the observers.

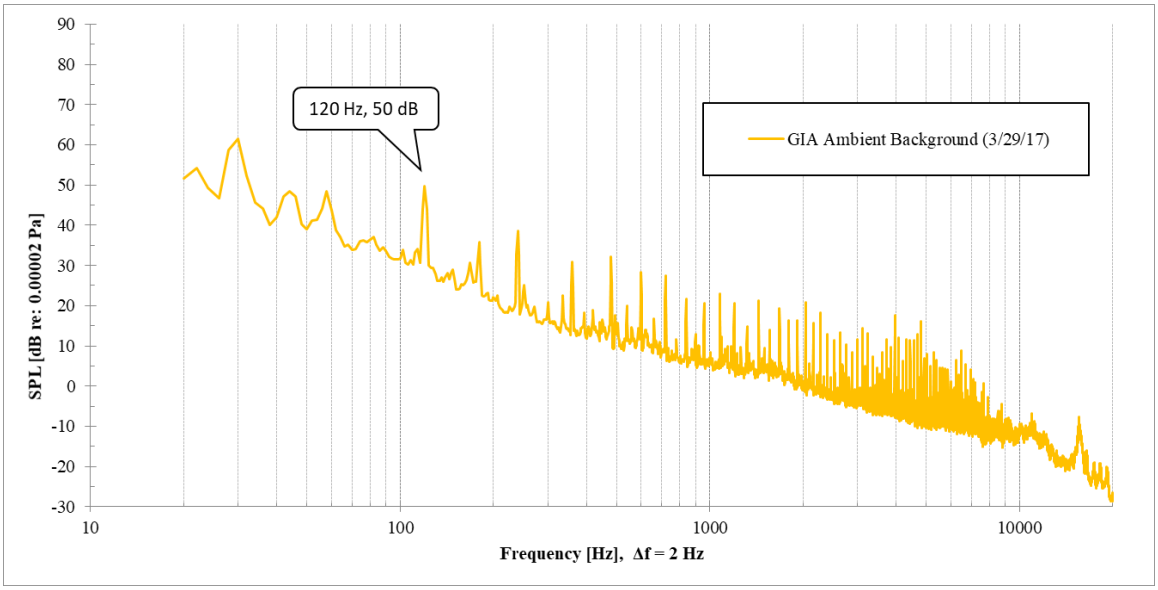

Figure 4-2: Comparison of narrowband acoustic spectra of OSU GIA ambient background noise

Figure 4-3 shows the comparison between the multiple narrowband ambient background spectra of the UAFS testing environment, which were gathered throughout various test setups of different days, as noted. This environment had the largest amount of variation in the ambient background noise, which is expected due to the numerous variables and potential noise sources that are indicative of outside sound measurements. Between the frequencies 230-1200 Hz, much of the broadband and tonal content is believed to be caused by the computer used for collecting the measurements. This computer has multiple onboard cooling fans which were constantly operating and provided a noticeable noise to the observers.

For the UAFS (4/12/17) spectrum, there were moderate winds of approximately 7.0 knots, causing a wire gate to make noise, which was observed to be the cause of the peak at 2258 Hz. For the UAFS (4/19/17) spectrum, there were higher winds of approximately 10.4 knots, causing a higher broadband noise over the spectrum. Also, the elevated broadband noise between approximately 3500 – 5000 Hz was determined to be caused by the constant chirping from bugs and birds. For the UAFS (6/19/17), there were low winds of approximately 4 knots at the beginning of the night, which then dissipated by the end of the test. However, towards the end of the test there

was a large about of noise from the wildlife which provided the elevated broadband noise between 1600-7000 Hz.

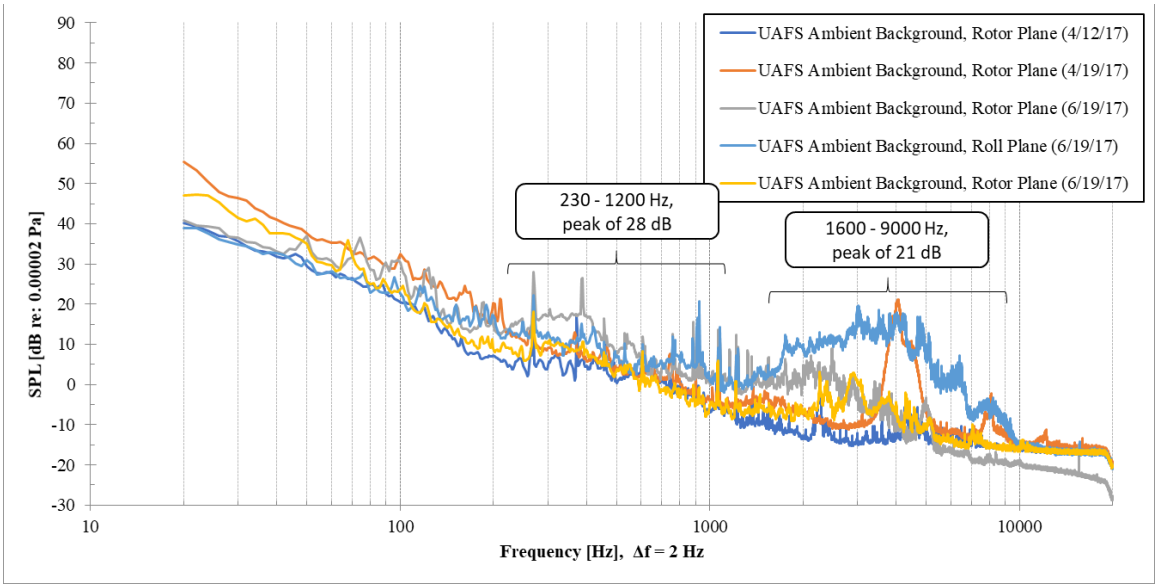

Figure 4-3: Comparison of narrowband acoustic spectra of OSU UAFS ambient background noise

Figure 4-4 shows a comparison of a narrowband acoustic spectrum for each testing environment. The figure only includes a representative spectrum from each set, in order to minimize clutter. The purpose of this figure is to show the differences between the ambient background noise in each environment. As expected, the anechoic chamber has the least amount of background noise with UAFS and GIA having comparable levels but varying frequency characteristics.

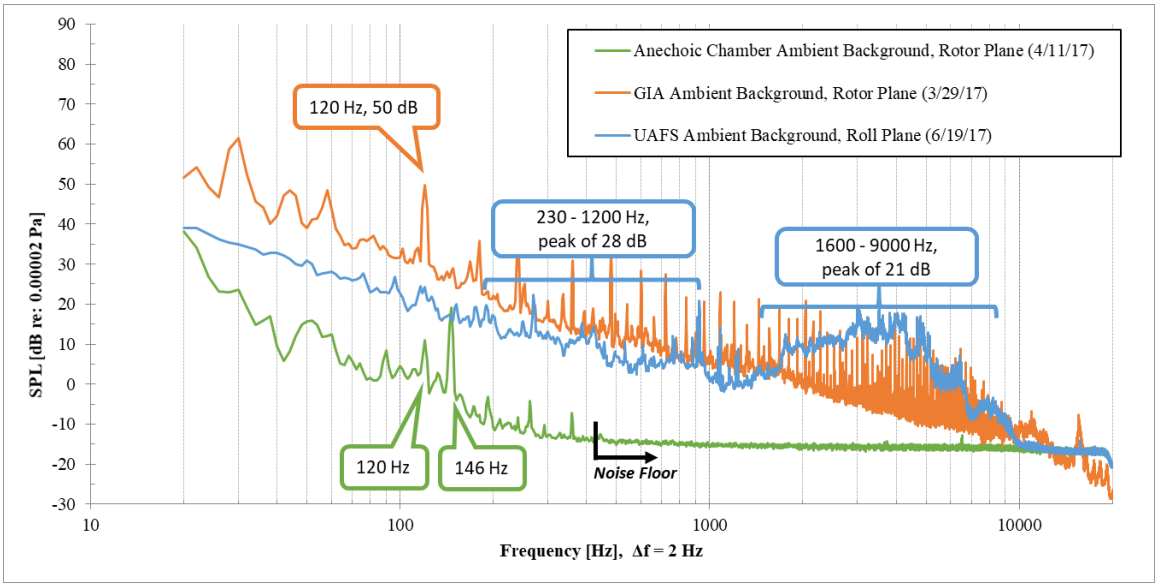

Figure 4-4: Comparison of narrowband acoustic spectra of ambient background noise for each testing environment

4.2. Spectral Characterization

As stated in the last chapter, multiple measurements were unable to be collected at the desired distance of 10D, which was required to assure measurements are in the geometric far field. It was assumed that the radius achieved was enough to successfully place the microphones in the geometric far field relative to the noise source. How does this assumption hold up in the OSU anechoic chamber or the OSU UAFS?

Measurements were made at increasing distances for microphone 1 and 5 with the Iris+ at 100% throttle, as discussed in the *Soft Mount Testing* section. For each measurement, the OASPL was calculated over the frequency range of 20-20k Hz, for each microphone. A comparison was performed between to the measured data and the Inverse-Square Law which should be followed in a relative small anechoic chamber. Figure 4-5 shows the measured data as a function of microphone distance with the representative Inverse-Square Law relationship superimposed. Note that the data appears to follow closely, if not exactly, with the Law (within 2dB). It is quite likely that the background ambient noise below 400 Hz contributes to the data not fitting the theory exactly.

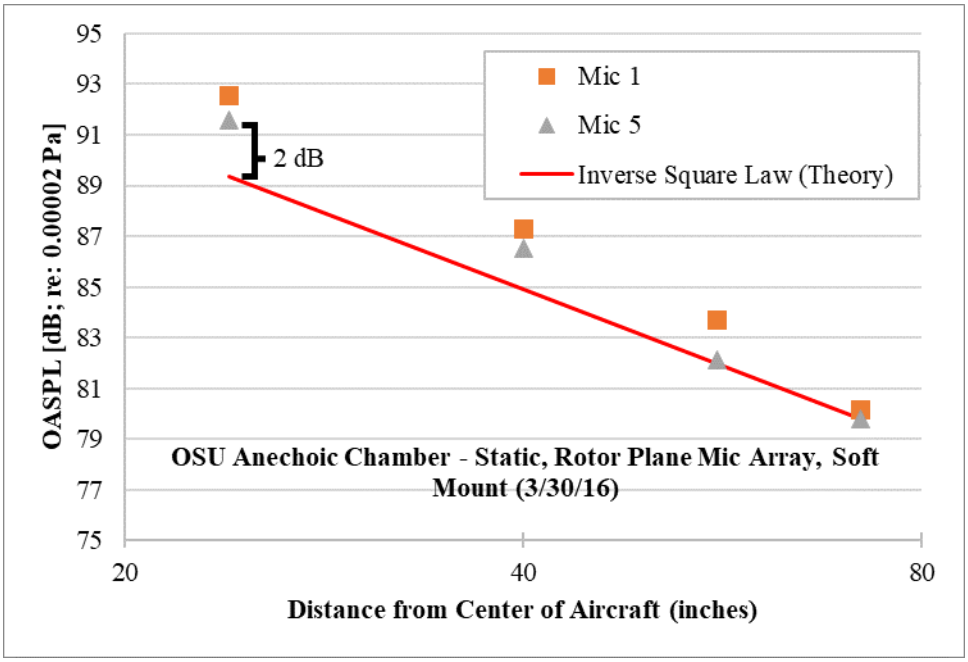

Figure 4-5: OSU Anechoic Chamber - Static, Rotor Plane Microphone Array, Soft Mount (3/30/16)

Figure 4-6 shows the narrowband acoustic spectrum of the Iris+ quadcopter with rotors attached (blue spectrum), operating in the OSU anechoic chamber. In addition, the acoustic spectrum of the Iris+ with only motors (orange spectrum) and the ambient background noise (yellow spectrum) are also included. This figure highlights the features of the acoustic spectra for the 3DR Iris+ multi-rotor and shows that it is consistent with that of typical rotor noise. The acoustic signature is characterized by a series of discrete tones with an underlying broadband base that increases in amplitude with increasing frequency. The Iris+ spectrum with rotors attached is visibly dominated by tonal noise including the motor shaft rate as well as the blade passing frequency (BPF) and its harmonics. However, there is the presence of additional tonal noise which is believed to be related to rotor-airframe interaction noise discussed by Zawodny [13]. The combination of these tones dominates the acoustic signature and contribute mostly to the audible sound.

It is also clear that broadband noise is present and significantly greater than the ambient background noise. The implication of all of the noise at higher frequencies is two-fold: 1) when close to an observer, the significant noise is in the sensitivity frequencies of human hearing and 2) all of that high frequency noise will be greatly affected by atmospheric absorption at large distances

from the observer. The Iris+ spectrum with motors only also contains a considerable amount of tonal noise including the motor shaft rate. In order to accurately compare the results with and without the rotors, the RPM of the motor was held constant (within a buffer range). From the results, it is apparent that the motor noise has a contribution to the tonal noise of the system. Also, a motor running with no rotor only affects the measured spectrum above the frequency where the shaft RPM is observed above the ambient.

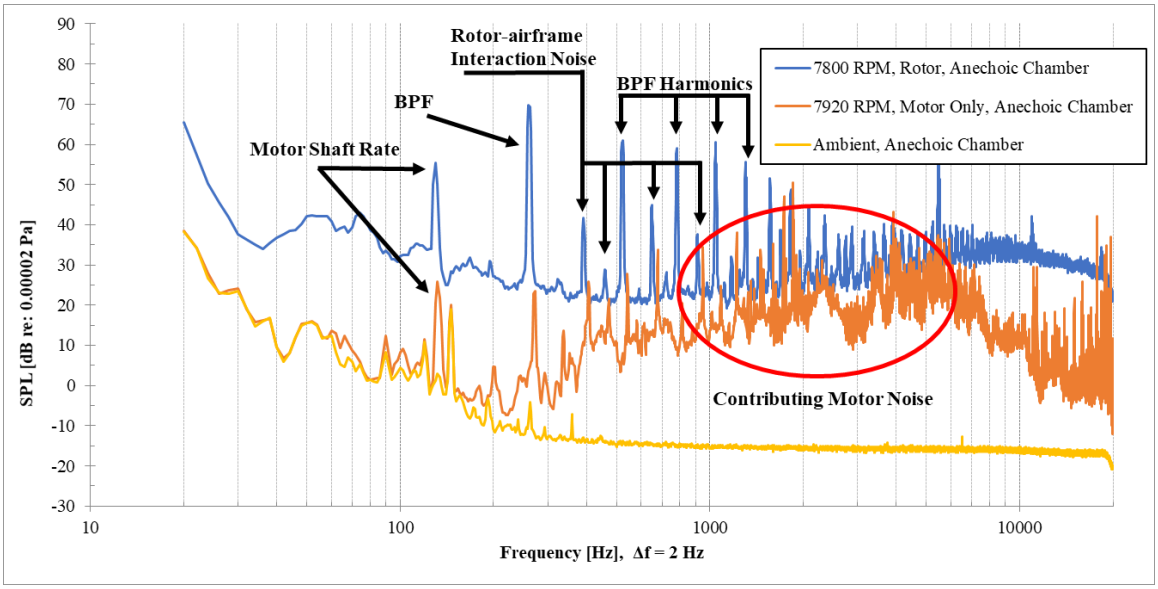

Figure 4-6: OSU Anechoic Chamber - Static, Rotor Plane Microphone Array, Hard Mount (4/11/17)

Figure 4-7 shows the narrowband acoustic spectrum of the Iris+ quadcopter with rotors attached (blue spectrum), operating at the OSU UAFS (4/12/17). In addition, the acoustic spectrum of the Iris+ with only motors (orange spectrum) and the ambient background noise (yellow spectrum) are also included. The test setup used to produce these results was consistent with that of Figure 4-6, which was the *Static, Rotor Plane Microphone Array with the Hard Mount* test setup used for the rotor RPM examination. Similarly, to what was found in Figure 4-6, the spectrum with rotors attached is dominated by tonal noise including the motor shaft rate, the BPF and its harmonics as well as the potential rotor-airframe interaction noise. Broadband noise is also present and the motor noise has a clear contribution to the tonal noise of the system. The results follow the same trend as what was presented for the results within the anechoic chamber.

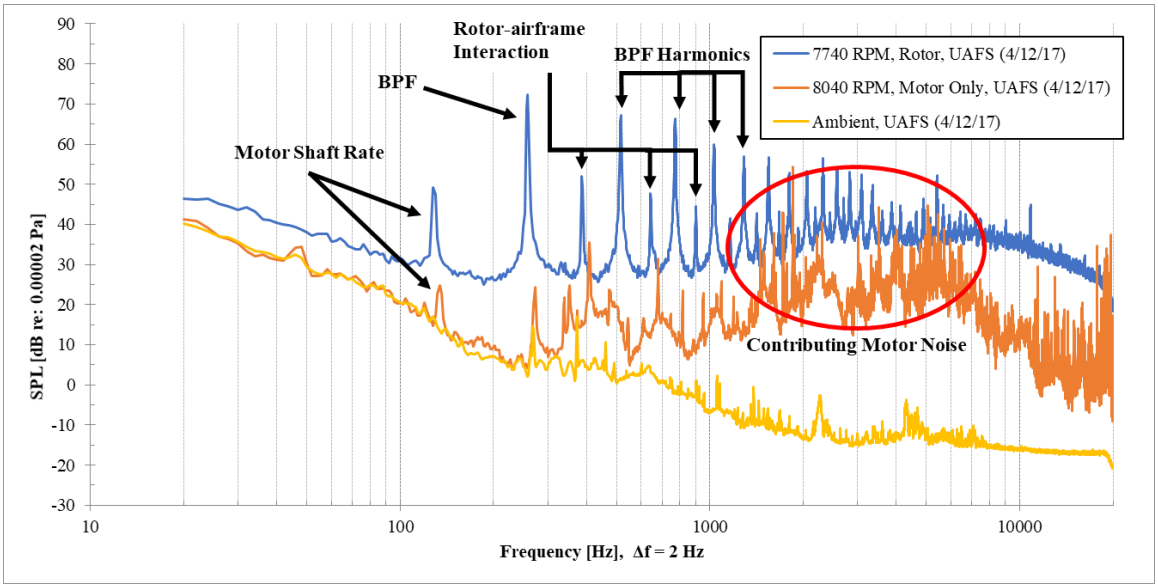

Figure 4-7: OSU UAFS- Static, Rotor Plane Microphone Array, Hard Mount (4/12/17)

Figure 4-8 shows the narrowband acoustic spectrum of the Iris+ quadcopter with at a height of 60 inches with the microphones at a height of 60 inches (blue spectrum), operating at the OSU GIA and the ambient background noise (yellow spectrum). The test setup which produced this result was the *Hover, Rotor Plane Microphone Array* test setup. This figure shows that the spectral features discussed above in Figure 4-6 are still present within the reverberant environment, however these features have been effected in various ways. The tonal content now has multiple tones with different amplitudes which span across a range of frequencies. The cause of this variation is the RPM of the rotors which is directly related to the operation of the aircraft. For this test, the aircraft was not fixed to a test stand and was allowed to fly under realistic conditions, albeit with the tether system restraining the motion of the aircraft. Due to this, the aircraft will have more variability in stability, orientation and location which will cause greater spread in the spectral content.

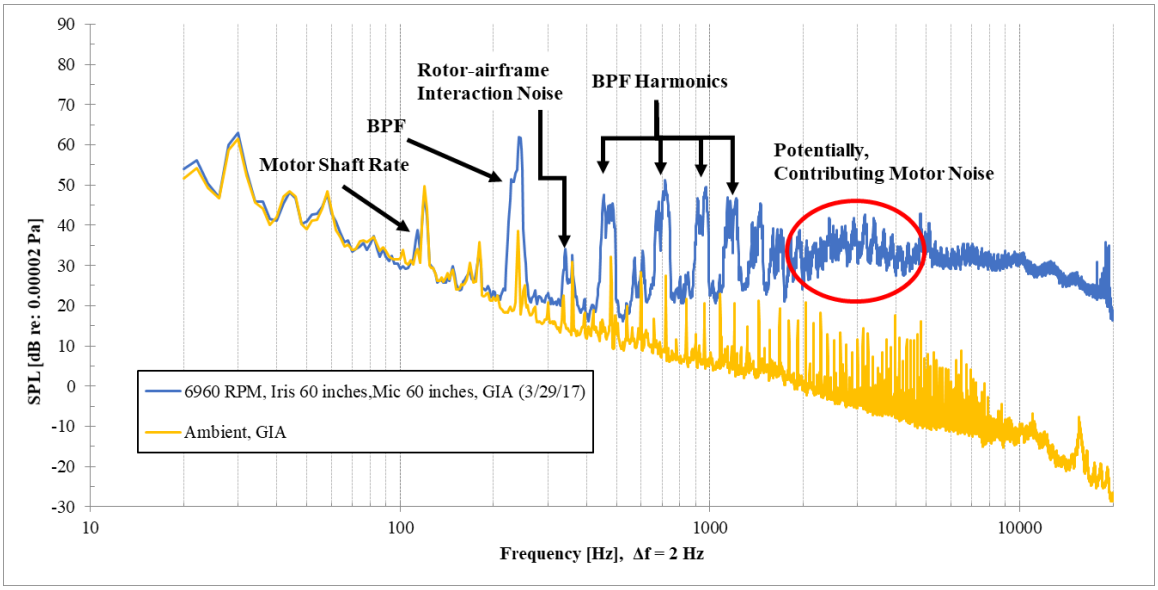

Figure 4-8: OSU GIA- Hover, Rotor Plane Microphone Array, Tether (3/29/17)

Figure 4-9 shows the narrowband acoustic spectrum of the Iris+ quadcopter with an altitude of 60 inches and the microphones at a height of 120 inches (blue spectrum), operating at the OSU UAFS (4/19/17) and the ambient background noise (yellow spectrum). The arrangement which produced this result was the *Hover, Rotor Plane Microphone Array* test setup. Similarly, to what was found in Figure 4-8, the spectrum contains the typical features of rotor noise which have multiple tones with different amplitudes which span across a range of frequencies. However, this test did not use the tether system but rather was controlled by the autopilot attempting to maintain a specific GPS location. While the amplitudes and frequencies vary between the two results, the trend is consistent. Also in Figure 4-6, Figure 4-7, Figure 4-8, and Figure 4-9 the noise produced by the Iris+ is clearly much louder than that of the ambient background noise for all the environments regardless of the differences between the test setups and operations, which is important when considering the detection of the system.

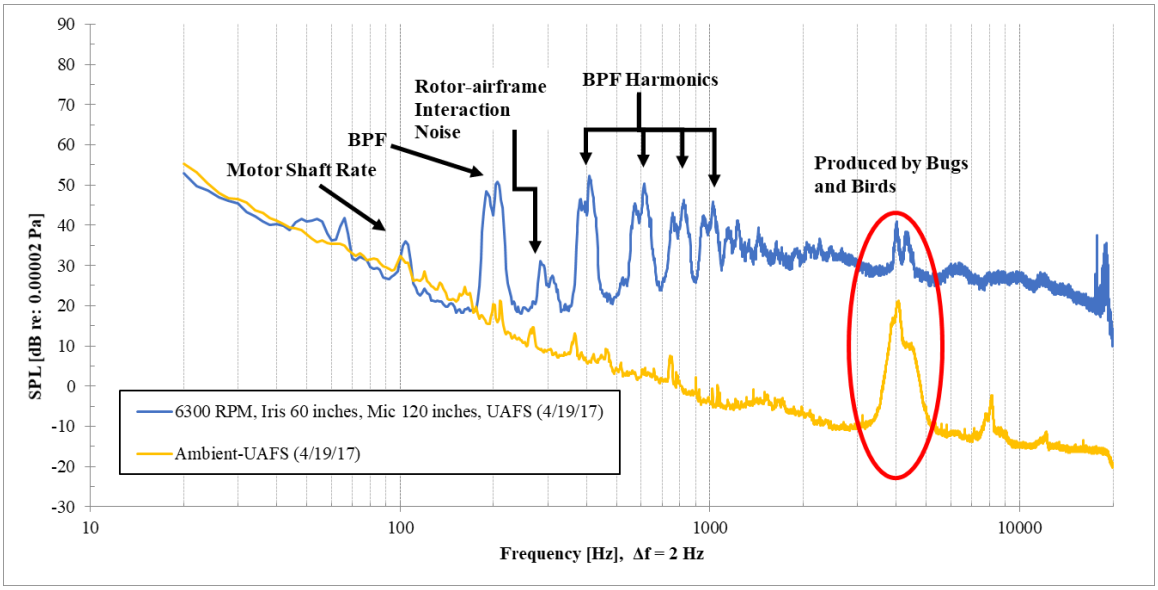

Figure 4-9: OSU UAFS- Hover, Rotor Plane Microphone Array, GPS Hold (4/19/17)

4.3. Effect of Increasing Throttle (RPM)

Figure 4-10 shows a comparison between the narrowband acoustic spectrums of the Iris+ quadcopter operating at 50%, 75%, and 100% throttle (5040 RPM, 6900 RPM, 7980 RPM, respectively), all tested on the static test stand in the anechoic chamber. The results show that the spectrum contains typical features of rotor noise as discussed earlier. When increasing the RPM of the motor, there is a clear increase in BPF frequency and amplitude, as well as all tonal content. This result is expected, especially since the BPF is defined as the frequency at which the blade makes one revolution and therefore simply equates to the motor rpm times the number of blades. Also, when increasing the RPM there is an increase in broadband noise amplitude but not in frequency.

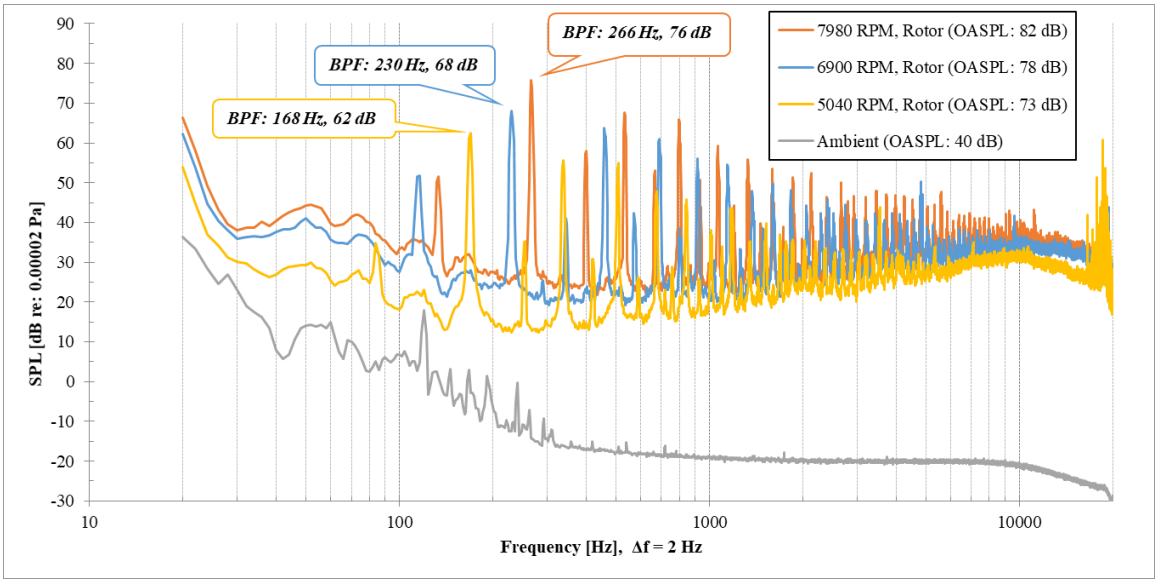

Figure 4-10: OSU Anechoic Chamber - Static, Rotor Plane Microphone Array, Soft Mount (3/30/16)

A clearer way to see the similarity in the acoustic signature characteristics is to normalize the frequency domain with the first BPF of each spectrum. Figure 4-11 shows this normalization for each throttle setting and the similarities of the features in each spectrum are evident. Doing this reveals the presence of high frequency motor noise which is independent of rotor noise. However, it also reveals the significant increase in rotor-aircraft interaction noise. There is also a significant increase in broadband noise between 11th and 14th BPF harmonic when increasing RPM from 5040 to 6900, when compared to increasing RPM from 6900 to 7980.

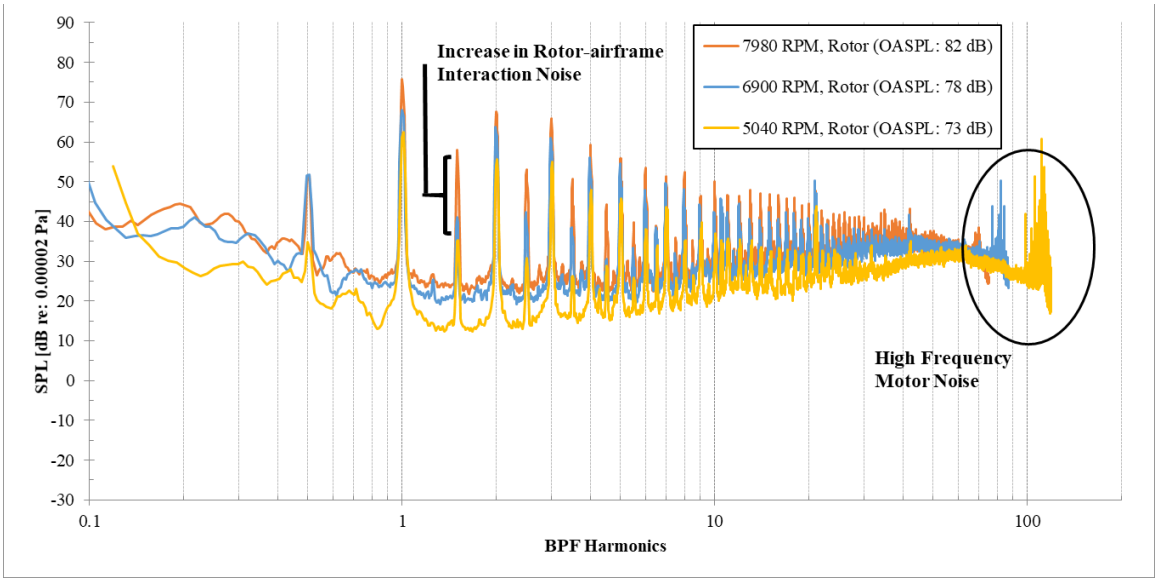

Figure 4-11: OSU Anechoic Chamber - Static, Rotor Plane Microphone Array, Soft Mount (3/30/16)

4.4. Effect of Multiple Rotors

Data was collected with different number of rotors operating on the quadrotor. Configuration 1, 3, and 5 represent cases where 4 rotors, 2 rotors, and 1 rotor are operating, respectively. Figure 4-12 shows a comparison of narrowband acoustic spectrums of the 3DR Iris+ quadcopter operating with 4 rotors (orange), 2 rotors (blue), and 1 rotor (yellow), all tested on the static test stand in the anechoic chamber at 100% throttle (7900 RPM ±120). The acoustic characteristics of the rotor noise is nearly identical whether all or one of the rotors are operating. There is a slight increase in amplitude of low frequency tonal content, specifically the BPF and its harmonics. Also, there is a large increase in rotor-airframe interaction noise and high frequency broadband noise. The increase in rotor-airframe noise is expected since it is directly related to the number of rotors used on the aircraft. The increase in high frequency broadband noise is likely due to the increase in prop wash.

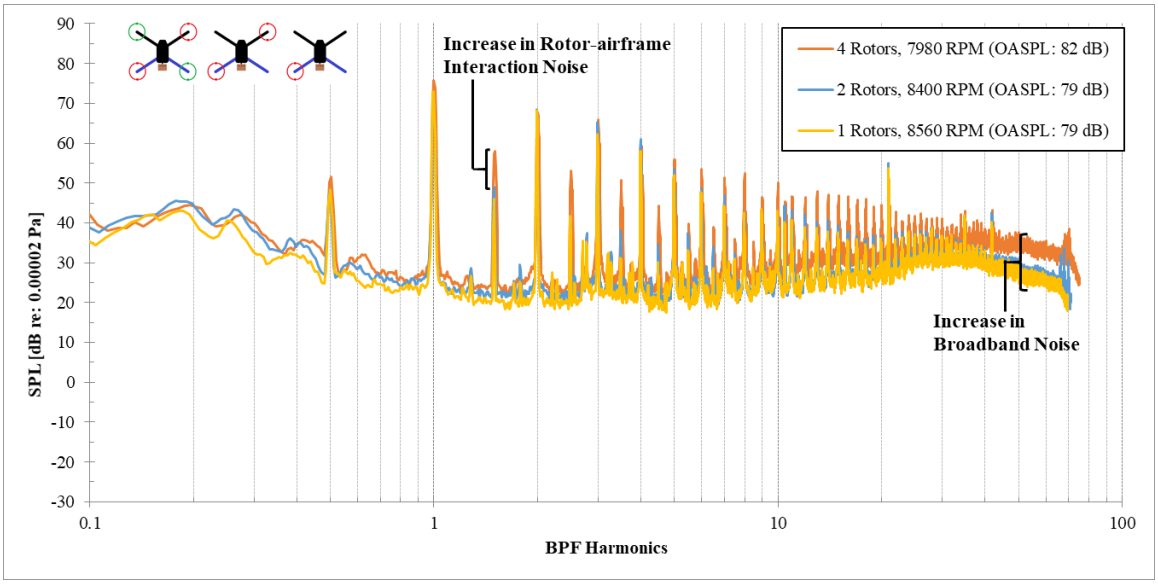

Figure 4-12: OSU Anechoic Chamber - Static, Rotor Plane Microphone Array, Soft Mount, Config 1a, 3a, 5a @100%, Microphone 3

4.5. Recirculation and Vibration Effects

Measurements were collected with varying mounting techniques, a "soft mount" and a "hard mount." The soft mount consisted of a wooden platform with foam attached to it and held the aircraft in place with zip ties, while the hard mount was a custom made, 3D printed, flush mount that was specifically designed to fit the aircraft. Figure 4-13 shows the narrowband acoustic spectrums of the Iris+ quadcopter operating with the soft mount (7980 RPM and orange), and hard mount (7800 RPM and blue), all tested on the static test stand in the anechoic chamber. Between the two studies, the only difference with the setup is how the aircraft was mounted to the test stand. From this knowledge, we have speculated that the large difference in amplitudes of tonal content is due to the reduced vibrations with the new "hard mount." While the RPM is greater for the previous study results, it is not believed to be the sole cause of the difference in amplitude. Also, the trend was consistent with all microphones.

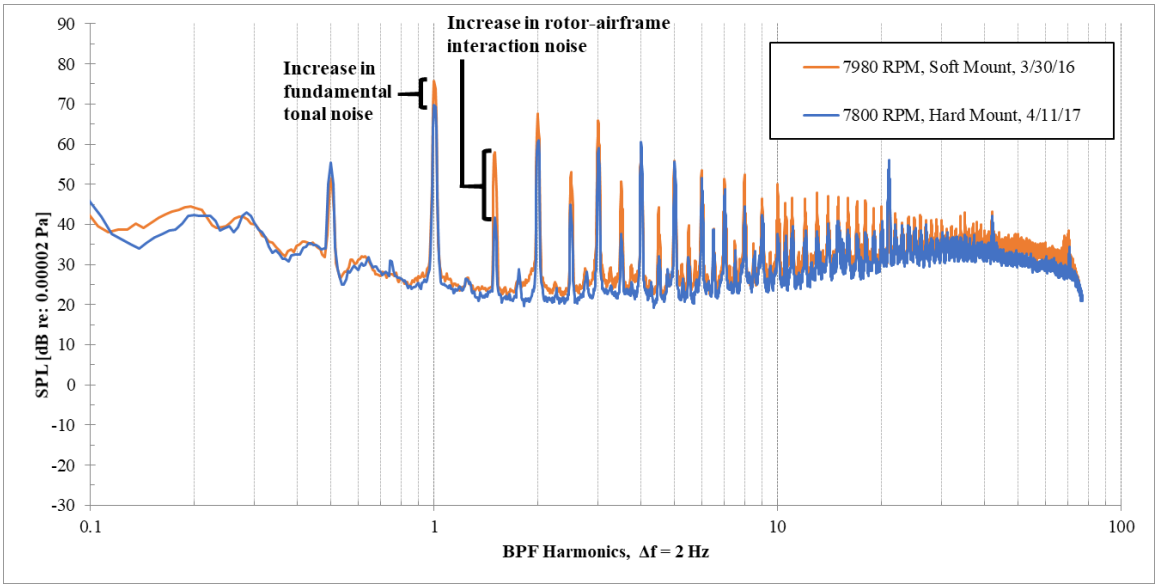

Figure 4-13: Comparison of narrowband acoustic spectra (Iris mounted with "hard mount," Iris mounted with "soft mount"), within OSU anechoic chamber, Static, Rotor Plane Microphone Array, Microphone 3

In terms of the potential effects of recirculation for this setup, it was determined that there was no apparent effect. The data shows that there was no recorded wind velocity at positions 4 and 5, as shown in Table 4-1 (a & b), and limited wind velocities at position 3. However, the data did show an interesting pattern with the measured wind velocities at position 3. An additional note, for position 3, the recorded values of zero are mainly along the walls of the anechoic chamber.

Table 4-1 (a & b): Wind velocities at recirculation measurement locations (knots), within OSU anechoic chamber, Static, Rotor Plane Microphone Array

Measurement Location	Rotor I	Rotor II	Rotor III	Rotor IV
1	2.3	1.7	2.1	2.4
2	7.6	9.9	7.4	8.7

Measurement Location	Mic 0	Mic 1	Mic 2	Mic 3	Mic 4	Mic 5	Mic 6	Mic 7
3	0.0	0.0	1.2	1.7	1.5	0.0	0.2	1.6
4	0.0	0.0	0.0	0.0	0.0	0.0	0.0	0.0
5	0.0	0.0	0.0	0.0	0.0	0.0	0.0	0.0

To further investigate the effects of recirculation, the test was repeated with foam sheets placed on the mesh floor. This was done to attempt to force recirculation within the anechoic chamber. The measured wind velocities at the are shown in Table 4-2. The data shows there was a more consistent wind velocity recorded at position 3, as well as limited wind velocities at position 5. These results suggest the likely hood of recirculation is higher.

Table 4-2 (a & b): Wind velocities at recirculation measurement locations (knots), within OSU anechoic chamber, Static, Rotor Plane Microphone Array, with Foam Sheets for forced recirculation

Measurement Location	Rotor I	Rotor II	Rotor III	Rotor IV
1	2.4	2.4	2.3	2.3
2	11.4	11.3	10.4	11.0

Measurement Location	Mic 0	Mic 1	Mic 2	Mic 3	Mic 4	Mic 5	Mic 6	Mic 7
3	1.3	1.3	0.8	1.2	0.9	0.9	1.5	1.5
4	0.0	0.0	0.0	0.0	0.0	0.0	0.0	0.0
5	0.0	0.0	0.0	1.1	0.0	0.0	0.0	1.1

Figure 4-14 shows narrowband acoustic spectrums of the Iris+ quadcopter operating with foam sheets (7980 RPM and yellow), and hard mount without sheets (7800 RPM and blue), all tested on the static test stand with the hard mount in the anechoic chamber. Between the two studies, the only difference with the setup is the foam sheets under the test stand. From these results, it is unclear if recirculation is effecting the spectrum. Figure 4-14 does show a decrease in broadband noise at low frequencies, however this is not caused by the recirculation but rather a decrease in ambient background noise. Also, there is an increase in rotor-airframe interaction noise. Again, this is not believed to be caused by recirculation but rather a result of the precision uncertainty.

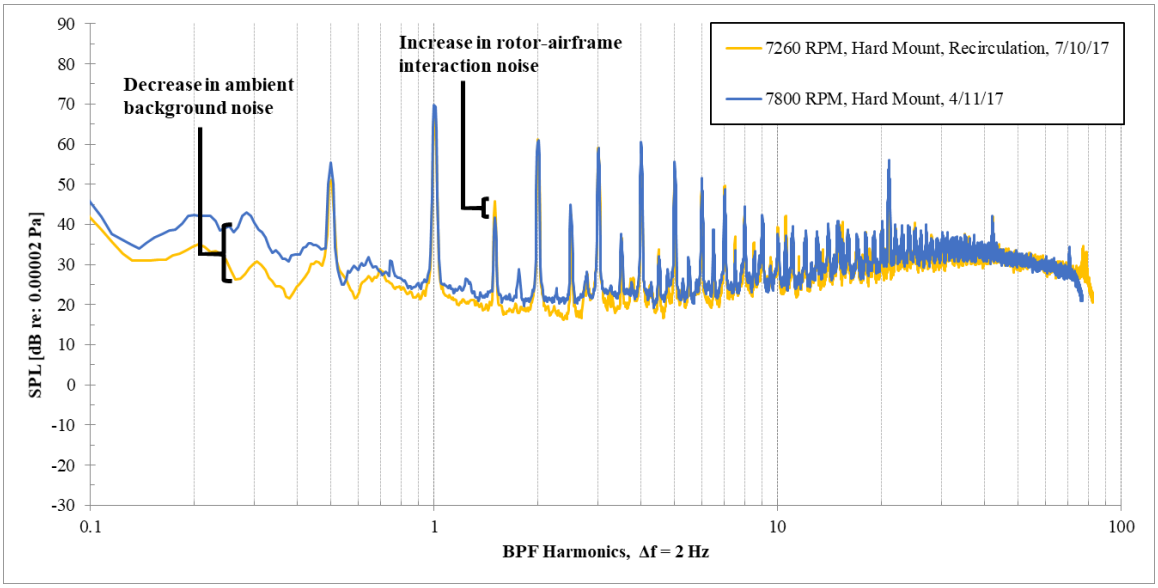

Figure 4-14: Comparison of narrowband acoustic spectra with/without Foam Sheets for forced recirculation, within OSU anechoic chamber, Static, Rotor Plane Microphone Array, Microphone 3

As stated above, the small variations shown in Figure 4-14 are believed to be caused by uncertainty which will affect the spectrum in various ways mainly with the amplitudes. To visualize the uncertainty, a plot with the hard mount without sheets (7800 RPM and blue) was plotted with the precision uncertainty (Figure 4-15) and the bias uncertainty (Figure 4-16). From these results, it can be seen that the majority of the small variations in Figure 4-14 fall in either of the uncertainty bounds. Interestingly, precision uncertainty is shown to have a larger effect on the tonal content while bias uncertainty has a larger effect on the broadband content. The bias uncertainty shown in Figure 4-16 will be consistent though out all measured data, with a value of ±2.01 dB.

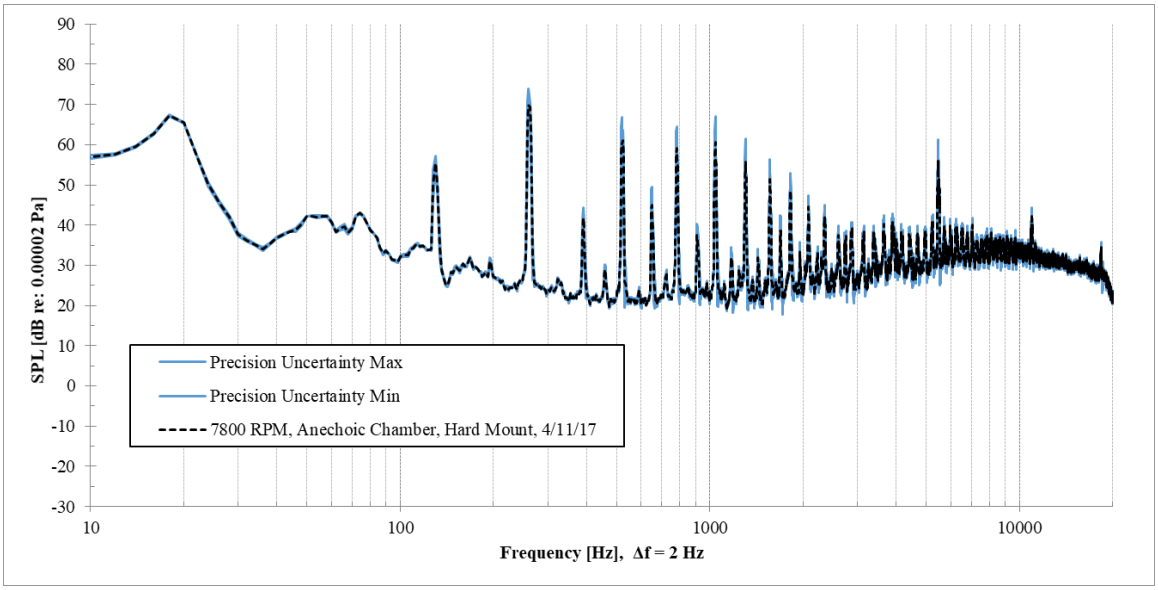

Figure 4-15: Narrowband acoustic spectra with precision uncertainty bounds, setup without Foam Sheets for forced recirculation within OSU anechoic chamber, Static, Rotor Plane Microphone Array, Microphone 3

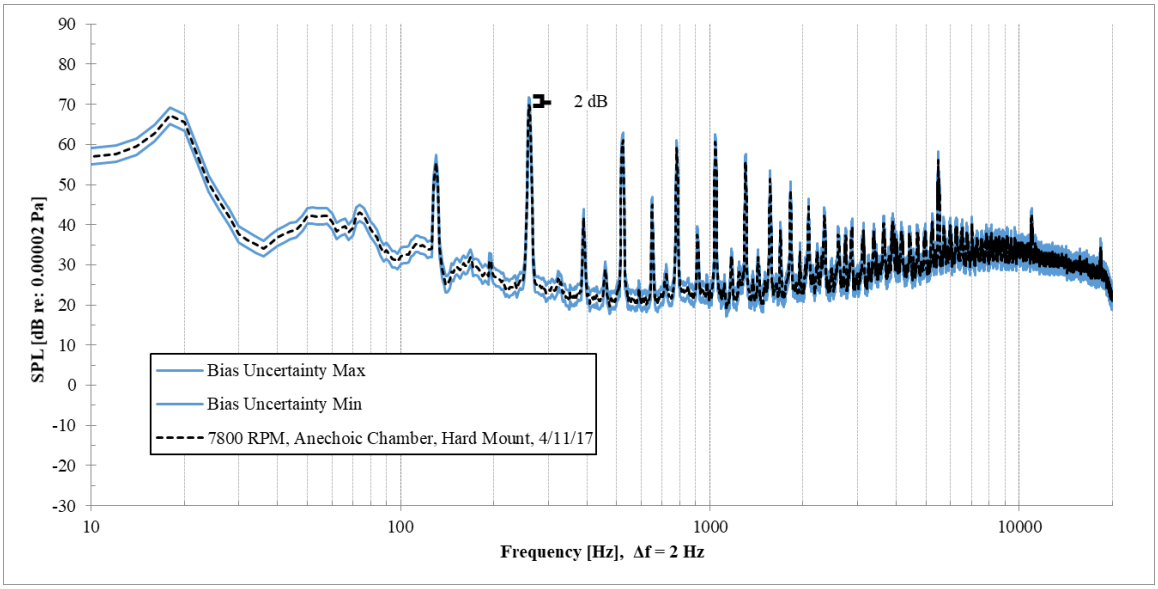

Figure 4-16: Narrowband acoustic spectra with bias uncertainty bounds, setup without Foam Sheets for forced recirculation within OSU anechoic chamber, Static, Rotor Plane Microphone Array, Microphone 3

To better understand the potential effects due to recirculation, more through experimental analysis is required. A larger aircraft with larger rotors are suggested in order to reassure recirculation is present.

4.6. Environmental Effects

For these results, only the OSU anechoic chamber and UAFS environments will be considered since static measurements in the OSU GIA were not conducted. When comparing the spectra from the anechoic chamber and UAFS (as seen in Figure 4-17), it was observed that there is no effect on spectral characteristics. However, there is an increased amplitude of BPF and harmonics as well as the broadband noise across the entire spectrum and specifically between 8th and 10.5 BPF harmonic. The cause of the increased broadband noise is undetermined; however, it is speculated to be related to the environment since that is the major difference between the two spectrums. Note that the RPM of the anechoic chamber test is greater than that of the UAFS test, which would typically result in the amplitude to also be greater but that is not the case with these results. This is believed to be due to the environment, and could possibly be caused by reflections from the ground. Lastly, the tones of the BPF and the respective harmonics have a greater gradient at the base than what is seen with the anechoic chamber results, the reason for this is still undetermined. The trend was consistent between all radial microphones, however at lower RPM values there was less variation in amplitude but the gradient and increase in broadband noise was present.

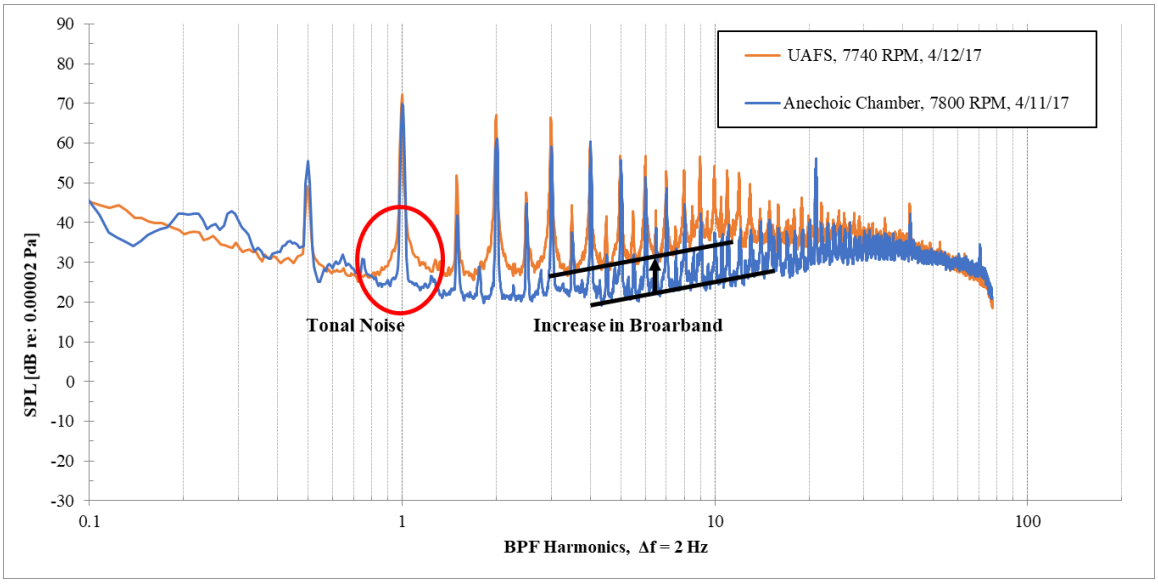

Figure 4-17: Comparison of narrowband acoustic spectra between OSU anechoic chamber (blue) and UAFS (orange), Static, Rotor Plane Microphone Array, Microphone 3

To better understand the potential effects due to environment, the UAFS results from Figure 4-17 was plotted with the precision uncertainty bounds, shown in Figure 4-18. Clearly the variation due to uncertainty is minute and therefore the observations on the content is likely due to the environmental differences.

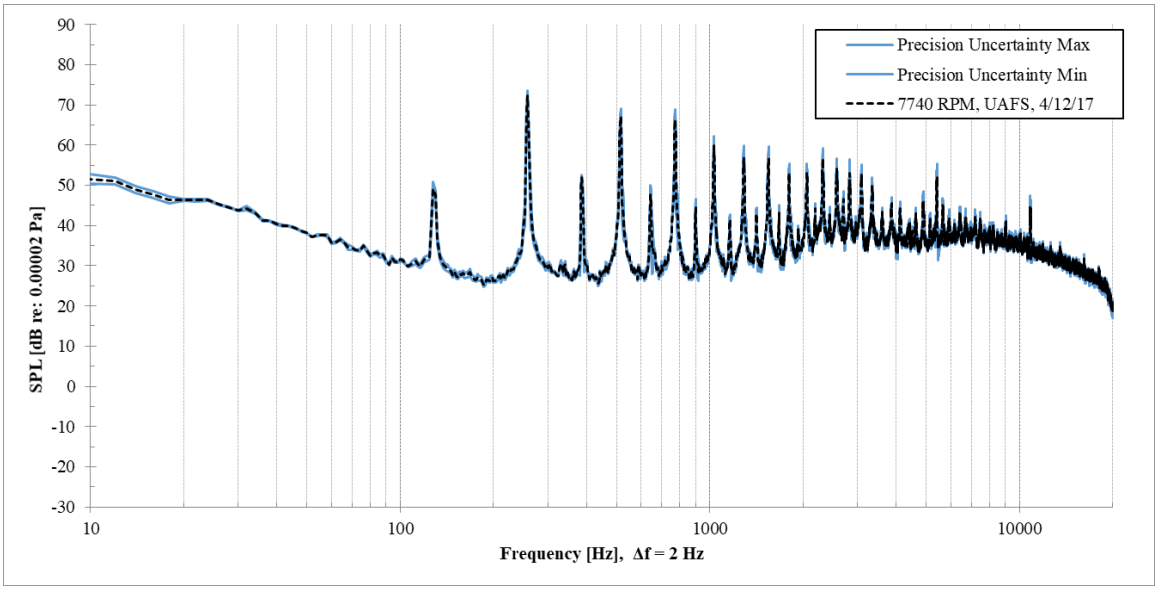

Figure 4-18: Narrowband acoustic spectra with precision uncertainty bounds, at UAFS with Static, Rotor Plane Microphone Array, Microphone 3

4.7. Directivity

6.7.1. Rotor Plane

The directivity of the Iris+ quadcopter was assessed first by examining the polar distribution of the OASPL (summed over the frequencies 100-20k Hz) for the three throttle settings in the rotor plane. Figure 4-19a, shows this distribution measured using the *Static, Rotor Plane Microphone Array* with the Hard Mount in the OSU anechoic chamber, while Figure 4-19b shows this distribution measured using the *Static, Rotor Plane Microphone Array* with the Hard Mount at the UAFS. The measurements show that the noise in the far field is very close to omnidirectional in the plane of the rotor rotation. This is true for all throttle settings tested. This trend becomes more evident as the RPM of the motor increases. Also, the OASPL values for the UAFS measurements are larger than the values for the anechoic chamber measurements with a larger separation between each throttle setting. It is suggested that the cause of this is the larger broadband noise and reflections, which was identified as a result of the UAFS environment.

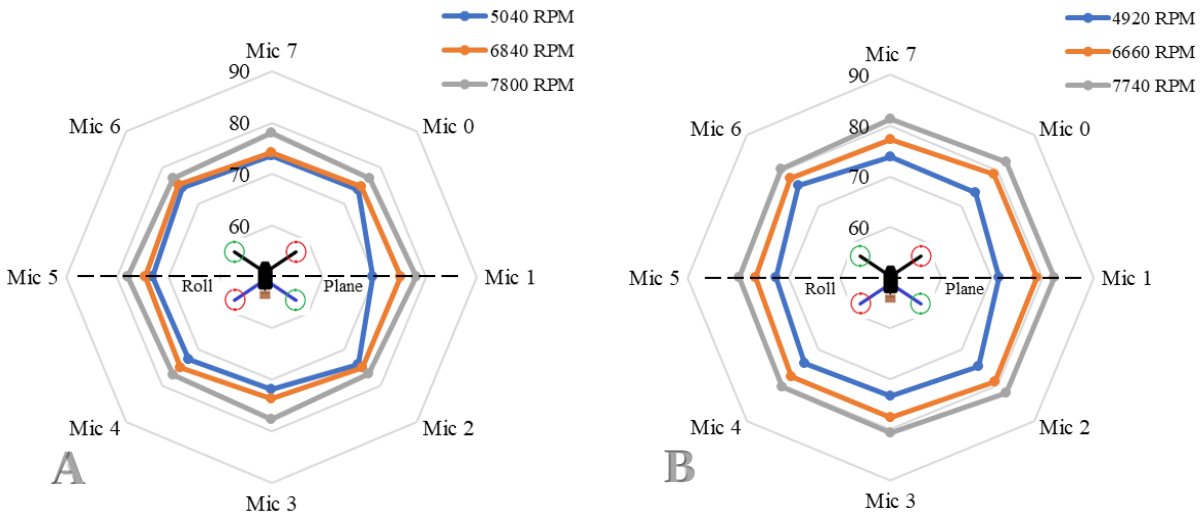

Figure 4-19: OASPL (dB, 100-20k Hz) - Static, Rotor Plane Microphone Array with Hard Mount tested in A) OSU Anechoic Chamber (4/11/17), B) OSU UAFS (4/12/17)

6.7.2. Roll Plane

To develop a three-dimensional representation for the directivity of the noise, measurements were also taken in the roll plane of the aircraft. The location of the measurements

was denoted by the angle θ which was defined in previous sections as the angle between the rotor plane and the observer (or microphone) location, as shown in Figure 4-20. The directivity in the roll plane was investigated with two different test setups, the *Static, Roll Plane Microphone Array*, the *Hover, Rotor Plane Microphone Array*, and the *Hover, Roll Plane Microphone Array*. The major differences between these setups is the microphone array. The *Rotor Plane Microphone Array* had a buildup approach for the angles while the *Roll Plane Microphone Array* collected the multiple angular measurements in one test. The directivity of the OASPL (100 – 20k Hz) for the aircraft under the *Hover, Rotor Plane Microphone Array* testing conditions, at GIA and UAFS, both tethered and GPS hold, is shown in Figure 4-21. This figure shows the directivity trend, with increasing values of θ, in terms of the OASPL measurements from each microphone location, parallel to the rotor plane (both above and below the rotor plane).

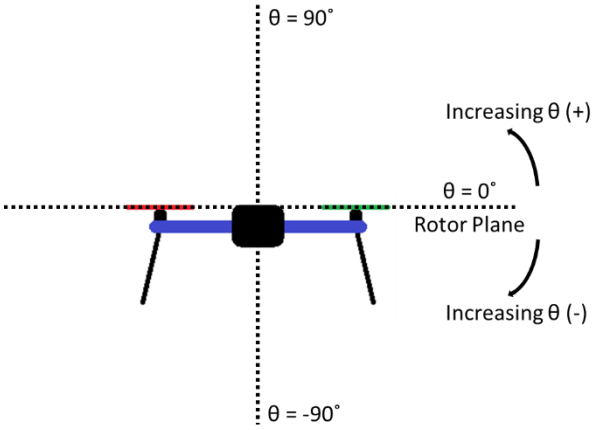

Figure 4-20: Visual representation of the angle θ, the angle between the rotor plane and the observer (or microphone) location

The *GIA Tether* results (Figure 4-21) indicate that the noise in the far field is very close to omnidirectional, when the microphone array is parallel to the rotor plane. However, the *GIA Tether* results also indicate that the OASPL increases as θ increases which is similar to what was found by Zawodny [10] and Sinibaldi [12], except for the position θ = -17.5˚ at the GIA environment with tether. This was determined to be caused by the location of the aircraft, as the aircraft was not centered within the microphone array and thus caused the response to be lower. From these results,

it can be assumed that the maximum OASPL will be achieved at θ = 90 degrees, however further tests are required to validate this assumption.

For the *UAFS Tether* results (Figure 4-21), the trend is different than what is presented for *GIA Tether*. The cause of this difference is believed to be rooted in the aircraft orientation as the aircraft was not only being operated in manual mode but also experienced winds. The results for the *UAFS Tether* test suggest that the noise in the far field is not omnidirectional, but the previous findings provide evidence that it is in fact omnidirectional.

The *UAFS GPS hold* results (Figure 4-21) show a similar trend to the *GIA Tether* results but have a larger variance, which further suggests that the noise in the far field is indeed omnidirectional. The variance is still believed to be caused by the wind but since the autopilot loiter mode is engaged for these flights, the aircraft is more stable and thus the results better represent what is expected.

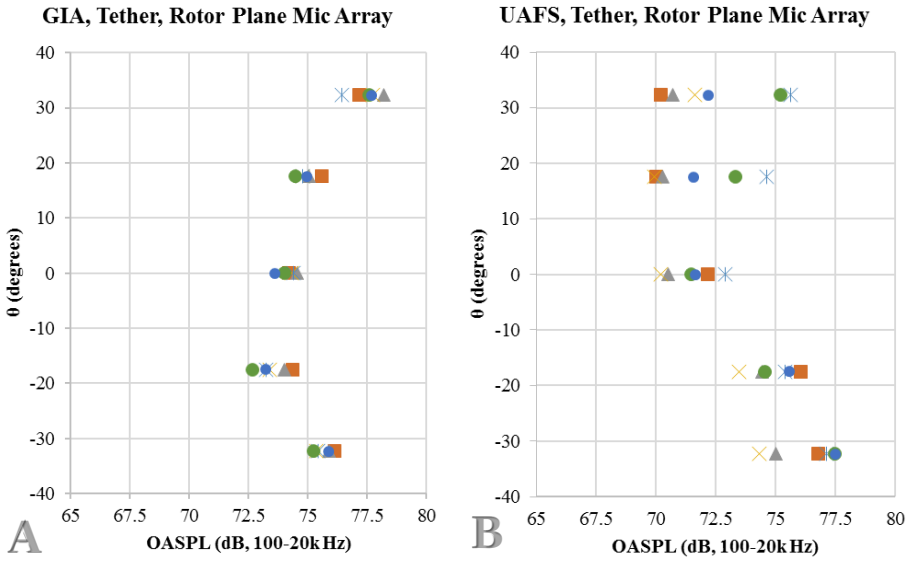

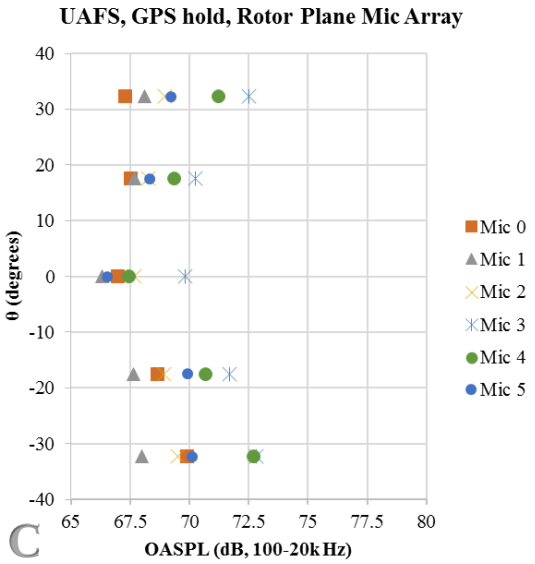

Figure 4-21: OASPL (dB, 100 – 20k Hz) directivity patterns of 3DR Iris+, for Rotor Plane Microphone Array tests (A: GIA Tether; B: UAFS Tether; C: UAFS GPS hold), with all microphones

To provide further evidence that the aircraft location could be the cause of the large variations in the *UAFS Tether* and *UAFS GPS hold* results, the microphone with the highest OASPL measurements for each directivity test was determined and plotted in Figure 4-22. For the *GIA Tether* results the microphone with the highest OASPL measurements was Microphone 0, while for both the *UAFS Tether* and *UAFS GPS hold* results the microphone was Microphone 3. Figure 4-22 shows that for each directivity test combination, the OASPL increases as θ increases. Also, the OASPL values for the *UAFS GPS* hold flight is lower than that of the *UAFS Tether* flight and the *GIA Tether* flight. This is believed to be caused by the increased weight (approximately 0.8 pounds) with the attached tether system, which in turn causes the aircraft to have to produce more thrust and therefore a larger RPM of the motor.

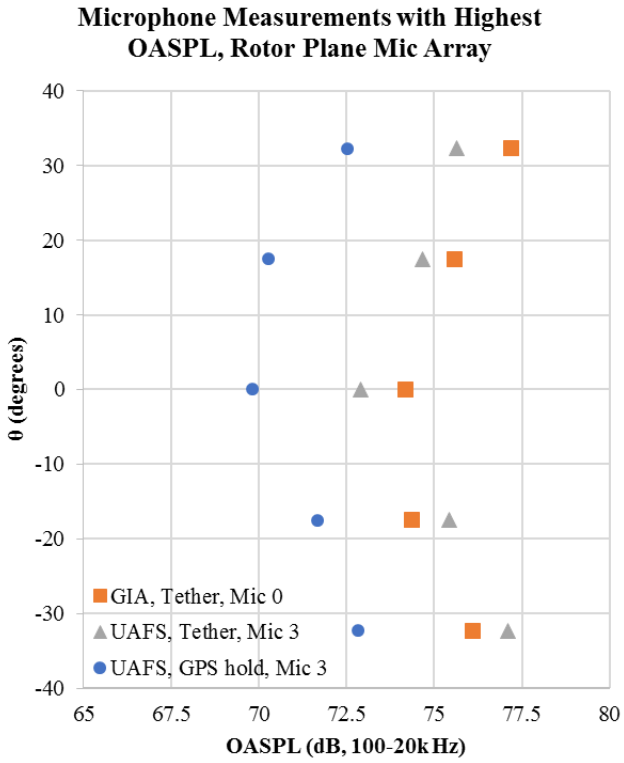

Figure 4-22: OASPL (100 – 20k Hz) directivity patterns of 3DR Iris+, for for Rotor Plane Microphone Array tests (A: GIA Tether; B: UAFS Tether; C: UAFS GPS hold), with highest microphone measurements

The directivity of the OASPL (100 – 20k Hz) for the aircraft under both *Static, Roll Plane Microphone Array* (blue) and *Hover, Roll Plane Microphone Array* (orange) testing conditions at UAFS is shown in Figure 4-23. This figure shows the directivity trend, with increasing values of θ, in terms of the OASPL measurements from each microphone location. The results show a consistent trend with what was shown in Figure 4-21, where the OASPL increases as the angle θ increases, until the maximum angle is reached at 90 degrees.

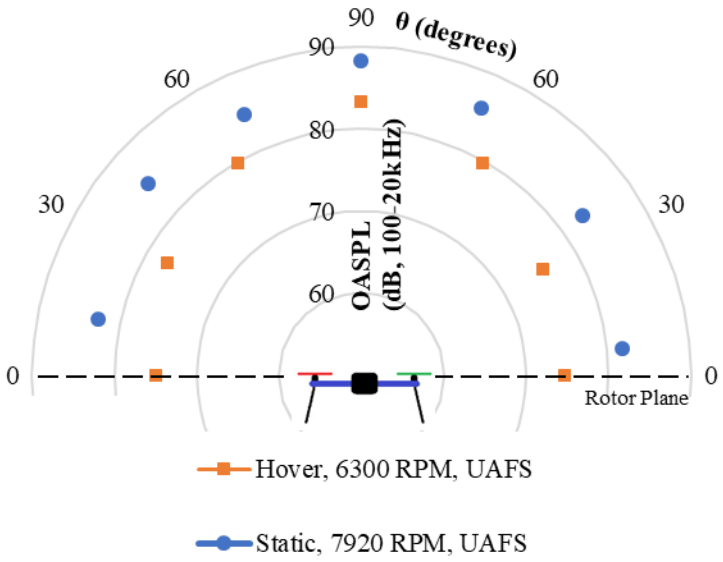

Figure 4-23: OASPL (dB, 100 – 20k Hz) directivity patterns of 3DR Iris+, for Roll Plane Microphone Array tests at static and hover testing conditions

The difference between the OASPL measurements in the rotor plane and 90 degrees above the rotor plane is approximately 8 dB. The values of the OASPL with their associated angles are presented in Table 4-3. This difference is large enough to be noticeable by the human ear however, it is not large enough to state that there is significant directivity. From these results, it can be assumed that the directivity in symmetric about the rotor plane and therefore the OASPL will reach a maximum at 90 degrees below the rotor plane. However, angular locations around 90 degrees below the rotor plane will be within the prop wash and therefore the propagation pattern and noise produced could be effected.

Table 4-3: OASPL (dB, 100 – 20k Hz) values of 3DR Iris+, for Roll Plane Microphone Array tests at static and hover testing conditions

Static, 7920 RPM, UAFS			Hover, 6300 RPM, UAFS	
θ (degrees)	OASPL (dB, 100-20k Hz)		θ (degrees)	OASPL (dB, 100-20k Hz)
12	82.7		**0**	74.8
40	84.8		**30**	77.1
65	84.8		**60**	79.8
90	88.3		**90**	83.3
65	85.7		**60**	79.7
40	83.1		**30**	75.6
12	81.8		**0**	74.8

4.8. Effects due to Operation of Aircraft

When considering the identification of these systems, it is important to recognize that these aircraft will be operated in many different flight conditions. These conditions could cause variations in the spectrum which will lead to a more complex method to identify the aircraft and therefore these operations and conditions need to be explored.

For this study, there is a significant difference in the control of the aircraft when considering the static and hover tests. For the static tests, there was no control from on-board flight computer and therefore the ESC controlled the RPM of the motors. For the hover tests, the flight computer had control over the motors and therefore the RPM would vary between each motor depending on flight conditions. This is present in the spectrum and is more evident when considering external forces like wind where the flight controller will have to command more thrust from specific motor in order to remain stable and/or stationary.

For the GIA tests, the tether system inhibited the aircraft from excessive pitching, rolling, and yawing, however the aircraft was able to climb and descend which caused the height to fluctuate if the aircraft climbed too quickly. For these tests, the aircraft would begin to lose altitude which then the pilot would input more throttle (in order to keep the aircraft in the correct position), causing the motors to increase the RPM and therefore increase the BPF. Figure 4-24 shows a comparison between narrowband acoustic spectrums of the Iris+ quadcopter operating in at GIA with fluctuating altitude (blue), more stable hover without fluctuations (orange), both with the Iris operating at an altitude of 60 inches and the microphone at a height of 60 inches. This figure highlights the effect on the acoustic spectrum caused by the flight maneuver of the aircraft, specifically climb, hover and descent. The BPF is clearly effected by this variation, as well as the harmonics and therefore causes the spectrum to be populated with more tonal noise. Since the BPF is a clear defining feature of the acoustic signature, it would likely be a factor when considering the

identification of the aircraft. However, this effect could potentially cause issues with identification of the aircraft, mainly since the tonal content will be greatly affected.

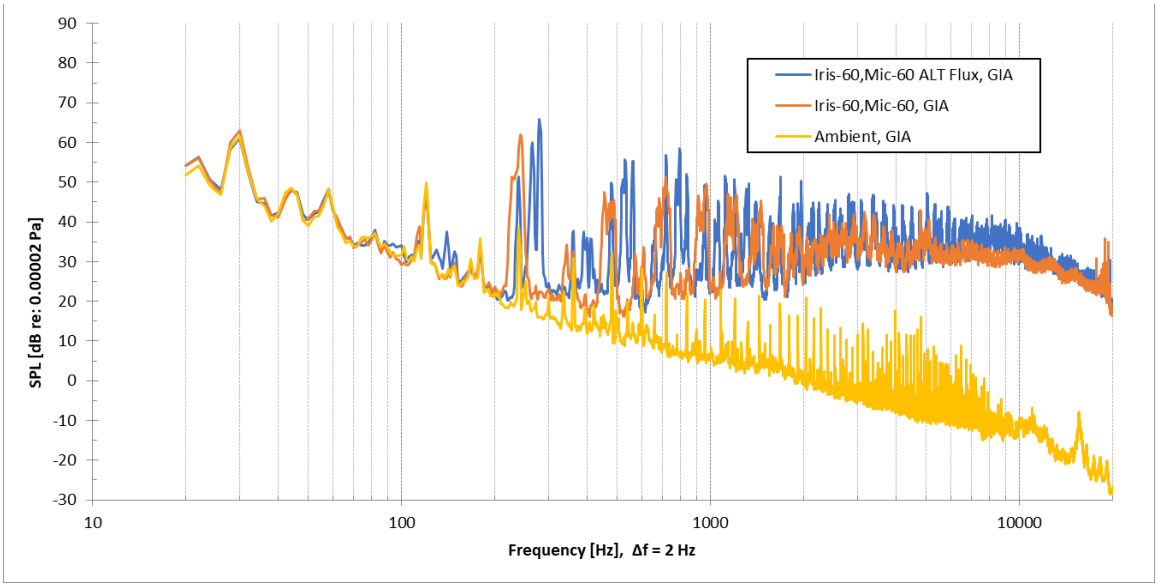

Figure 4-24: Comparison of stable flight (orange) with altitude fluctuation flight (blue) and ambient background, Iris flown at 60 inches with mics at 60 inches taken at GIA

Figure 4-25 shows the same spectra but between the frequencies 100 – 2000 Hz. Here the BPFs for each spectrum are clearly visible. The figure also shows the BPF values and the associated sound pressure level (SPL). For the stable flight (orange) the aircraft was able to hover with little variation about principle axes and altitude which resulted in a peak BPF tone at 242 Hz, however there is still the presence of an increase of rotor RPM. It is important to keep in mind that no flight was 100% stable and stationary and therefore the spectrum was effected. For the fluctuating altitude flight (blue) the aircraft was unable to stabilize and therefore resulted in multiple BPF values at 240 Hz, 266 Hz and 280 Hz. The stable flight (orange) spectrum has less variation in BPF due to a less pilot interference, which caused more of a 'smearing' effect with the tone. The fluctuating altitude flight (blue) spectrum has the deterministic tones rather than smearing due to the clear distinction between the flight maneuvers rather than the orange spectrum which maintained a more consistent flight maneuver.

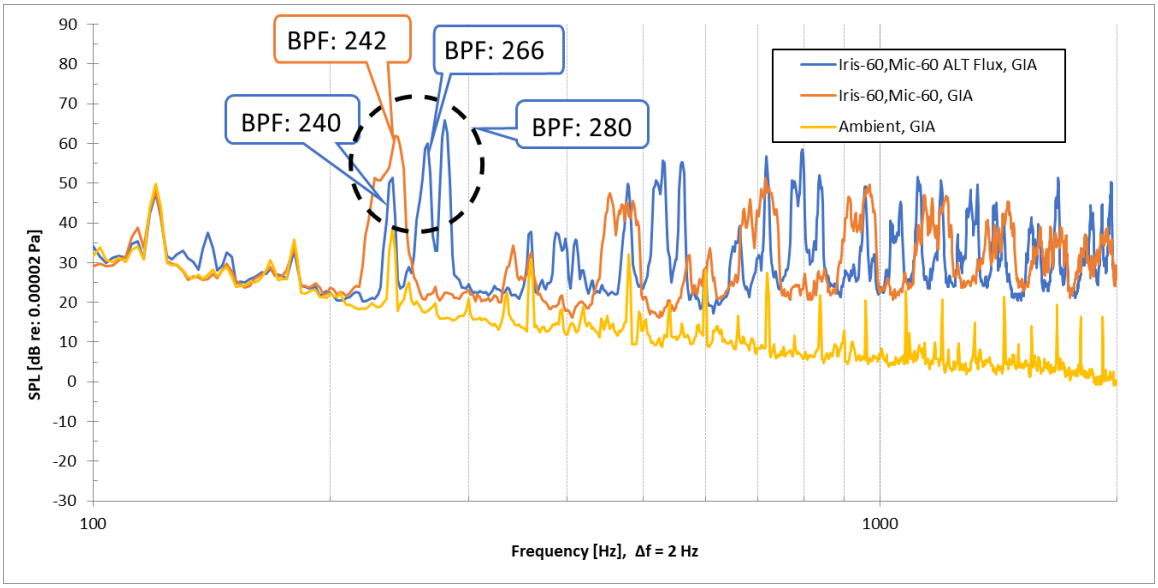

Figure 4-25: Comparison of stable flight (orange) with altitude fluctuation flight (blue) and ambient background, Iris flown at 60 inches with mics at 60 inches taken at GIA (frequencies 100 – 2000 Hz)

These large variations cause a significant amount of uncertainty and create an issue when considering identification of the noise source, as shown in Figure 4-26. This figure shows the stable flight from Figure 4-24 compared with the precision uncertainty bounds. Clearly there is a significant amount of uncertainty revolving the tonal content, which is expected due to the instability of the aircraft without a sophisticated positioning system, such as GPS.

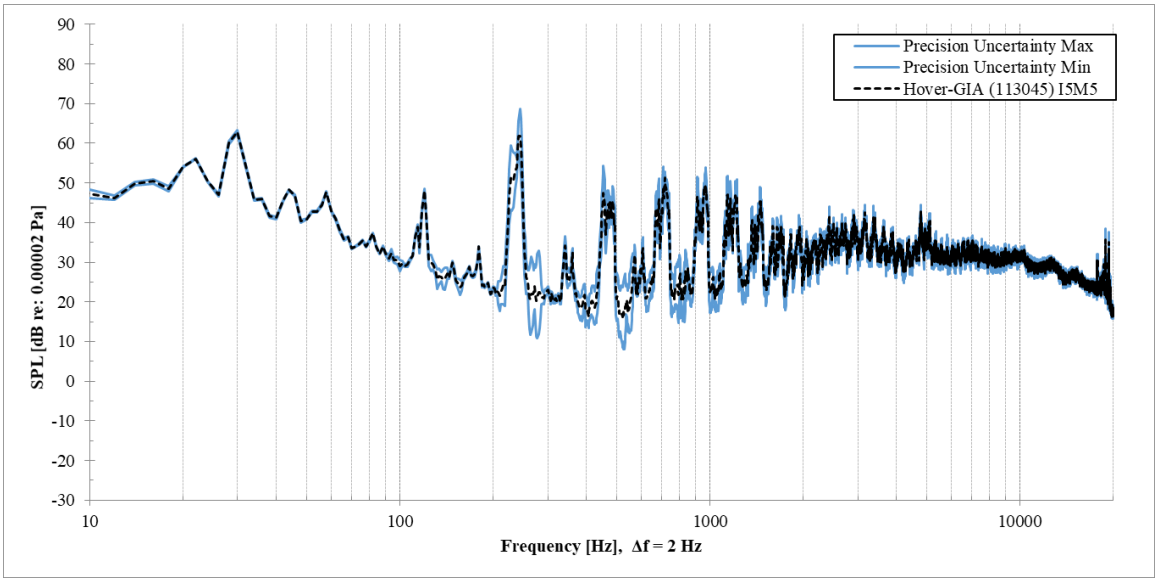

Figure 4-26: Narrowband acoustic spectra with precision uncertainty bounds, at UAFS with Static, Rotor Plane Microphone Array, Microphone 3

If operating in a constant flight maneuver (excluding hover) then multiple tones will be present (related to the different motor RPM values). Figure 4-27 shows the narrowband spectrum of the Iris flown at 60 inches with the microphone height also at 60 inches and a wind speed of approximately 10.4 knots, taken at the UAFS. This figure highlights the effect on the acoustic spectrum caused by the flight maneuver of the aircraft, specifically forward flight. This spectrum shows a distinct pair of BPF tones at 194 Hz and 208 Hz, which are believed to correspond with the orientation of the aircraft. During this test, the aircraft was attempting to maintain a constant position within a windy environment, which caused the aircraft to alter the RPM of the motors to compensate and provide a thrust vector in the opposite direction of the wind. Figure 4-27 also has a representation of the approximate aircraft orientation, in the top right.

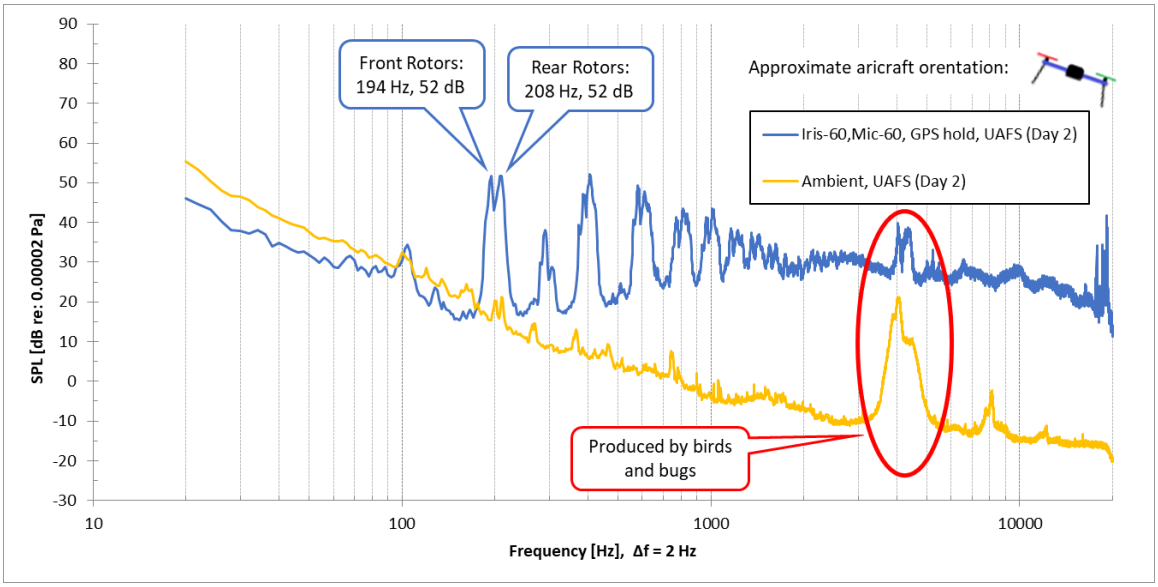

Figure 4-27: Narrowband spectrum of stable flight with wind speed of 10.4 knots, Iris flown at 60 inches with mics at 60 inches taken at UAFS

CHAPTER V

5. CONCLUSION

5.1. Summary

A common quadrotor (3DR Iris+) was tested in multiple testing conditions at multiple testing environments where the characteristic acoustic signature could be established. This is a continuation in research that will help in the noise prediction of sUAS for community noise studies as well as the basis for detection and counter-UAS applications. Tests were conducted that provided evidence in the validity of the previous work as well as providing further knowledge in the directivity of the acoustic signature of the aircraft as well as the effects caused by the operational state of the aircraft. These results were comparable to what was found in other literature. Figure 5-1 summarizes the effects and causes on the spectral content found through this study. The spectra in this figure are not measured data, but created to show the effects. The exact numbers are not correct however the treads are.

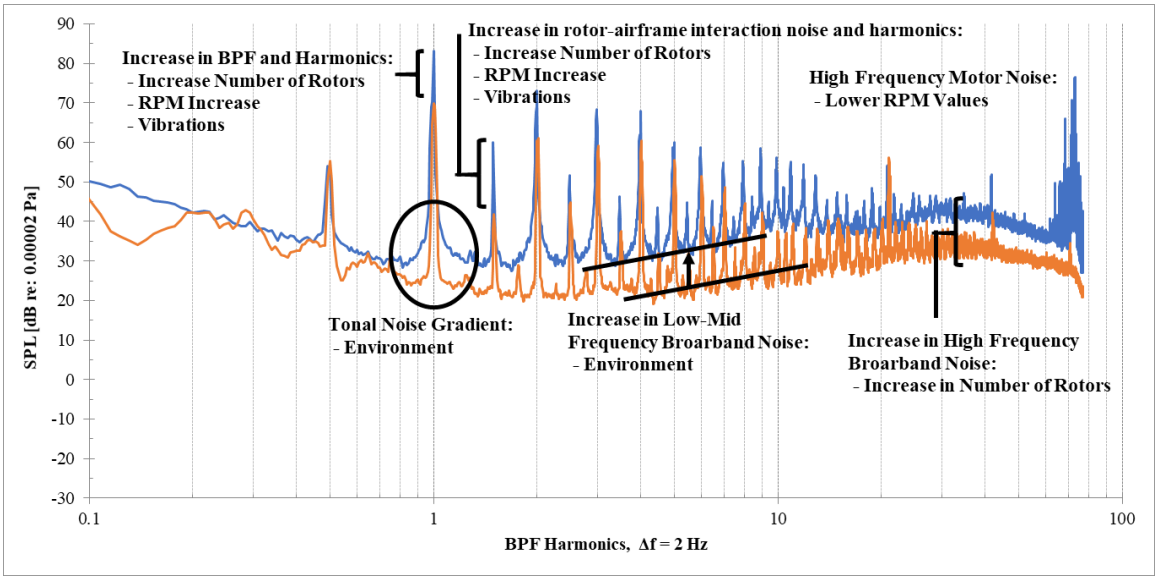

Figure 5-1: Fabricated compilation of cause and effect found through this study

The salient points from this study are as follows:

- Spectral Characterization
    - It was shown that the acoustic signature contains typical features of rotor noise, such as the shaft rate, BPF and harmonics, and broadband noise. The tonal noise dominates the low-mid frequencies while the broadband noise dominates the higher frequencies. It was also shown that there is the presence of additional tonal content which is suggested to be caused by rotor-airframe interaction.
- Effect of Increasing Throttle (RPM)
    - The spectral characteristics appears to be invariant to the speed of the rotors operating. However, typical effects such as increasing amplitude of tonal and broadband noise and increasing frequency of tonal noise is present.
- Effect of Multiple Rotors
    - The spectral characteristics of the acoustic signature appears to be invariant to the number of rotors. Nevertheless, this results in increasing high frequency broadband noise and rotor-airframe interaction noise.

- Recirculation and Vibration Effects
    - Recirculation was determined to not have affected the results due to the variations present being within the uncertainty bounds. However, there is a clear difference in amplitude between the results from the different mounting techniques which is speculated to be caused by the vibrations within the mount.
- Environment Effects
    - There was no apparent effect on characteristic acoustic signature due to the environment. The only effects that were observed were changes in amplitude of the tonal content and an increase in broadband noise which was speculated to be caused by reflections.
- Directivity
    - The directivity in the rotor plane was shown to be omni-directional, regardless of the varying parameters. While there was a noticeable amount of directivity above and below the rotor plane, which represent the expected dipole pattern. The directivity results show that as θ increases, so does the OASPL.
- Flight Operation
    - The flight maneuver of the aircraft significantly effects the tonal content in the acoustic signature. It was speculated that this could cause problems when considering identification. Additionally, this creates more tonal noise, which is perceived to be more annoying to humans.

5.2. Conclusions

The goal of this project was to provide a base understanding of the noise produced by an sUAS that will lead towards answering the question: Is it feasible to detect and/or identify an sUAS via the acoustic signature produced during flight operations? Based on the results presented in this study, it is too early to make a solid conclusion on the feasibility of this technique. However, from

the knowledge gained through this research it is reasonable to begin the development of an algorithm that will analyze the sound scape looking for potential noise sources that follow the typical rotorcraft acoustic features.

The results indicate that the signature contains typical characteristic acoustic features associated with rotorcraft which is both beneficial and not. Due to this, it is more difficult to differentiate between rotorcraft, however it is easier to guarantee that a rotorcraft indeed causes the noise source. Also, though observation of the acoustic spectra it has been suggested that identification of the aircraft could be difficult if the only defining features under inspection is the typical characteristic acoustic features. With this in mind, further research is required in order to identify additional parameters that could be used for the identification. This study showed that one of the most definable features of the acoustic signature was found to be the rotor-airframe interaction noise. This feature was present throughout all results and was shown to be related to the number of rotors, which is a defining variable for different multi-rotor aircraft. However, this feature is related to the RPM of the motors which will be continuously changing throughout typical operation of the aircraft. Due to this, the rotor-airframe interaction feature might not be suitable as a detection characteristic. The propagation pattern of the noise emitted by the aircraft is also not significant enough to be able to utilize it as a detection characteristic.

5.3. Future Work

Based on the results and conclusions there are a number of areas for future research. An initial consideration would be to fill out the missing data from this study. While the environment was a parameter under investigation for this study, not all environments were able to be compared. Static measurements were not performed in the OSU GIA. This was mainly due to scheduling conflicts rather than any technical issues. Collecting this data will help bridge the gap in the environmental study and allow for more conclusions to be drawn involving the effect due to the testing environment. It is expected to have similar results with what was presented for UAFS,

however there could be more reflections. Another consideration would be to perform *Hover, Roll Plane Microphone Array* tests in pitch plane and incremental planes between the roll and pitch plane. This would provide further evidence to show that the directivity of the noise source is omni-directional in the rotor plane and all planes parallel. Lastly, it would be beneficial to repeat the rotor-airframe interaction study performed by Zawodny [18] except with a 3DR Iris+ motor and arm. This will help identify the actual contribution rotor-airframe interaction noise has on the system noise and further define the concept of rotor-airframe interaction noise in whole.

This study only considered static and hover tests, which does not cover all forms of flight available for rotorcraft. Another direction for future work would be to investigate fly over measurements. This is important to consider since non-axial flight is the typical operation of these aircraft. A great starting point for this direction would be anechoic wind tunnel testing. While the setup for these measurements is fairly sophisticated and difficult, it allows for much more control over the parameters. This would also allow for a more direct comparison with hover and static data prior to the complex fly over data.

When considering the detection and identification of the aircraft, future work could be done in comparing different noise sources such as a weed eater, chainsaw, fixed-wing aircraft, or even typical military equipment with the 3DR Iris+. By performing these comparisons, conclusions could be drawn on which features best represent each individual noise source. Once these features have been identified, an algorithm could be created that will monitor the sound scape, looking for defining features that will allow for the detection and identification of the noise source. In terms of the logic for such system, the flow for the decision making and output signal should be similar to the following:

1. Monitoring Ambient Soundscape
2. Feature Detection
    2.1. Notify detection of noise source
3. Identify Friend or Foe

3.1. Run signature against known signatures for friendly vehicles

3.2. Notify if vehicle is friend or foe

4. Identify Details of Vehicle

4.1. Run diagnostics on signature to determine details of vehicle

4.2. Is it a rotorcraft, fixed wing?

4.3. How fast is it traveling?

4.4. How large is it?

Finally, the last consideration for future work is testing the accuracy of numerical prediction by comparing with experimental results. Work is progressing towards accurate noise prediction of these low tip Mach number rotors and validation of noise measured during flight. The insight gained will be used to improve predictions of noise and help in the development of counter-UAS devices as well as the development of quiet UAS for commercial and community use.

REFERENCES

[1] U.S. Department of Transportation & Federal Aviation Administration, "Small Unmanned Aircraft Systems Regulations, 14 CFR part 107," Washington, D.C., 2016.

[2] J. W. R. Taylor, Jane's pocket book of remotely piloted vehicles: Robot aircraft today, London: Collier Books, 1977.

[3] V. K. Saxena, The Amazing Growth and Journey of UAV's and Ballastic Missile Defence Capabilities: Where the Technology is Leading to?, Vij Books India Pvt Ltd, 2013.

[4] S. C. Tucker and P. M. Roberts, The Encyclopedia of the Arab-Israeli Conflict: A Political, Social, and Military History, Santa Barbara, California: ABC-CLIO, Inc., 2008.

[5] L. Daigle, "Air Force agreement aims to reduce UAS noise pollution," 10 April 2017. [Online]. Available: http://mil-embedded.com/news/air-force-agreement-aims-to-reduce-uas-noise-pollution/. [Accessed 13 April 2017].

[6] M. S. Rosenwald, "The Washington Post," 13 10 2016. [Online]. Available: https://www.washingtonpost.com/local/prisons-try-to-stop-drones-from-delivering-drugs-porn-and-cellphones-to-inmates/2016/10/12/645fb102-800c-11e6-8d0c-fb6c00c90481_story.html?utm_term=.aebc86508fed. [Accessed 13 4 2017].

[7] A. Mairaj, "Detection and Identification of an Aircraft by Processing its Acoustic Signature," in *International Conference on Network and Electronics Engineering,* 2011.

[8] B. Kaushik, D. Nance and K. Ahuja, "A Review of the Role of Acoustic Sensors in the Modern Battlefield," *11th AIAA/CEAS Aeroacoustics Conference,* 2005.

[9] HGH Infrared Systems, "Definition of DRI : Detection, Recognition, Identification ranges," [Online]. Available: http://www.hgh-infrared.com/FAQ/Perimeter-Security/Definition-of-DRI-Detection-Recognition-Identification-ranges.

[10] K. S. Brentner and F. Farassat, "Modeling aerodynamically generated sound of helicopter rotors," *Progress in Aerospace Sciences,* vol. 39, pp. 83-120, 2003.

[11] H. H. Hubbard, Aeroacoustics of Flight Vehicles: Theory and Practice. Volume 1. Noise Sources, Ft. Belvoir: Defence Technical Information Center, 1991.

[12] Y. H. Yung, "Rotor blade–vortex interaction noise," *Progress in Aerospace Sciences,* vol. 36, no. 2, pp. 97-115, 2000.

[13] N. S. Zawodny, D. D. Boyd Jr. and C. L. Burley, "Acoustic Characterization and Prediction of Representative, Small-Scale Rotary-Wing Unmanned Aircraft System Components," in *AHS 72nd Annual Forum*, West Palm Beach, Florida, 2016.

[14] N. Intaratep, W. N. Alexander, W. J. Devenport, S. M. Grace and A. Dropkin, "Experimental Study of Quadcopter Acoustics and Performance at Static Thrust Conditions," in *22nd AIAA/CEAS Aeroacoustics Conference*, Lyon, France, 2016.

[15] G. Sinibaldi and L. Marino, "Experimental analysis on the noise of propellers for small UAV," *Applied Acoustics,* vol. 74, pp. 79-88, 2013.

[16] R. K. Amiet, "Acoustic radiation from an airfoil in a turbulent stream," *Journal of Sound and VIbration,* vol. 41, no. 4, pp. 407-420, 1975.

[17] R. K. Amiet, "Noise due to turbulent flow past a trailing edge," *Journal of Sound and Vibration,* vol. 47, no. 3, pp. 387-393, 1976.

[18] N. Zawodny, D. D. Boyd Jr. and H. H. Haskin, *Progress on Small Unmanned Aerial System (sUAS) Noise Characterization,* Hampton, VA, 2017.

[19] 3. Robotics, "3DR," 2016. [Online]. Available: https://3dr.com/kb/iris/.

[20] T. Motor, "T-MOTOR, The safest propulsion system," 2016. [Online]. Available: http://www.rctigermotor.com/html/2014/Propeller_1205/280.html.

[21] J. B. Brandt, R. W. Deters, G. K. Ananda and M. S. Selig, "UIUC Airfoil Database," University of Illinois at Urbana-Champaign, [Online]. Available: http://m-selig.ae.illinois.edu/ads/coord_database.html. [Accessed 12 2016].

[22] O. S. University, "Unmanned Aircraft Flight Station," [Online]. Available: https://unmanned.okstate.edu/node/52. [Accessed 6 July 2017].

[23] K. K. Ahuja, "Reliable Acoustic Measurements of Ducted and Unducted Rotors for use in Predicting Flyover Data," in *DARPA/NASA Propeller-Rotor Acoustics Workshop*, NASA Langley Research Center, 2010.

[24] J. M. Seitzman, *Experimental Errors and Uncertainty: An Introduction*, Georgia Tech College of Engineering, Class Notes from AE 3051.

APPENDICES

6. APPENDIX A

6.1. Ambient Background Noise Characterization Additional Results

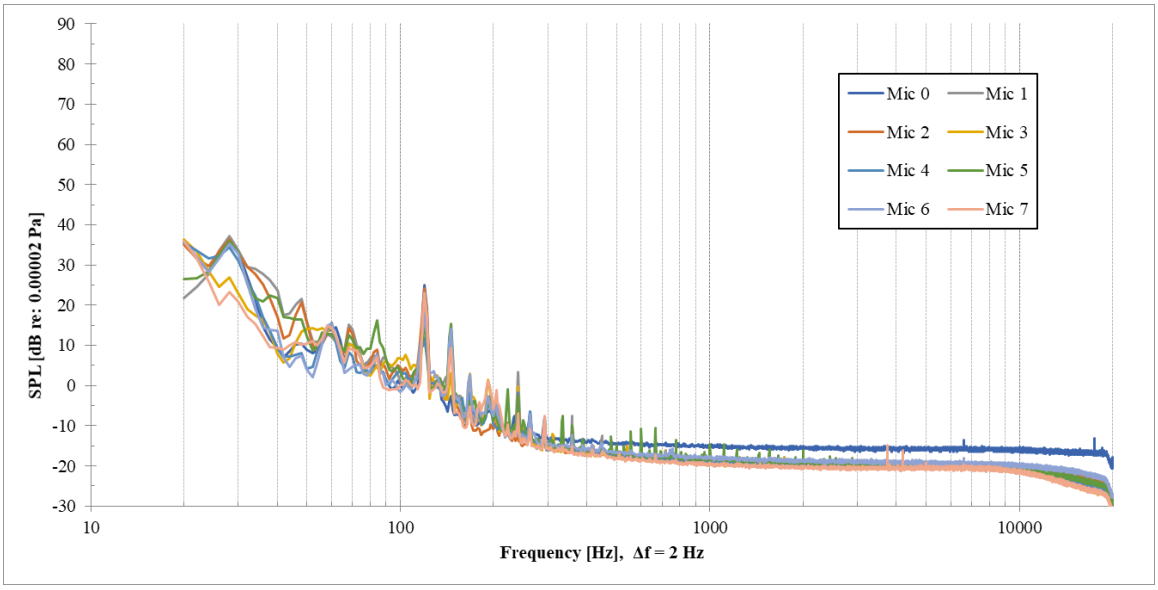

Figure 6-1: OSU Anechoic Chamber - Ambient Background Noise - Static, Rotor Plane Microphone Array, Soft Mount with all microphone responses (3/30/16)

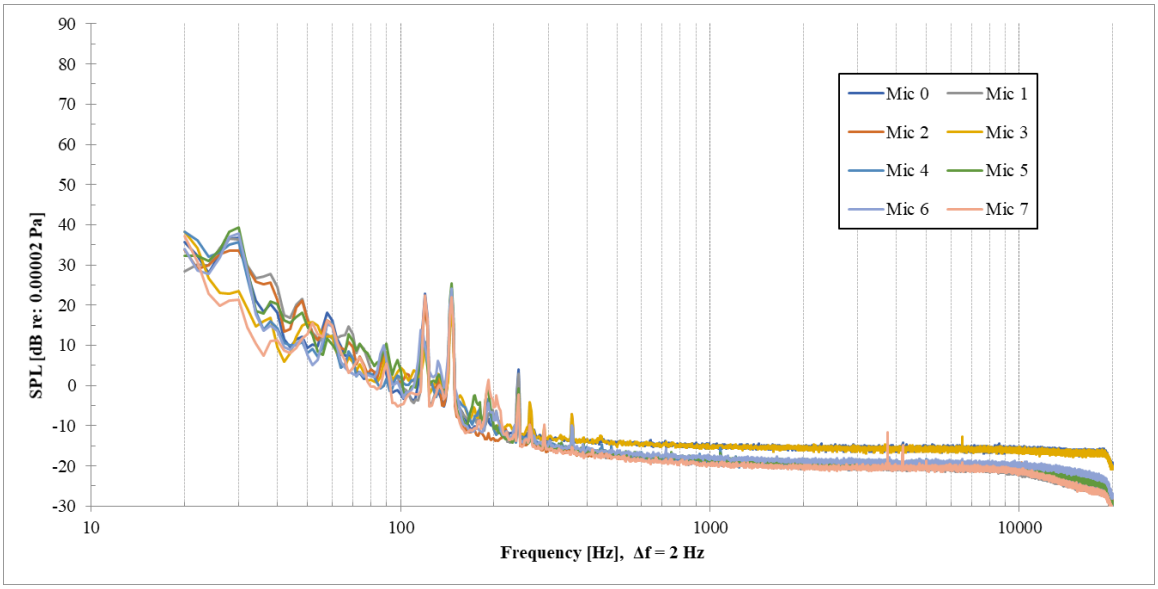

Figure 6-2: OSU Anechoic Chamber - Ambient Background Noise - Static, Rotor Plane Microphone Array, Hard Mount with all microphone responses (4/11/17)

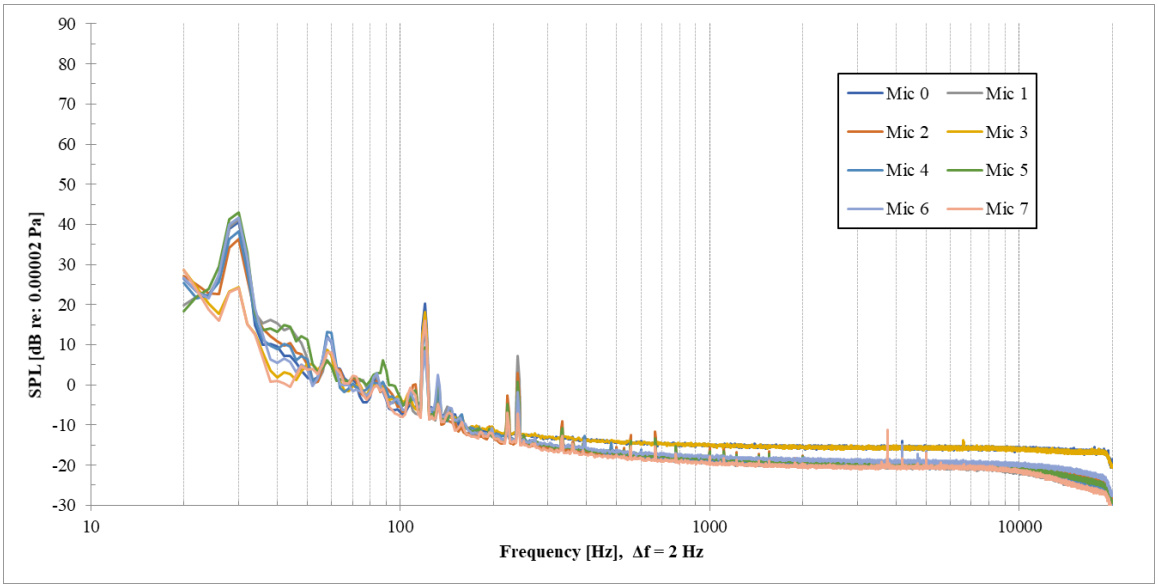

Figure 6-3: OSU Anechoic Chamber - Ambient Background Noise - Static, Rotor Plane Microphone Array, Hard Mount with all microphone responses (6/15/17)

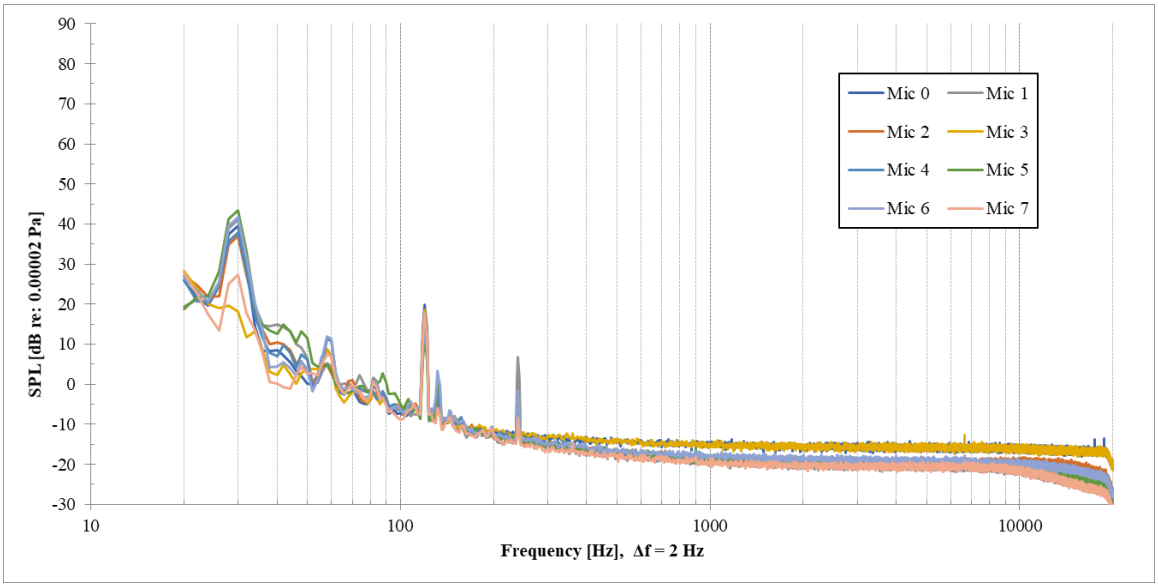

Figure 6-4: OSU Anechoic Chamber - Ambient Background Noise - Static, Rotor Plane Microphone Array, Hard Mount with all microphone responses (7/11/17)

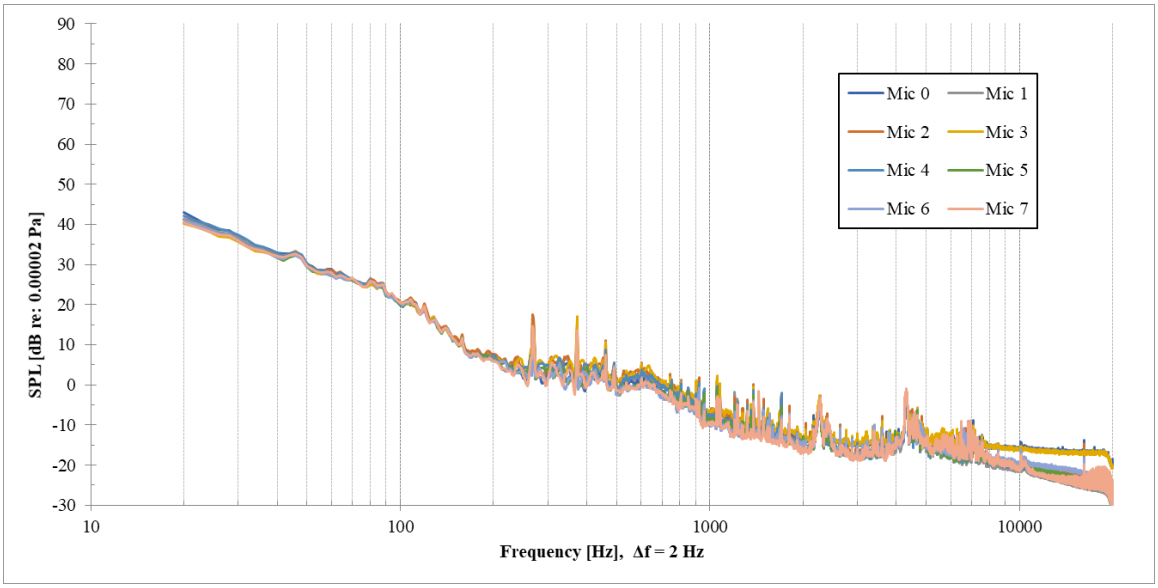

Figure 6-5: OSU UAFS - Ambient Background Noise - Static, Rotor Plane Microphone Array, Hard Mount (4/12/17)

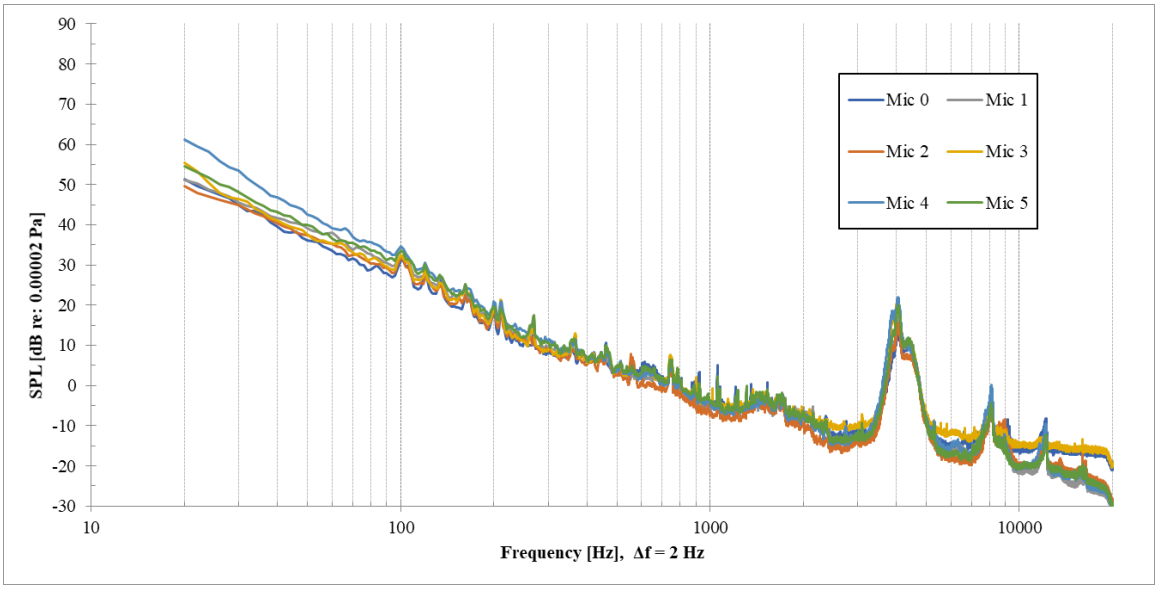

Figure 6-6: OSU UAFS - Ambient Background Noise - Hover, Rotor Plane Microphone Array (4/19/17)

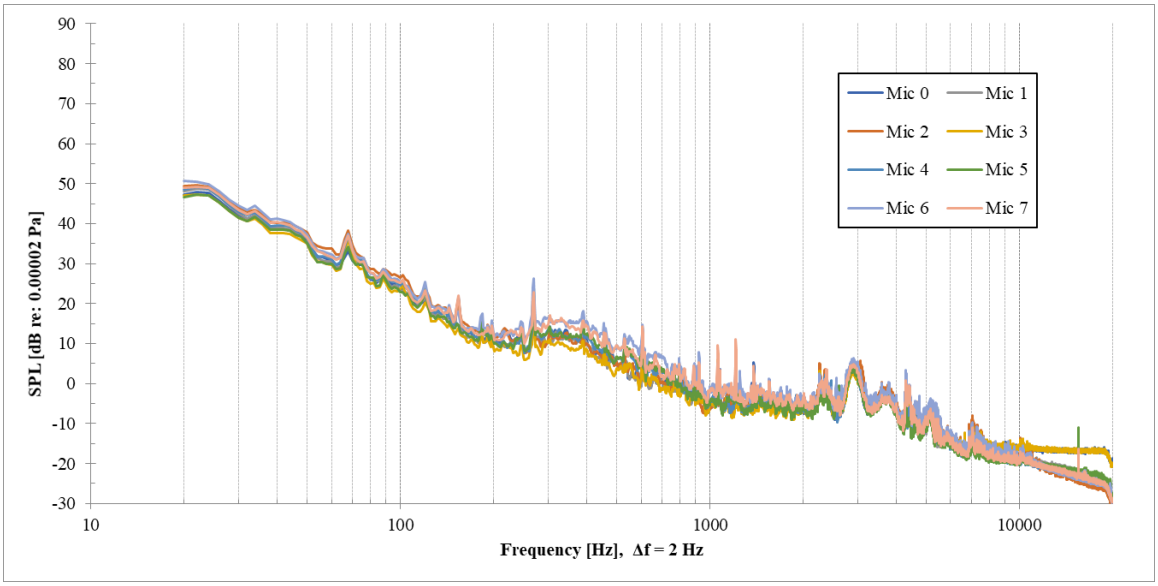

Figure 6-7: OSU UAFS - Ambient Background Noise - Static, Rotor Plane Microphone Array (6/19/17)

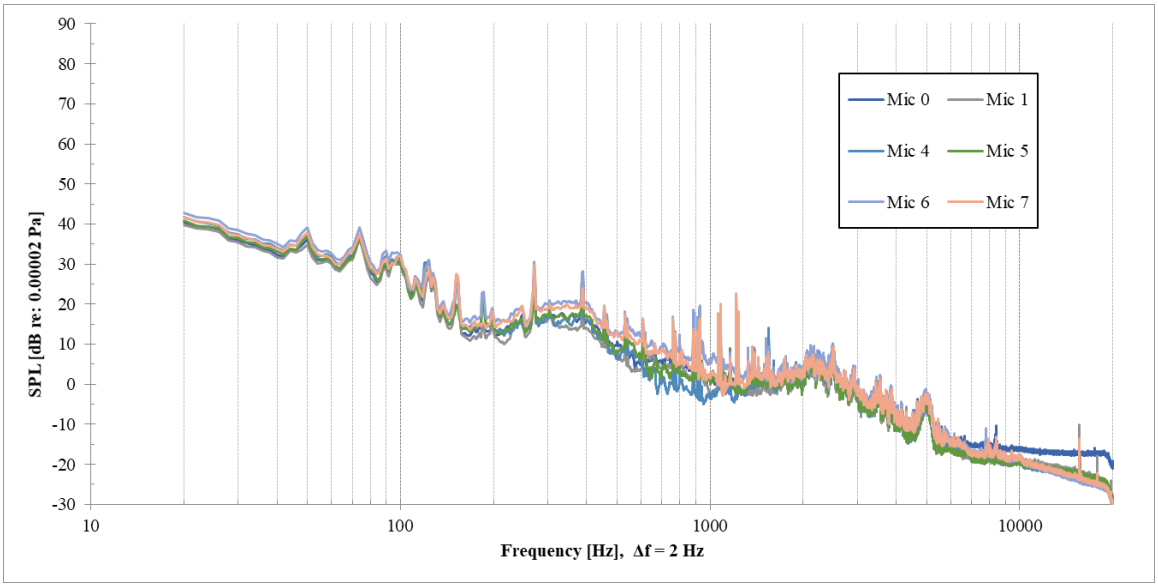

Figure 6-8: OSU UAFS - Ambient Background Noise - Hover, Rotor Plane Microphone Array (6/19/17)

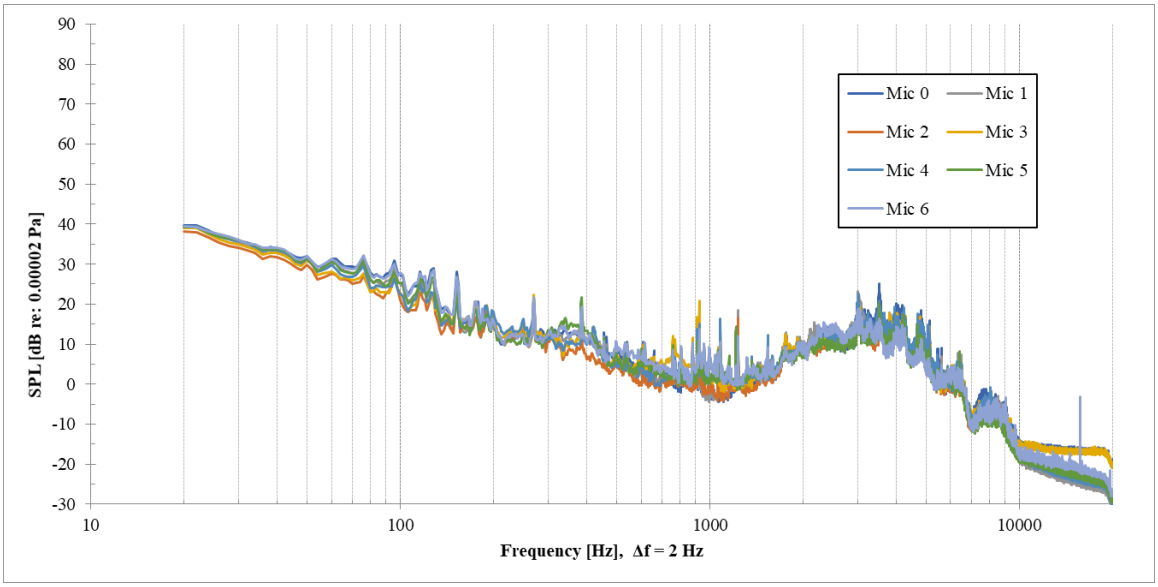

Figure 6-9: OSU UAFS - Ambient Background Noise - Hover, Roll Plane Microphone Array (6/19/17)

Table 6-1: Atmospheric and weather conditions at specified testing environments on testing day

Date	Test Environment	Start Time	End Time	Temp. (F)	Bar Pressure (Hg)	Wind Speed (mph)	Wind Gusts (mph)	Wind Direction
3/30/2016	Anechoic Chamber	10:37:00 PM	12:45:00 AM	65	29.5	--	--	--
3/29/2017	GIA	9:26:00 PM	12:44:00 AM	47	29.75	--	--	--
4/11/2017	Anechoic Chamber	11:33:00 PM	11:59:00 PM	50	30.2	--	--	--
4/12/2017	UAFS	3:41:00 AM	4:32:00 AM	56	30.2	6	8	ESE
4/19/2017	UAFS	1:36:00 AM	5:56:00 AM	61	30	9	10	S
6/15/2017	Anechoic Chamber	3:07:00 AM	3:59:00 AM	75	29.75	--	--	--
6/19/2017	UAFS	1:16:00 AM	1:45:00 AM	66	29.95	4	5	S
6/19/2017	UAFS	2:30:00 AM	3:51:00 AM	63	29.95	2	4	S
6/19/2017	UAFS	5:30:00 AM	5:35:00 AM	58	29.95	0	0	--
6/19/2017	UAFS	5:48:00 AM	5:50:00 AM	59	29.98	0	0	--
7/11/2017	Anechoic Chamber	2:15:00 AM	4:40:00 AM	77	29.87	--	--	--

6.2. Spectral Characterization Additional Results

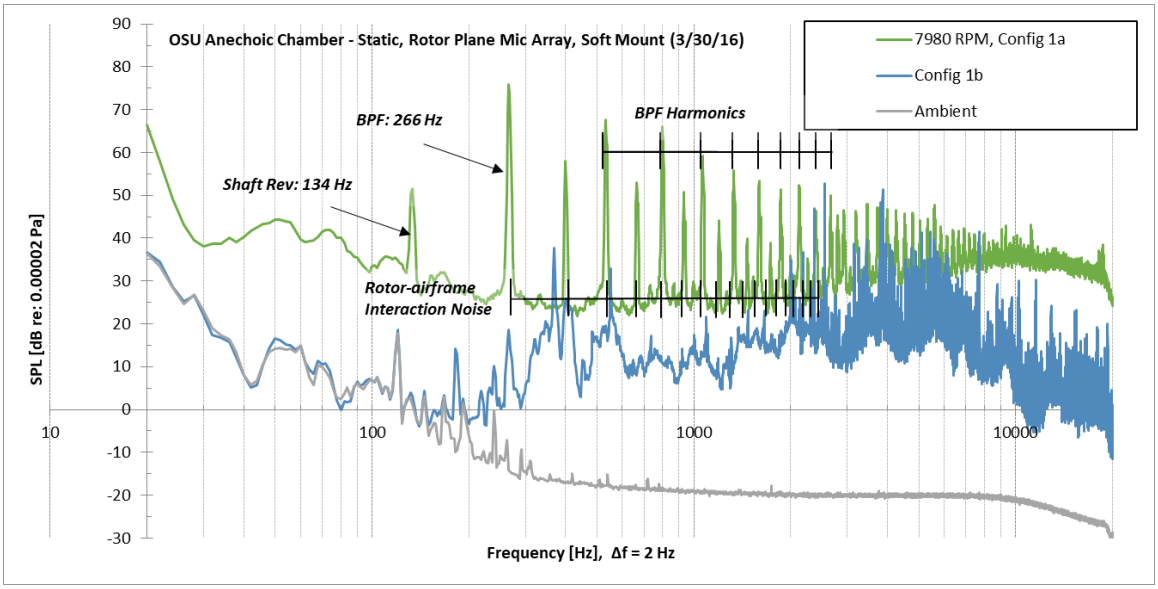

Figure 6-10: OSU Anechoic Chamber - Static, Rotor Plane Mic Array, Soft Mount (3/30/16)

6.3. Effect of Increasing Throttle (RPM) Additional Results

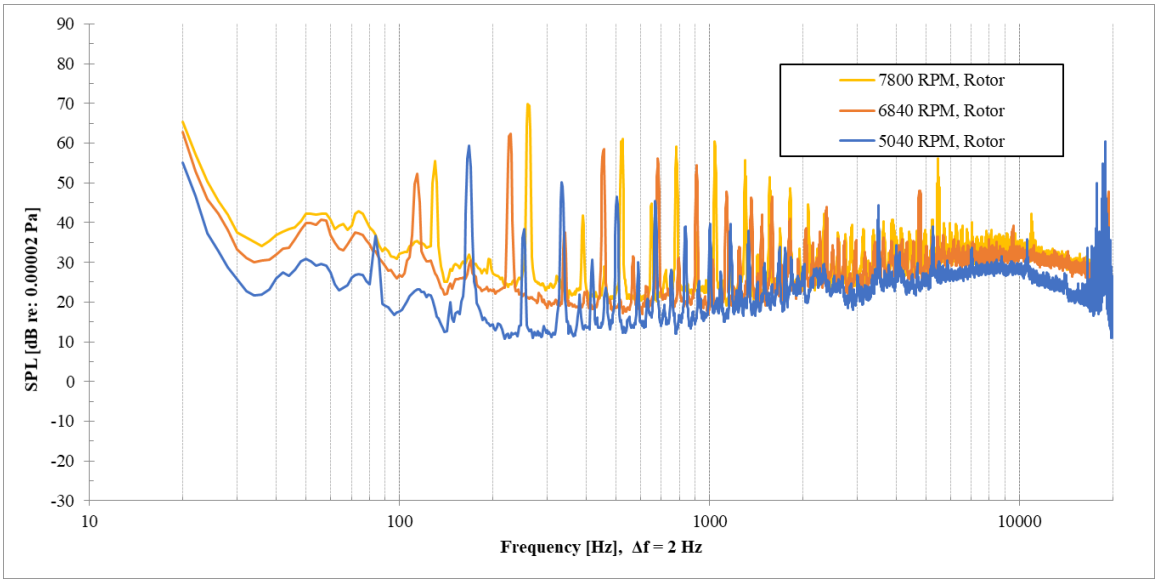

Figure 6-11: OSU Anechoic Chamber – Varying RPM, Static, Rotor Plane Microphone Array, Hard Mount (4/11/17)

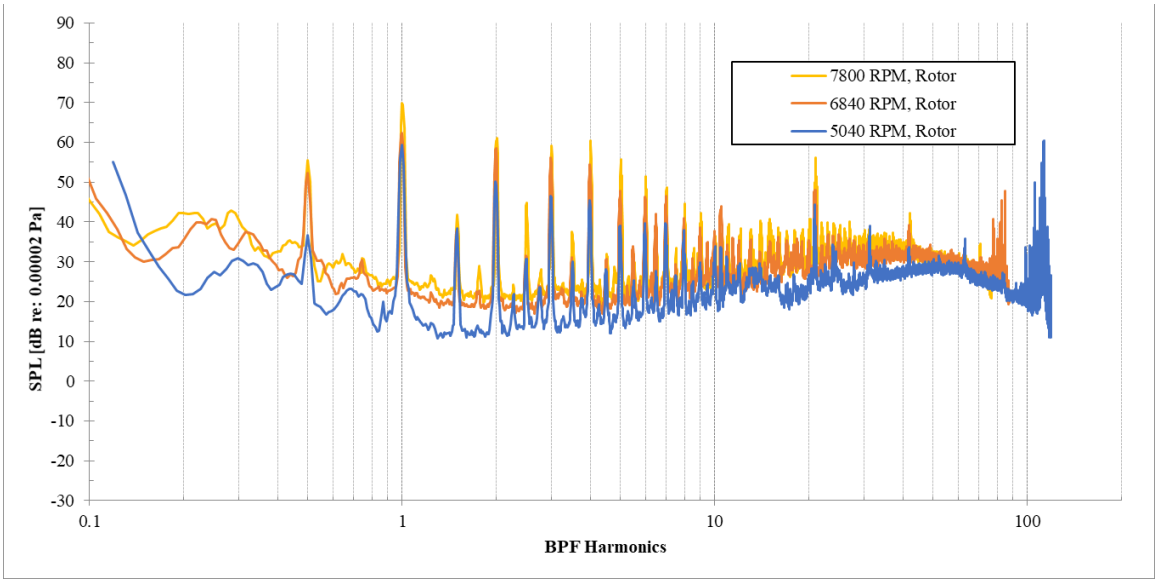

Figure 6-12: OSU Anechoic Chamber – Varying RPM, Static, Rotor Plane Microphone Array, Hard Mount, Normalized to BPF (4/11/17)

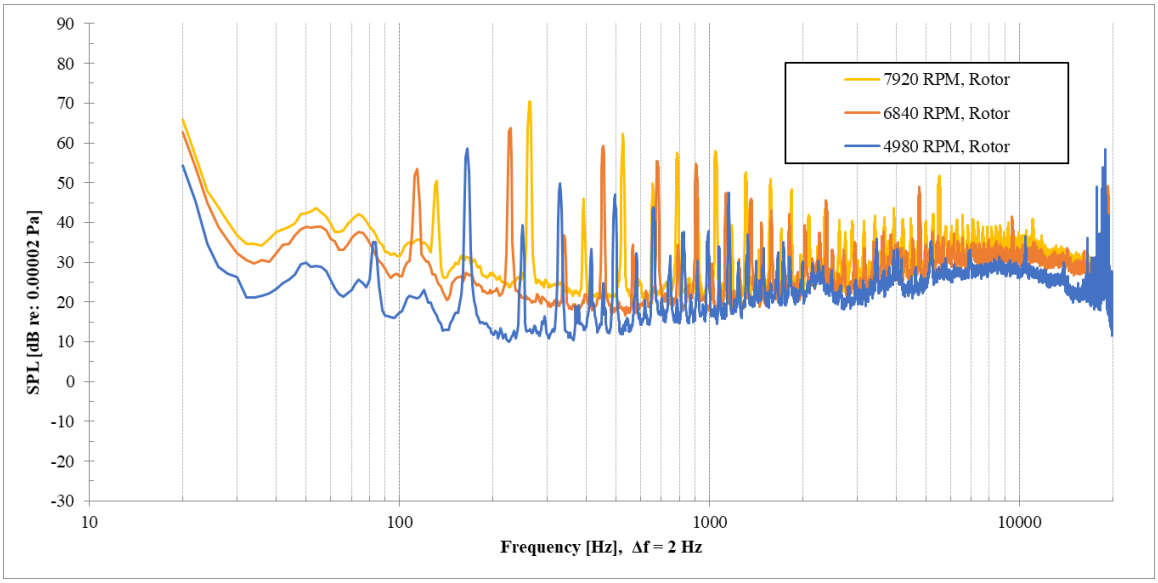

Figure 6-13: OSU Anechoic Chamber – Varying RPM, Static, Rotor Plane Microphone Array, Hard Mount (6/15/17)

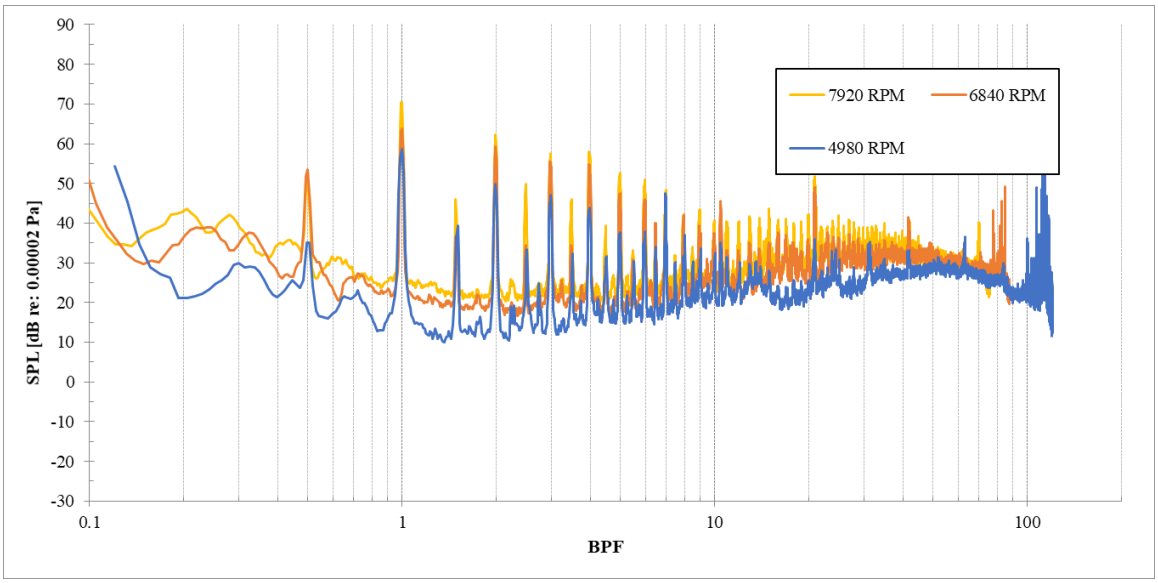

Figure 6-14: OSU Anechoic Chamber – Varying RPM, Static, Rotor Plane Microphone Array, Hard Mount, Normalized to BPF (6/15/17)

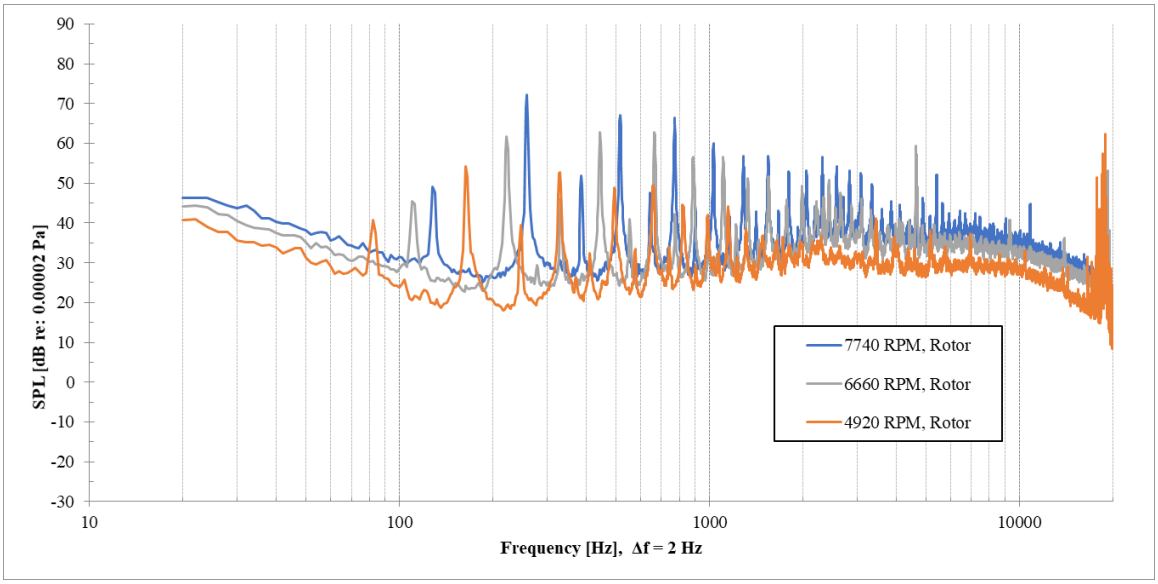

Figure 6-15: OSU UAFS- Varying RPM, Static, Rotor Plane Microphone Array, Hard Mount (4/12/17)

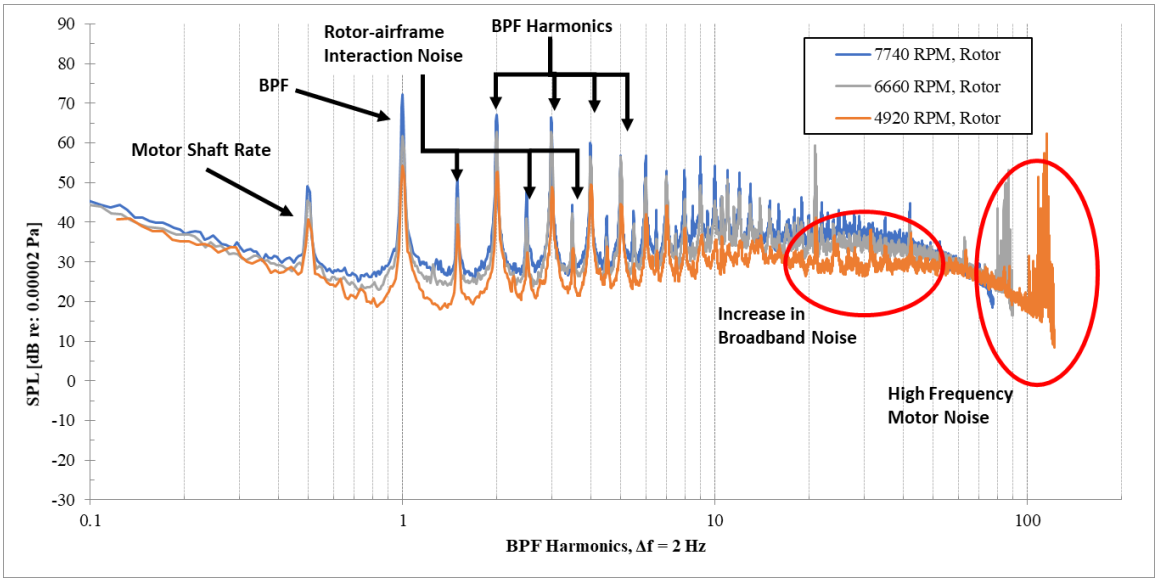

Figure 6-16: OSU UAFS- Varying RPM, Static, Rotor Plane Microphone Array, Hard Mount, Normalized to RPM (4/12/17)

6.4. Effect of Multiple Rotors Additional Results

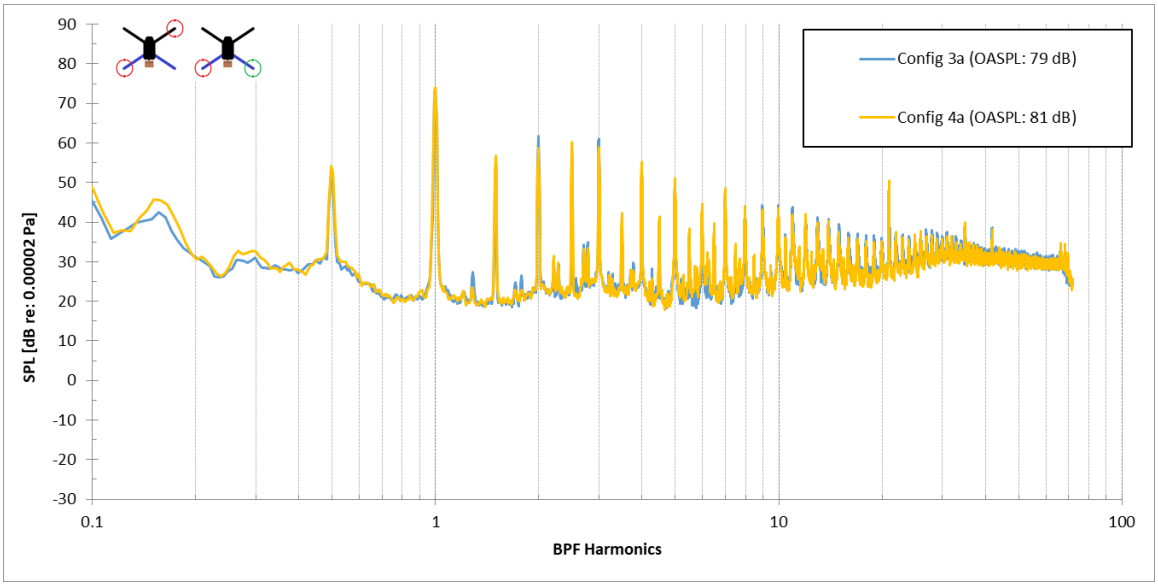

Figure 6-17: OSU Anechoic Chamber Config 3a, 4a @ 100% Throttle; Mic 5

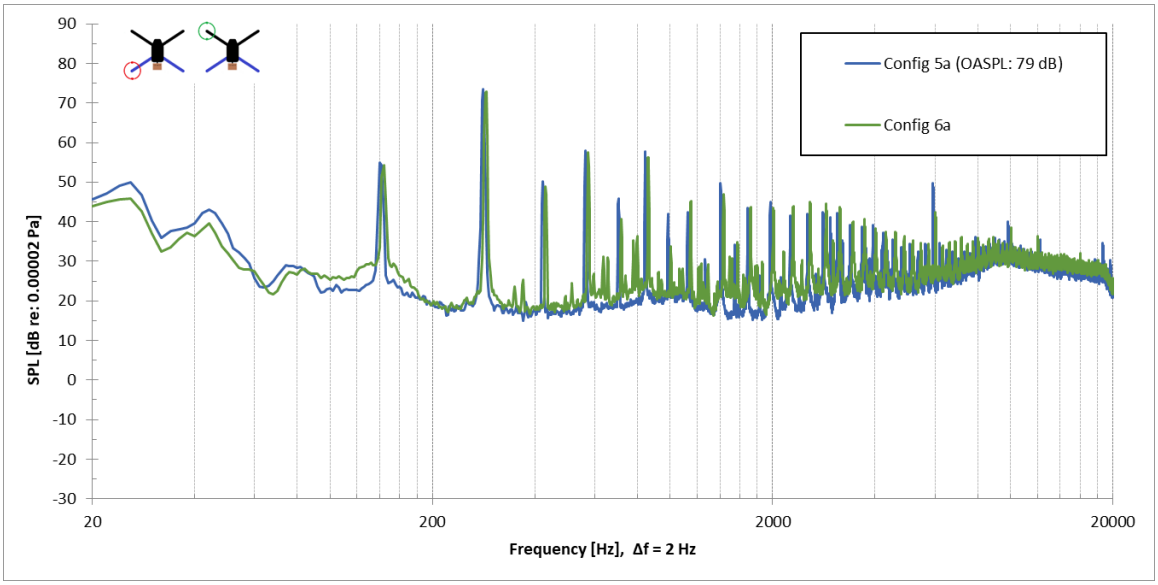

Figure 6-18: OSU Anechoic Chamber 3DR Iris+; Config 5a, 6a @ 100% Throttle; Mic 5

6.5. Recirculation and Vibration Effects Additional Results

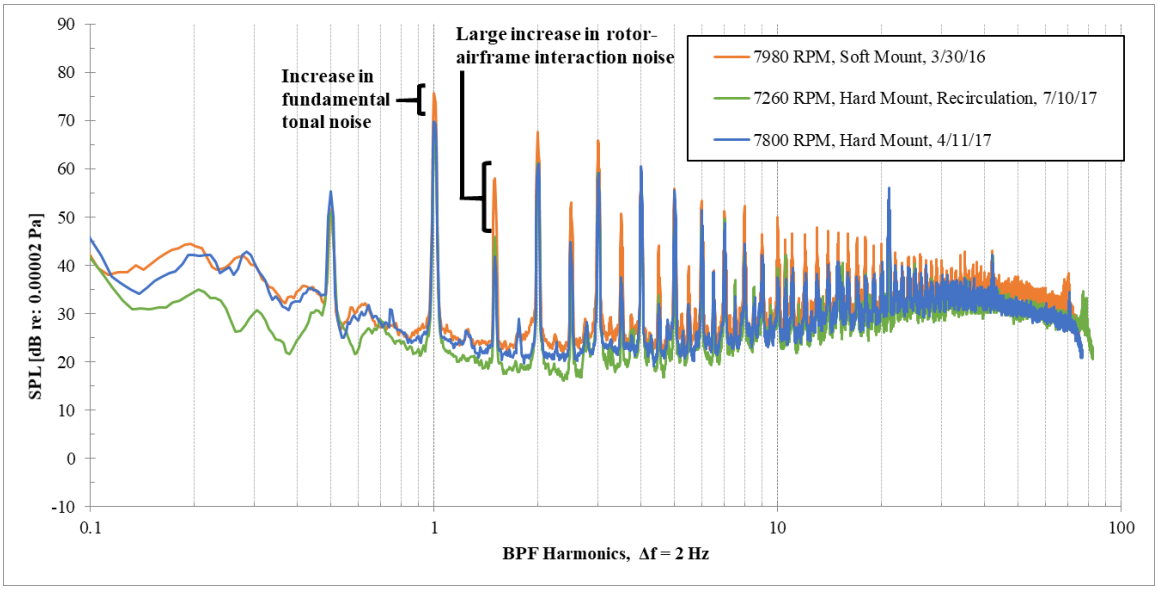

Figure 6-19: Comparison of narrowband acoustic spectra with Hard Mount (blue), without Foam Sheets for forced recirculation, within OSU anechoic chamber, Static, Rotor Plane Microphone Array, Microphone 3

6.6. Directivity Additional Results

6.6.1. Rotor Plane

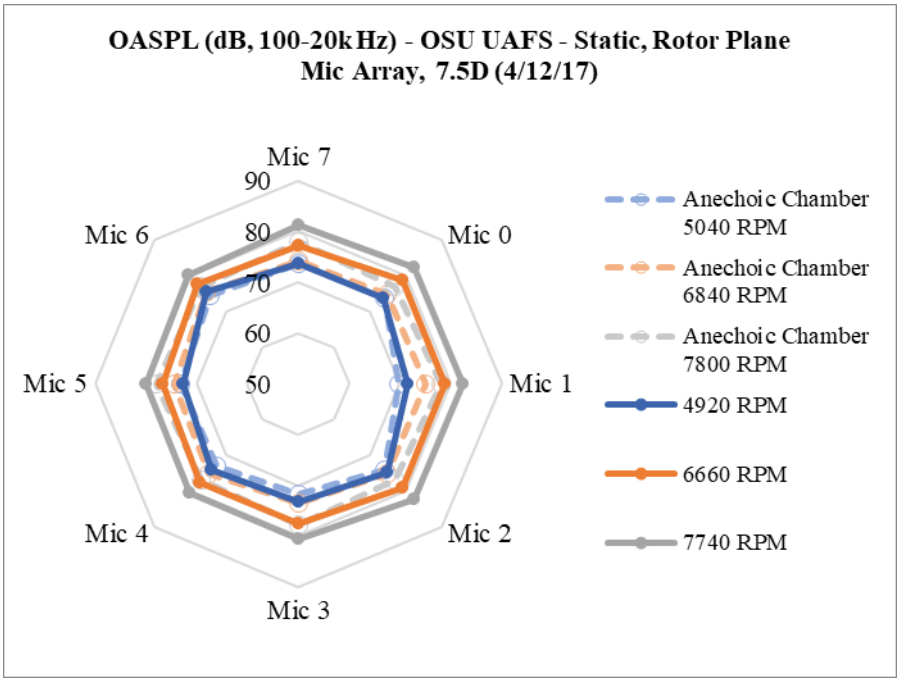

Figure 6-20: OASPL (dB, 100-20k Hz) - Static, Rotor Plane Microphone Array with Hard Mount shown with dotted line comparison with OSU Anechoic Chamber (4/11/17), B) OSU UAFS (4/12/17)

6.6.2. Roll Plane

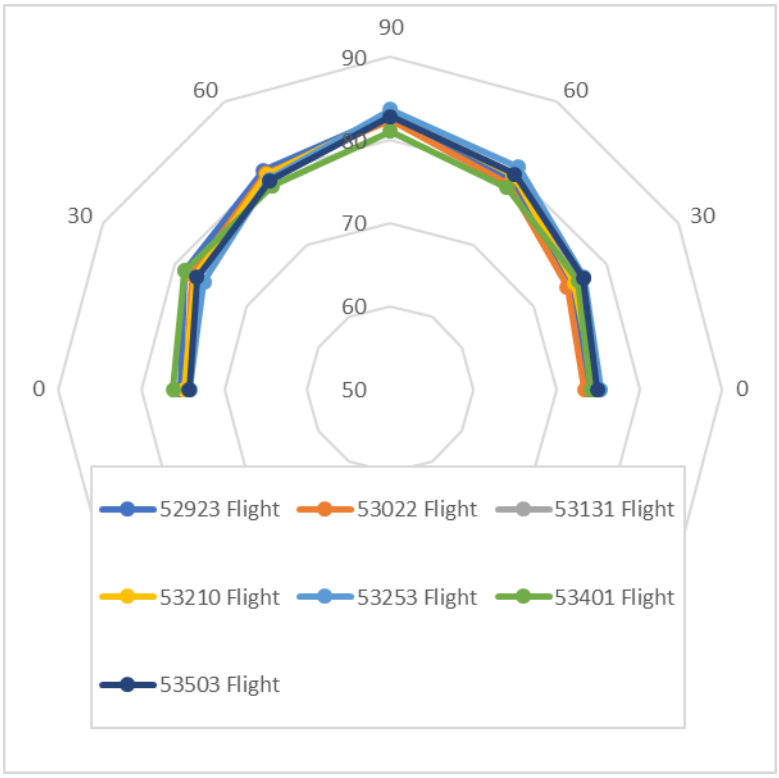

Figure 6-21: OASPL (dB, 100 – 20k Hz) directivity patterns of 3DR Iris+, for Roll Plane Microphone Array tests at hover testing conditions, 7 different measurements

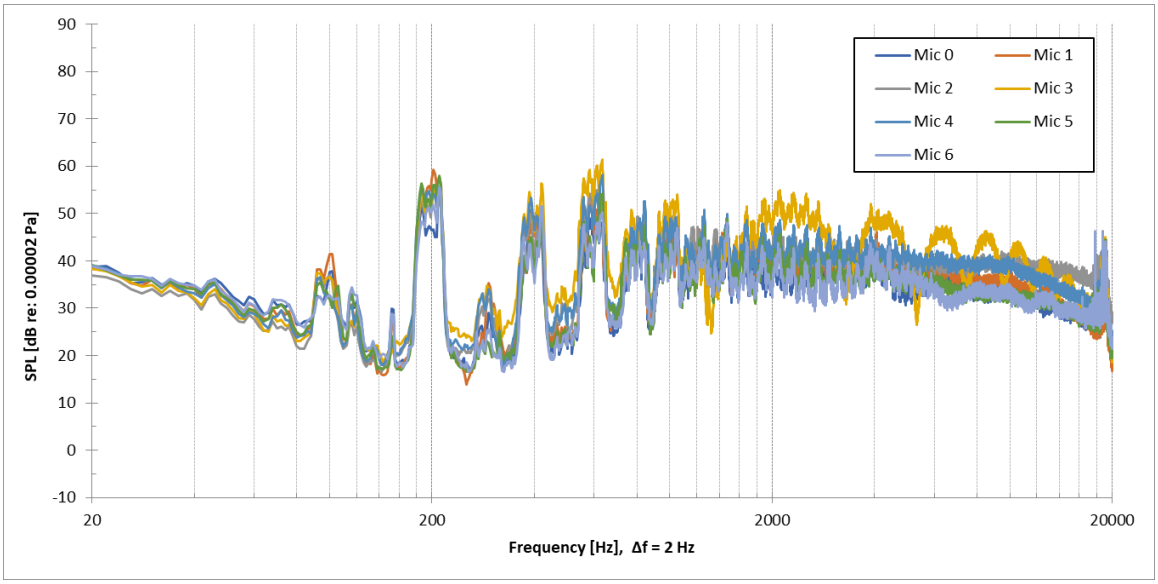

Figure 6-22: OSU UAFS- Flight, Roll Plane Mic Array, GPS Hold (6/19/17)

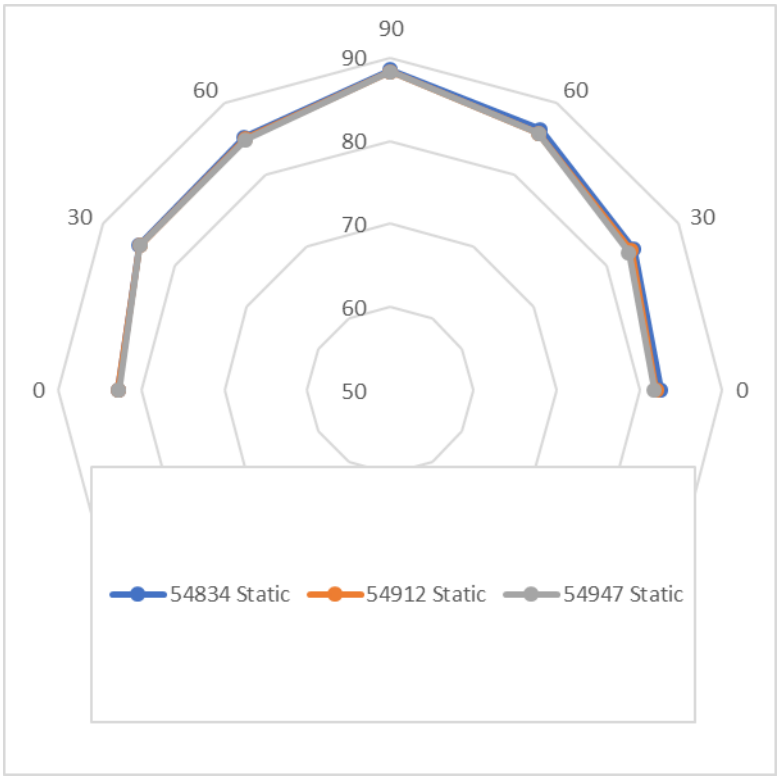

Figure 6-23: OASPL (dB, 100 – 20k Hz) directivity patterns of 3DR Iris+, for Roll Plane Microphone Array tests at static testing conditions, 2 different measurements

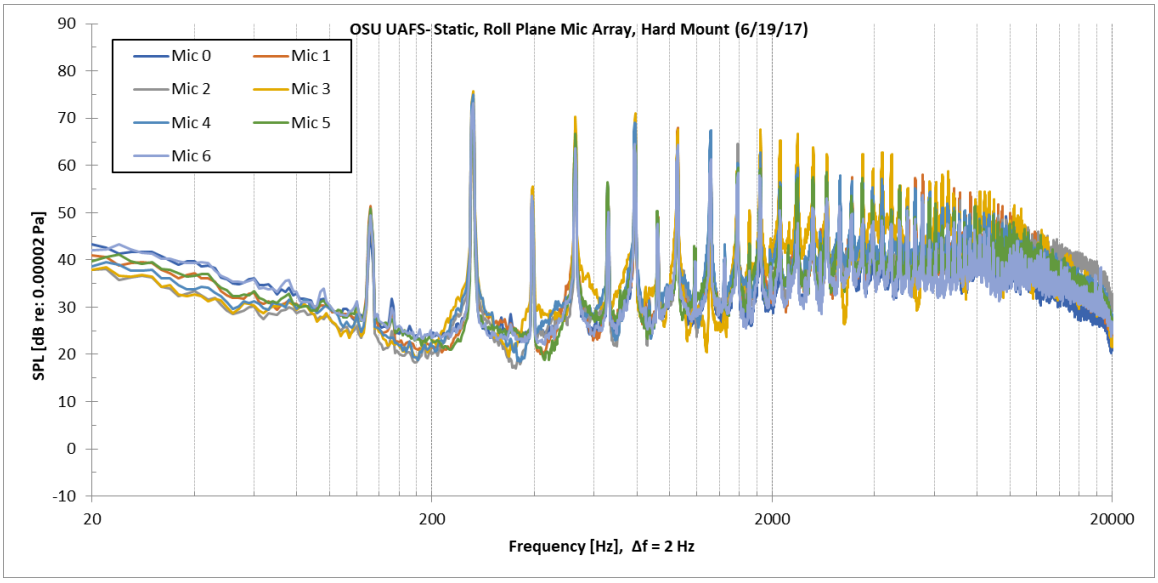

Figure 6-24: OSU UAFS- Static, Roll Plane Mic Array, Hard Mount (6/19/17)

6.7. Effects due to Operation of Aircraft Additional Results

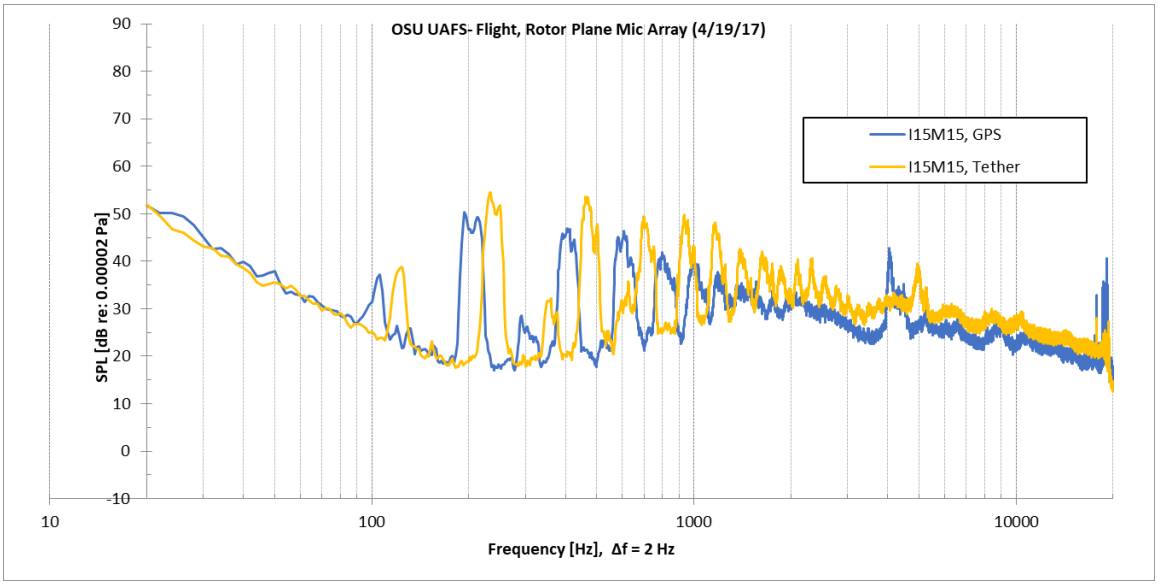

Figure 6-25: Difference in narrowband data from GPS Hold and Tether control

VITA

Jordan Ambrose Feight

Candidate for the Degree of

Master of Science

Thesis: ACOUSTIC CHARACTERIZATION OF A MULTI-ROTOR SUAS AS A FIRST STEP TOWARDS DETECTION AND IDENTIFICATION VIA ACOUSTIC SIGNATURE

Major Field: Mechanical and Aerospace Engineering

Biographical:

Education:

Completed the requirements for the Master of Science in Mechanical and Aerospace Engineering at Oklahoma State University, Stillwater, Oklahoma in July, 2017.

Completed the requirements for the Bachelor of Science in Mechanical Engineering and Aerospace Engineering at West Virginia University, Morgantown, West Virginia in December, 2014.

Experience:

Research Assistant – Oklahoma State University, Stillwater, OK
Research Assistant – West Virginia University, Morgantown, WV

Professional Memberships:

AIAA